Universidade de Lisboa
Faculdade de Ciências
Departamento de Física

Dynamics and steady-state properties of adaptive networks

Stefan Wieland

Doutoramento em Física

2013

Universidade de Lisboa
Faculdade de Ciências
Departamento de Física

Dynamics and steady-state properties of adaptive networks

Stefan Wieland

Tese orientada pela Prof.ª Doutora Ana Maria Ribeiro Ferreira Nunes e pela Doutora Maria Gabriela Miranda Gomes, especialmente elaborada para a obtenção do grau de doutor em Física

2013

Professor Ana Nunes for insisting that precise language precedes analytical rigor, for the many insights provided in frequent discussions, and for being patient enough to put up with my stubborn soul. Professor Gabriela Gomes for a warm welcome in Lisbon, and for a crucial first year at the IGC in Oeiras. Professor Nico Stollenwerk for offering me a platform to spread ideas and interact with other researchers.

FCT for the key SFRH/BD/45179/2008 that opened many doors. Andrea and Tomás for their research contributions. Andrea, Heinrich, Ramona, Atle, Ganna, Sílvia and Miguel for proofreading, as well as for hilarious and much-needed coffee breaks. Marta and Pedro for tickling my brain during shared lunches. Patrícia for being a good sport, and for identifying with the plight of Germans living abroad.

Dani for putting things into perspective while sharing drinks at Bica. Marlene and Mariana for doing the same through riding Portugal's waves with me.

Most of all, I would like to thank Ale. You are family.

Abstract

Collective phenomena often arise through structured interactions among a system's constituents. In the subclass of adaptive networks, the interaction structure coevolves with the dynamics it supports, yielding a feedback loop that is common in a variety of complex systems. To understand and steer such systems, modeling their asymptotic regimes is an essential prerequisite. In the particular case of a dynamic equilibrium, each node in the adaptive network experiences a perpetual change in connections and state, while a comprehensive set of measures characterizing the node ensemble are stationary. Furthermore, the dynamic equilibria of a wide class of adaptive networks appear to be unique, as their characteristic measures are insensitive to initial conditions in both state and topology.

This work focuses on dynamic equilibria in adaptive networks, and while it does so in the context of two paradigmatic coevolutionary processes, obtained results easily generalize to other dynamics. In the first part, a low-dimensional framework is elaborated on using the adaptive contact process. A tentative description of the phase diagram and the steady state is obtained, and a parameter region identified where asymmetric microscopic dynamics yield a symmetry between node subensembles. This symmetry is accounted for by novel recurrence relations, which predict it for a wide range of adaptive networks. Furthermore, stationary node-ensemble distributions are analytically generated by these relations from one free parameter.

Secondly, another analytic framework is put forward that detects and describes dynamic equilibria, while assigning to them general properties that must hold for a variety of adaptive networks. Modeling a single node's evolution in state and connections as a random walk, the ergodic properties of the network process are used to extract node-ensemble statistics from the node's long-term behavior. These statistical measures are composed of a variety of stationary distributions that are related to one another through simple transformations. Applying this fully self-sufficient framework, the dynamic equilibria of three different flavors of the adaptive contact process are subsequently described and compared.

Lastly, an asymmetric variant of the coevolutionary voter model is motivated and proposed, and as for the adaptive contact process, a low-dimensional description is given. In a parameter region where a dynamic equilibrium lets the infinite system display perpetual dynamics, this description can be further reduced to a one-dimensional random walk. For finite system sizes, this allows to analytically characterize longevity of the dynamic equilibrium, with results being compared to the symmetric variant of the process. A nontrivial parameter combination is identified for which, in the low-dimensional description of the process, the asymmetric coevolutionary model emulates symmetric voter dynamics without topological coevolution. This emerging symmetry is partially confirmed for the full system and

subsequently elaborated on. Slightly varying the original asymmetric model, an additional asymptotic regime is shown to occur that coexists with all others and complicates system description.

Resumo

A estrutura das interacções entre os constituintes elementares de um sistema está frequentemente na origem de comportamentos colectivos não triviais. Em redes adaptativas, esta estrutura de interacção evolui a par com a dinâmica que nela assenta, traduzindo uma retroacção que é comum encontrar em vários sistemas complexos. Resultados analíticos sobre os estados assimptóticos destes sistemas são uma peça essencial para a sua compreensão e controlo. O equilíbrio dinâmico é um caso particular de estado assimptótico em que cada nodo da rede adaptativa vai sempre mudando o seu estado e as suas ligações a outros nodos, enquanto que um conjunto de medidas que caracterizam estatisticamente o ensemble dos nodos mantêm valores fixos. Além disso, uma classe muito geral de redes adaptativas apresenta equilíbrios dinâmicos que parecem ser únicos, no sentido em que aqueles valores estacionários não dependem das condições iniciais, quer em termos do estados dos nodos quer em termos da topologia da rede.

Este trabalho incide no estudo do equilíbrio dinâmico de redes adaptativas no contexto particular de dois modelos paradigmáticos de coevolução, mas os principais resultados podem ser facilmente generalizados a outros processos. Na primeira parte, revisita-se e desenvolve-se uma abordagem da variante adaptativa do processo de contacto baseada num modelo de baixa dimensão. Obtem-se uma descrição aproximada do diagrama de fases do sistema e do equilíbrio dinâmico, e identifica-se nessa fase uma combinação de parâmetros para a qual a dinâmica microscópica, que é assimétrica nos estados dos nodos, dá origem a uma simetria entre os dois subconjuntos de nodos. Esta simetria é explicada através da derivação de relações de recorrência para as distribuições de grau, que a prevêem para uma ampla classe de redes adaptativas. Estas relações permitem também gerar analiticamente as distribuições de grau estacionárias de cada subconjunto de nodos a partir de um parâmetro livre.

Na segunda parte, desenvolve-se uma outra abordagem analítica que permite detectar e descrever o equilíbrio dinâmico, a partir de propriedades gerais que se têm que verificar em muitas redes adaptativas. Na base desta abordagem está a descrição do processo estocástico associado à evolução do estado e das ligações de cada nó, e as propriedades ergódicas que permitem obter as estatíticas de ensemble na rede a partir do comportamento a longo termo de um nó. Estas medidas estatísticas podem ser calculadas a partir de várias distribuições estacionárias que se relacionam umas com as outras através de transformações simples. Como aplicação desta abordagem completa, os equilíbrios dinâmicos de três diferentes variantes do processo de contacto adaptativo são descritos e comparados.

Finalmente, motiva-se e propõe-se uma variante assimétrica do *voter model* coevolutivo. A fase activa metastável é tentativamente descrita como uma *random walk* ao longo de uma variedade lenta, à semelhança do que foi feito na literatura

para o modelo simétrico, e os resultados para os dois casos são comparados. É identificada uma combinação de parâmetros particular para a qual este modelo assimétrico emula o modelo simétrico em rede fixa, o que é mais um exemplo da simetria emergente prevista pelas relações de recorrência estabelecidas na primeira parte. Considera-se ainda uma outra variante assimétrica, mais complexa, do *voter model* co-evolutivo, que apresenta um diagrama de fases essencialmente diferente, e cuja descrição se mostra requerer novas abordagens.

Contents

Glossary

BR	blind rewiring
CST	composite stage transition
DD	(joint) degree distribution
DE	dynamic equilibrium
ER	Erdős-Rényi
ICD	distribution in initial coordinates / in (joint) degrees
MC	Monte-Carlo
MR	media-driven rewiring
NC	node cycle
ODE	ordinary differential equation
PA	pair approximation
PDE	partial differential equation
RW	random walk
SIS	Susceptible-Infected-Susceptible
SR	selective rewiring

1 INTRODUCTION

1.1 Understanding complex systems

In the past centuries, science has replaced narcissistic narratives about the origin of man [1], his place in the cosmos [2, 3] and his self-determination [4]. More recently, some discoveries additionally challenged the rationalist approach that builds a worldview solely around common sense: Frameworks like quantum mechanics and relativity showed that on extreme spatial and fast time scales, the world is counterintuitive. This is in turn plausible, as perception and comprehension of processes on those extreme scales were not beneficial to our survival.

What does increase our species' fitness is to explore, understand and steer phenomena in our - the intermediate - spatio-temporal domain [5]. Among others, these include geological and meteorological events, immunological and epidemiological processes as well as ecological and social interactions. Is for instance a just society best achieved through a collective push for utopia [6], or will it come as a natural result of numerous individuals each pursuing personal interests [7]?

One could describe aforementioned processes solely based on heuristic principles, but this strategy fails on two grounds. Firstly, extreme events by definition rarely influence the formulation of such principles and are therefore not captured by them [8]. Secondly, intellectual vanity demands for an elegant and coherent *view* on the world - as a consolation prize for aforementioned loss of our special *status* in it. This implies the quest for a minimal set of first principles that accounts for observations at all length and time scales.

Whereas the trailblazers in fundamental physics are mainly looking for these principles, complexity science is the rear guard that maintains coherence in our worldview: It engages in an essentially reductionist research program, showing that and how observed aggregate processes arise from the realm of fundamental physics. In the course of that, it tries to bridge the gap between the different branches of science through stringently relating phenomena at different length and time scales. The idea that complex macroscopic behavior can emerge from simple microscopic rules is indeed a powerful one and crucial to this endeavor. An extremely reduced proof of concept is provided by Conway's game of life, where neighboring cells of

a cellular automaton interact according to a small set of elementary rules, giving rise to an astonishing variety of elaborate patterns [9].

Encouraging results in this research domain were first obtained in the middle of the nineteenth century, when statistical mechanics gave a rigorous justification for the phenomenological laws of thermodynamics. Those laws describe systems in thermodynamic equilibrium, where the absence of driving gradients prohibits net flows in both matter and energy[1]. Complex behavior however usually arises far from thermodynamic equilibrium in so-called dissipative systems - open systems that exchange matter and energy with their environment. A unifying framework for the description of such systems has not been established yet [10, 11], but several tools and methods can be used for ad-hoc modeling. Of particular interest in a dissipative system are regimes of uniform long-term behavior - its stationary (or *steady*) states. By definition, the longevity of steady states make them most amenable to study and manipulation.

An aggravating aspect in the description of dissipative systems is that they are almost exclusively nonlinear, i.e. their macroscopic behavior is a nontrivial consequence of their interacting constituents (the output of a linear system on the other hand is just the superposition of the individuals' dynamics). In that regard, the nonlinearity blurs the correspondence between microscopic rules and macroscopic behavior. Consequently, emergent properties in such systems can range from being plausible or at least conceivable to being downright counterintuitive [12], having given rise to the rather vague term *complex systems* as a synonym.

Stochastic modeling

To nonetheless be able to tackle the large set of degrees of freedom in a complex system, one generally needs to identify a far smaller subset sufficient for an understanding of the dynamics of the full system. The neglected degrees of freedom then account for stochasticity in this reduced description, transforming the remaining ones into time-dependent random variables that span the reduced state space. These state variables are usually chosen to yield a Markov process, i.e. a stochastic process whose future behavior only depends on its variables' current values, not their past ones. Assuming the absence of memory in the process simplifies stochastic modeling enormously and, in case the system possesses a countable number of states (that is, discrete state variables), enables one to set up Master equations. These are ordinary differential equations (ODEs) that describe the temporal evolution of the state variables' probability distribution. If $p_l(t)$ is the probability[2] of the system to be in state l at time t, then the Master equation of

[1] This definition applies to system outside critical regimes, that is, away from phase transitions (see below).

[2] In a dynamical context, $p_l(t)$ is often referred to as *probability mass*.

the system is given as

$$\frac{\mathrm{d}}{\mathrm{d}t}p_l(t) = \sum_{l'} \left(W_{ll'}p_{l'} - W_{l'l}p_l\right) . \tag{1.1}$$

Here $W_{ll'} \geq 0$ is the (not necessarily constant) transition rate that mediates the flow of probability mass from state l' to l. Hence, Eq. 1.1 models a stochastic process with a deterministic gain-loss equation for the underlying probability mass in state space, with stochasticity encapsulated in the governing rates.

If in Eq. 1.1, i) jumps between system states are small as quantified by corresponding changes in state variables and ii) the state probability distribution evolves slowly compared to state-variable increments, the Fokker-Planck equation yields an approximate description of the process. This is a partial differential equation (PDE) in - now continuous - state variables, and describes the evolution of the probability distribution by means of its drift and diffusion, i.e. through its first two moments [13]. Although rarely solvable analytically, its PDE character can significantly facilitate modeling in comparison with Eq. 1.1. Alternatively, stochasticity can be dealt with heuristically in stochastic differential equations known as Langevin equations. There, the neglected degrees of freedom constitute a stochastic process in the state variables, which is represented by a noise term and added to known evolution equations of averaged (continuous) state variables. In rare circumstances however, the Master equation can be solved exactly, so that then a full probabilistic account of the system is given.

Dynamical systems theory

For sufficiently large system sizes, stochastic fluctuations become negligible[3]. Then averaged state variables adequately mirror the system state, and their time evolution is given by ODEs obtained from the Master equation. This further reduces the complexity of the system description, and the tools of dynamical systems theory [15] can be applied to explore dynamics. The averaged state variables x_1, x_2, ..., x_n obviously are continuous in the thermodynamic limit, with the state space they span now being referred to as phase space. With $\mathbf{x} \equiv (x_1, x_2, ..., x_n)$, the time evolution of the dynamical system can then be written as

$$\frac{\mathrm{d}\mathbf{x}}{\mathrm{d}t} \equiv \dot{\mathbf{x}} = F(\mathbf{x}) , \tag{1.2}$$

where $F \equiv (F_1(x_1, x_2, ..., x_n), ..., F_n(x_1, x_2, ..., x_n))$ is a n-component function.

The long-term behavior of Eq. 1.2 is of particular interest: Parameter regions that yield qualitatively similar asymptotic regimes are identified as system phases

[3]Note that for some systems, this so-called thermodynamic limit does not exist [14].

and allow for a classification of the plethora of dynamical systems. Consequently, asymptotic regimes are an essential characteristic and formalized through the concept of attractors, which loosely speaking are regions of phase space to which nearby trajectories converge. More precisely, an attractor is a closed subset A of phase space so that

1. A evolves into itself - every trajectory $\mathbf{x}(t)$ starting in A remains in A.
2. There exists an open subset U of phase space that contains A, and that if $\mathbf{x}(0) \in U$, then $\mathbf{x}(t)$ converges to A.
3. No proper subset of A satisfies both 1) and 2).

All subsets meeting criterion 1) are called invariant sets, whereas the basin of attraction of an attractor is defined as the largest set U in 2).

The simplest and a very common invariant set is the fixed point, where A is just a single point and associated with a steady state in the full system. To determine whether a given fixed point $\mathbf{x}^*$ actually is an attractor, its stability - that is, the behavior of nearby trajectories - needs to be investigated. One usually considers a small deviation $\delta\mathbf{x}$ from $\mathbf{x}^*$ and linearizes its time evolution according to

$$\frac{\mathrm{d}}{\mathrm{d}t}\delta\mathbf{x} = J(\mathbf{x}^*)\delta\mathbf{x}\,. \tag{1.3}$$

Here $J(\mathbf{x}^*)$ is called the Jacobian at $\mathbf{x}^*$, and is a $n \times n$ matrix with real entries $J_{ij}(\mathbf{x}^*) = \partial F_i(\mathbf{x})/\partial x_j|_{\mathbf{x}^*}$. The Hartman-Grobman theorem [16, 17] then states that the linearized system in Eq. 1.3 captures the qualitative behavior of the nonlinear system in Eq. 1.2 in the vicinity of $\mathbf{x}'$ if that fixed point is hyperbolic, that is, if all of the eigenvalues of $J(\mathbf{x}^*)$ have a nonzero real part. If that is the case, the fixed point is stable and an attractor if all of the real parts are negative (as then small perturbations $\delta\mathbf{x}$ decay [15]), and unstable otherwise (repelling nearby trajectories). With this at hand, model parameters can be identified at which local bifurcations occur and a given fixed point becomes non-hyperbolic. If accompanied by a change of the fixed point's stability, a phase transition is triggered, locally changing the qualitative asymptotic behavior of the system[4].

Stable fixed points capture steady states in dissipative systems and will thus be of prime interest in this work. Another prominent example of an attractor is the limit cycle: It yields oscillatory dynamics, as the aforementioned subset A is a closed trajectory that is isolated, i.e. there is no other closed trajectory arbitrarily close to A. In general, attractors can display much more convoluted geometrical shapes, as can their basins of attraction [18].

[4]Global bifurcations on the other hand are changes of phase space topology that are not confined to the neighborhood of a given fixed point [18].

Achieving conceptual shortcuts

As indicated above, the steady states in complex systems can be modeled through stationary stochastic processes. These are stochastic processes for which all moments of the underlying probability distribution in system states do not depend on time. Consequently, the probability distribution itself - as obtained through different realizations of the same process - is time-independent. A stationary stochastic process is then called ergodic if the same distribution arises through a long-term sampling of a *single* realization of the process. This conveniently eliminates the need for sampling different realizations of a given system, so that its stochastic properties can be fully investigated by long-term observation of the often only realization there is. Considerations on the particular system presented in Chapters 3 to 5 are based on that property.

Another aspect that enhances the understanding of some stochastic processes concerns their transient regimes, more specifically system behavior outside a given steady state. In the deterministic description through Eq. 1.2, this steady state could be given by a non-hyperbolic fixed point $\mathbf{x}^*$ whose Jacobian in the linearized system of Eq. 1.3 moreover contains at least one eigenvalue that is *precisely* zero. The corresponding eigenvectors span the slow subspace of $\mathbf{x}^*$, and the set of trajectories in the nonlinear system that are tangential to the slow subspace of $\mathbf{x}^*$ is called slow manifold. Along the latter, the system evolves relatively slowly compared to fast variables that quickly relax to the manifold. The ensuing fast-slow dynamics allow for the elimination of the fast degrees of freedom, confining system description to the slow manifold and simplifying modeling even further [19]. In the following however, the definition of a slow manifold is widened to *any* set of trajectories that the system quickly relaxes to and then slowly proceeds along towards an attracting fixed point. This is for instance the case if the eigenvalues of the respective Jacobian can be grouped into two subsets, each consisting of real parts of similar magnitude, but differing vastly from the ones in the other set. For the system that will be dealt with in Chapter 6, the occurence of a slow manifold is used to model the stochastic transition from one steady state to another.

A complementary approach to facilitate the understanding of complex systems was offered by the advent of computers. Not only is analytic insight enhanced through symbolic computation with speeds vastly superior to the human mind [20], but, in case the system in question is analytically intractable, sophisticated approximations can be obtained through quick implementations of numerical recipes. It has furthermore become feasible to directly simulate dynamics with a large number of degrees of freedom, letting one explore and manipulate full systems *in silico*. In the case of stochastic systems, the probability distribution of system states can be sampled through individual-based Monte-Carlo (MC) simulations. There a single realization of the full system is obtained through iterated realizations of elementary stochastic processes with the help of random (or pseudorandom)

number generators (such as [21]). It follows that computation can guide the modeler's intuition, test analytic approaches as well as uncover previously unknown dynamical regimes essential to the understanding of a given system. Hence it can, right next to theory and experiment[5], be considered the third pillar complexity science rests on [11]. The majority of analytical results obtained in this work will be verified by means of MC simulations, which are considered implementations of the full system modeled.

1.2 Collective dynamics with structured interactions

Complex networks

A variety of complex systems consist of an agglomeration of agents that engage in collective dynamics. The simplest models of collective dynamics replace interactions between agents with a mean field that is computed as the effective interaction of the average constituent with the rest of the system. In many instances, the system departs from this homogeneous-mixing assumption in a twofold way: Not everyone interacts with everybody else, and the ensuing sparse number of interactions is not evenly distributed among the system's agents. In the past two decades, complex networks - multiple agents (nodes) engaging in structured interactions (links connecting nodes) - have become a prominent paradigm in describing collective dynamics [22, 23, 24, 25]. With nodes being assigned a (countable or uncountable) set of possible states, the network provides the topological background for the dynamics acting on node states. In the following, *graph* will be used as a synonym when referring to purely topological aspects of a network.

A graph can be represented by its adjacency matrix, whose entries A_{ij} are 1 if nodes i and j are connected, and 0 otherwise. The graph is connected if every node can be reached from every other, and features a giant component if there exists a connected subgraph consisting of a node fraction that does not vanish in the thermodynamic limit. Links, triplets (three nodes joined by two links) and higher-order network motifs are classified according to the node states they connect, and their per-capita numbers are averages that offer a coarse-grained understanding of network structure.

While this understanding can be widened through a variety of other averages (see [23] for a review), this work focuses on distributions that comprehensively describe a network and dynamical processes running on it. With a node's degree being its

[5]Which itself recently gained new momentum under the banner of *big data*.

number of connections to other nodes, the degree distribution (DD) is the probability distribution of degrees over the whole node ensemble. To construct an Erdős-Rényi (ER) graph of N nodes and mean degree $\langle k \rangle$, $N \cdot \langle k \rangle / 2$ randomly selected node pairs are linked, so that a Poissonian DD of the form $P(k) = \langle k \rangle^k \cdot e^{-\langle k \rangle}/k!$ ensues [26]. The ER graph serves as a null model to investigate degree correlations in other networks, and will thus be used as a initial network configuration for the majority of MC simulations performed in this work. Other standard topologies include i) the regular random graph that constrains an ER graph to feature the same degree for every node ii) the small-world network that interpolates between an ER graph and regular random graph through randomly rewiring each link in the latter with a given probability [27] iii) the Barabási-Albert graph in which nodes are linked through a preferential attachment rule, resulting in a scale-free degree distribution $P(k) \sim k^{-3}$ for sufficiently large degrees [28].

The concept of DDs can be extended to describe the topology of a network with consideration of its dynamical state: In a network with n possible node states, the joint degree $(k_1, k_2, ..., k_n)$ of a node is the set of numbers k_j of its connections to nodes of type $j \in \{1, 2, ..., n\}$, so that the joint-degree distribution yields ensemble statistics on the state composition of a node's neighborhood. Moreover, each node subensemble - defined as the set of nodes with the same state - can be assigned its own DD, describing state-specific connectivity in the network. Apart from DDs, several other distributions that also capture stochastic network dynamics will be introduced and computed in Chapters 3 and 4.

Adaptive networks

Many instances of collective dynamics with structured interactions are coevolutionary, in the sense that the dynamics of node states and linking structure are coupled [29, 30]. This coevolution is formalized in the field of adaptive networks and has been the subject of abundant literature, capturing such diverse phenomena as the emergence of cooperation [31, 32, 33, 34, 35], opinion formation [36, 37, 38, 39], disease spreading [40, 41, 42, 43], speciation [44, 45] as well as traffic and communication flows [46, 47, 48]. While some contributions explore the respective phenomenology with individual-based simulations [32, 33, 49, 50], others also focus on providing explanatory frameworks for observed dynamics [31, 34, 38, 42, 43, 51, 52].

Like for many dynamical systems, the long-term behavior is an important characteristic of adaptive networks and can usually be assessed by low-dimensional ODE models. Frozen states are classified according to how dynamics come to a halt: At absorbing consensus, a single node state is adopted globally, while updating relies on node-state heterogeneity and thus ceases. The absorbing fragmented state on the other hand features node-state heterogeneity, but lacks active links that con-

nect different nodes types and drive network dynamics. Instead, all links are inert, i.e. do not carry dynamics. Transitions to and between those absorbing states in adaptive networks have been dealt with using mean-field approximations or small perturbations of the fragmented state [38, 41, 53, 54, 55].

Cyclic processes on adaptive networks, that is, nodes going through a cyclic sequence of states while changing their connections, may yield adaptive networks displaying perpetual node-state and link dynamics [29]. Those processes correspond to the active phase of the system, as opposed to the frozen phase where the system reaches a static equilibrium. Node-state and link dynamics in the active phase of adaptive networks can be highly complex [56, 57], and stationary (as well as oscillatory) steady states have been shown to occur for a variety of frameworks both in MC simulations and in their approximate mean field descriptions [30]. For such networks in dynamic equilibrium (DE), nodes undergo permanent state and degree evolution, while global statistics characterizing ensemble dynamics and network topology settle down to a steady state. In many instances, the shape of these dynamic equilibra does not depend on initial conditions - neither in node states nor in network topology - but just on parameters governing the coevolutionary dynamics.

Many adaptive networks are particular realizations of nonequilibrium systems, and describing network statistics in DE is essential to understanding the relation between dynamics and network structure, as well as to applying these ideas to real-world examples. To describe the latter, one usually considers finite-size networks in the active phase, where stochastic fluctuations induce transitions from a prolonged active to a frozen state. Describing such a metastable regime is known as a *first-passage problem* [58], and the scaling of system size with several relevant averages can be uncovered.

Understanding the emergence of DEs, as well as analytically detecting and describing them, will be the core theme of Chapters 2 to 5, whereas metastability in adaptive networks will be focused on in Chapters 6 and 7. Unless indicated otherwise, all following chapters will consist of original research based on two paradigmatic models in the study of collective dynamics: The contact process (presented in Chapter 2) and the voter model (outlined in Chapter 6).

2 THE ADAPTIVE CONTACT PROCESS

As an example for simple cyclic dynamics, the contact process on an adaptive network is proposed in [42] to model the spreading of a disease in a population without immunity, but with disease awareness. The traditional contact process is also called Susceptible-Infected-Susceptible (SIS) model, owing to the cyclic sequence of node states it imposes: Infected nodes (*I-nodes* of fraction $[I]$ of the total node number N) turn adjacent susceptible nodes (*S-nodes* of fraction $[S] = (1 - [I])$) into I-nodes with rate p, while themselve recovering to S-nodes with rate r. In the adaptive SIS model (interchangeably used with *adaptive contact process* in the following), S-nodes additionally evade infection by retracting links to infected neighbors with rate w and rewiring them to randomly selected S-nodes. This rewiring mechanism conserves the total number of links and ties the network's topological evolution to its node-state dynamics, yielding an adaptive network with constant mean degree $\langle k \rangle$. In these coevolutionary dynamics[1], infection and rewiring occur along active links that connect S- and I-nodes, whereas recovery acts on I-nodes regardless of their neighborhood. Inert links that connect nodes of same state have no immediate impact on dynamics, but become active as soon as one of their end nodes changes state.

The SIS model is just one in a wide range of compartmental epidemic models, where a population is divided into compartments that mirror different infection states. The spreading of the respective disease is then described through transitions between these compartments, and the model named after the sequence of states an individual goes through in that process. If recovery in the traditional SIS model happens on a significantly slower time scale than infection, the onset of spreading is well-captured by the acyclic Susceptible-Infected model [59]. In case a disease confers permanent immunity to its carrier, Susceptible-Infected-Recovered models are appropriate acyclic frameworks to resort to. To account for the in part elaborate patterns of host infection, the spreading of many diseases is described by introducing additional compartments or permutating node-state sequences.

[1] One usually prohibits self- and double-connections of nodes as dynamics can mostly be expressed without them.

2.1 The model in the pair approximation

The time evolution of both node fractions and the various link densities $[AB]$ (the per-capita number of AB-links connecting A- with B-nodes, $A, B \in \{S, I\}$) are approximately captured by the pairwise framework proposed in [42]. This pair approximation (PA) is a subclass of moment expansions, where generally a set of evolution equations is compiled for the per-capita density of network motifs (also called *moments*). In the particular case of the PA, only node and link densities are tracked, while at the same time approximating higher-order motif densities needed to describe their evolution. This moment closure thus caps the hierarchy of motif equations at the level of links, yielding a coarse-grained description of the network process. The triplet density $[ISI]$ - the per-capita number of triplets with a central S-node connected to two I-nodes - is then for instance approximated as

$$[ISI] \approx \eta \frac{[SI]^2}{2[S]}\,, \tag{2.1}$$

with the parameter η being determined by the first two moments of the underlying network's DD [54, 60]. Hence in the PA, no further node correlations are assumed beyond those implicitly given by η and explicitly given by the pair densities.

The biased rewiring rule introduced above enforces a strict degree gain among S-nodes (the *S-ensemble*), whereas I-nodes (making up the *I-ensemble* of nodes) can only lose neighbors through being rewired from. Hence for sufficiently high rewiring rates, the full system explores large degree ranges, so that a choice of η representing a wide DD is desirable (see further below). It has been shown that with $\eta = 1$, capturing the Poissonian DD of an ER graph, the respective moment closure maintains validity for networks with even broader DDs [42, 54]. With that choice of η and the network's constant link density $\langle k\rangle/2 = ([SS] + [SI] + [II])$, the PA of the adaptive contact process yields [42]

$$\begin{aligned}
\frac{d[I]}{dt} &= p[SI] - r[I] \\
\frac{d[II]}{dt} &= p[SI]\left(\frac{[SI]}{[S]} + 1\right) - 2r[II] \\
\frac{d[SS]}{dt} &= [SI]\left((w + r) - 2p\frac{[SS]}{[S]}\right)\,.
\end{aligned} \tag{2.2}$$

The constant mean degree $\langle k\rangle$ thus closes the system of ODEs and becomes an additional system parameter that does not characterize dynamics, but its topological background. In the following, mean degrees with $\langle k\rangle < 1$ are not considered, as a corresponding ER graph would not yield any giant component [26]. The result would be an all-encompassing frozen phase for the full system, as a giant component obviously is a necessary prerequisite for sustaining any node dynamics that rely on active links.

With

$$\langle k_{\mathrm{S}} \rangle = \frac{2[SS] + [SI]}{[S]}$$
$$\langle k_{\mathrm{I}} \rangle = \frac{2[II] + [SI]}{[I]} \tag{2.3}$$

for the mean degrees of the S- and I-ensemble, respectively, Eqs. 2.2 also offer a coarse-grained view of coevolving network topology. In the following, the long-term limit of Eqs. 2.2 is investigated, with the bracket notation for motif densities and mean degrees denoting their steady-state values.

The phase diagram

To investigate the asymptotic behavior of the system, time can be rescaled by setting $(w + p + r) = 1$ without loss of generality. The model can then be reparameterized through

$$w = \omega$$
$$p = (1 - \omega)\rho$$
$$r = (1 - \omega)(1 - \rho) \tag{2.4}$$

with just two parameters $\omega, \rho \in [0, 1]$ (conversely $\omega = w$ and $\rho = p/(p + r)$). Parameter space is hence reduced and compactified, so that compilation and exploration of the phase diagram are facilitated. If in the following being subject of considerations, the phase diagram will be referred to through this reparametrization, whereas the more intuitive initial choice of parameters is used to convey general properties of the system in dynamic equilibrium.

The structure of Eqs. 2.2 allows for a largely analytic steady-state analysis, with its principal steps demonstrated in Appendix A.1. It is found that the adaptive SIS model yields a frozen phase with $[I] = 0$ when rewiring or recovery occur too frequently for the disease to persist. In its active phase, this simple coevolutionary process already features a rich dynamical behavior. The dominant regime possesses a DE (referred to as the simple endemic phase) also found in classic SIS dynamics, where the disease persists in a steady nonzero fraction of the population. Large-enough rewiring rates additionally yield small parameter regions of simple bistable and oscillatory bistable regimes [42], where a stable absorbing state $[I] = 0$ coexists with either a stable DE or a stable limit cycle (Fig. 2.1).

The onset of the simple endemic phase generally depends on the particular choice of η [62]. For $\eta = 1$, this *epidemic threshold* is approximated in [42], and in Appendix A.1 exactly calculated as

$$\frac{w}{w + p + r} < \frac{p\langle k \rangle - r}{p\left(\langle k \rangle + 1\right)}\,. \tag{2.5}$$

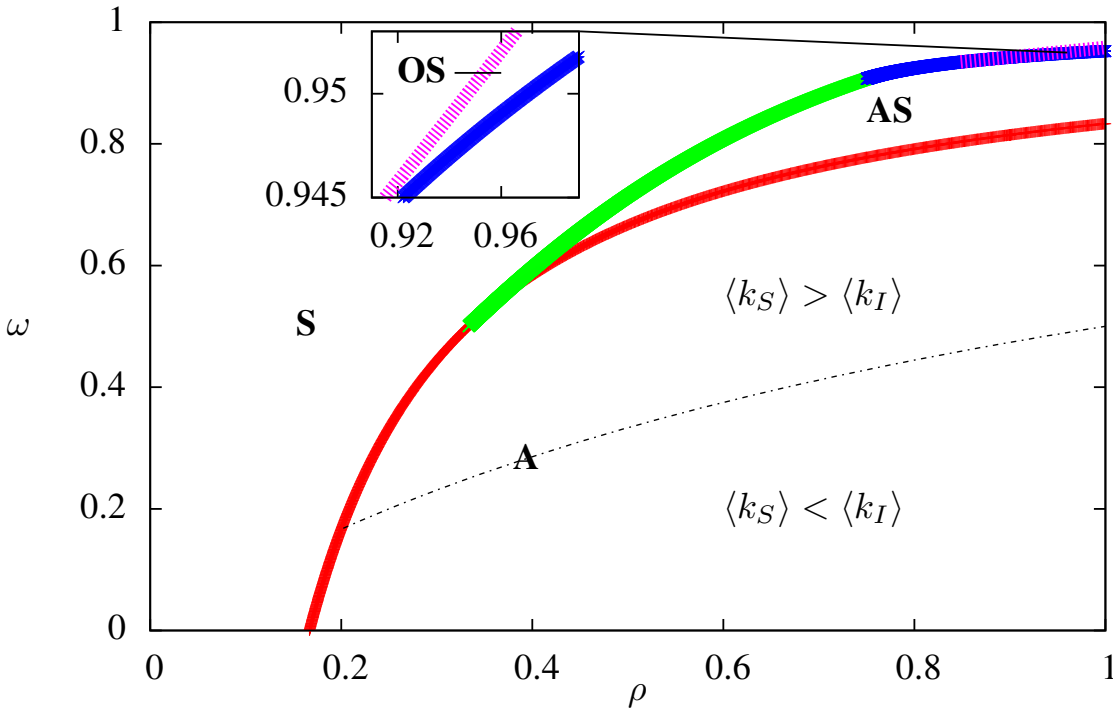

Figure 2.1: Phase diagram of the PA of the adaptive SIS model. Transcritical bifurcations (red line), fold bifurcations (green line), Andronov-Hopf bifurcations (blue line) and cycle-fold bifurcations (purple line) mark the following phases: Frozen phase with $[S] = 1$ (**S**), simple endemic phase (**A**), simple bistable phase (**AS**), oscillatory bistable phase (**OS**, inset). The dotted line represents $\langle k_S \rangle = \langle k_I \rangle$ in DE. Mean degree $\langle k \rangle = 5$, compiled with [61].

Consequently, rewiring increases the epidemic threshold from its classically-given value $p/r = 1/\langle k \rangle$ in degree-homogeneous static networks. The latter value is a special case of the fraction of the first and second moment of the static network's DD, and thus may be even zero for sufficiently heterogeneous static graphs [63]. Generally, the conditions for the existence of an epidemic threshold have been the subject of much debate even for static networks. While just dealing with the network's *annealed* structure (solely focusing on degree distributions and disregarding dynamical or topological correlations) conceivably delivers different results than considering the *quenched* structure of real networks (i.e. their actual adjacency matrix), even frameworks all pursuing the latter, more sophisticated route yield conflicting predictions (see [64] and references therein).

For Eqs. 2.2, it can furthermore be shown that, for any given $\langle k \rangle > 1$,

$$w > p + r \tag{2.6}$$

is a necessary condition for the advent of bistability or an oscillatory regime (Appendix A.1). Hence a qualitative departure from classic SIS dynamics without

rewiring is only possible in the pairwise framework if topology change outweighs disease dynamics.

From Eqs. 2.3 and steady-state motif densities in Appendix A.1 it follows that in the active phase,

$$\langle k_{\mathrm{S}} \rangle - \langle k_{\mathrm{I}} \rangle = \frac{w}{p} - 1 \tag{2.7}$$

regardless of imposed $\langle k \rangle > 1$. Therefore in DE, the S-ensemble will have a larger mean degree than the I-nodes if and only if rewiring outperforms infection (see also [65]). This may seem counterintuitive, as rewiring retracts links from I-nodes and increases connectivity among S-nodes. But this topologically induced bias in subensemble mean degrees can be offset dynamically by the rapid infection of resulting high-degree S-nodes.

Both Eqs. 2.6 and 2.7 are simple balance relations between the rewiring rate on the one hand and parameters governing classic SIS dynamics on the other, and are in particular independent of any chosen $\langle k \rangle > 1$. The advent of bistability in the phase diagram as well as of the topological symmetry of the two steady-state subensembles are hence determined by the coevolutionary dynamics alone, not by the underlying network's connectivity.

According to Eq. 2.5, the line of transcritical bifurcations in the phase diagram is given by

$$\omega = 1 - \frac{1}{\rho(\langle k \rangle + 1)} \tag{2.8}$$

and marks the onset of the simple endemic phase (Fig. 2.1). Moreover, Eq. 2.7 predicts that this regime is further partitioned by $\omega = \rho/(\rho+1)$into two parameter regions where either the S- or the I-ensemble in DE displays a mean degree larger than $\langle k \rangle$. As obtained from Eq. 2.6, a cusp bifurcation gives rise to the simple bistable phase at exactly $\omega = 1/2$, and a generalized Hopf bifurcation yields the onset of the oscillatory bistable phase; both codimension-two bifurcations mark triple points in the phase diagram. At a point consistent with a Bogdanov-Takens bifurcation, the simple bistable regime switches from being bordered by fold bifurcations to being bounded by Andronov-Hopf bifurcations (see [18] for a general treatment of local and global bifurcations). All three regimes of the active phase are widened as $\langle k \rangle$ increases, as an increased connectivity fosters transmission and hinders network fragmentation through rewiring.

Additional DE measures

The link densities introduced above encode node-state correlations in the network: If a fraction $[I]$ of randomly chosen nodes are primed as I-nodes and the remaining fraction $[S]$ as S-nodes, then in the thermodynamic limit a randomly picked link i) features two S-nodes with probability $[S]^2$ ii) consists of two I-nodes with

probability $[I]^2$ iii) is an active link with the remaining probability $2 \cdot [S] \cdot [I]$. It follows that in a network of link density $\langle k \rangle / 2$ and without node-state correlations, $[SS] = [S]^2 \cdot \langle k \rangle / 2$, $[II] = [I]^2 \cdot \langle k \rangle / 2$ and $[SI] = [S] \cdot [I] \cdot \langle k \rangle$ hold[2].

A steady-state analysis of Eqs. 2.2 reveals that only trivial parameter combinations in the active phase fulfill aforementioned equalities (that is, only for $[I] = 0$), so that node states are always correlated in DE. Since it can be shown for any DE that $[SI] < [S] \cdot [I] \cdot \langle k \rangle$, the rewiring rule induces assortative mixing of node states with node-state clustering ensuing (see Fig. 2.4).

The motif densities used in the pairwise framework also encode average lifetimes of any node and link type of the network. In DE, the average lifetime τ_{S} of a S-node equals the inverse of the mean force of infection exerted on it. This force is in turn given by the infection rate times the average number of infected neighbors of the node, so that

$$\tau_{\mathrm{S}} = \frac{[S]}{p[SI]} = \frac{1}{r} \left(\frac{1}{[I]} - 1 \right) , \tag{2.9}$$

with the second equality stemming from the first of Eqs. 2.2.

In contrast, an active link can vanish in multiple ways: Through recovery of the infected node, or through a breakup induced by rewiring or infection of the susceptible partner. The link's average lifetime τ_{SI} is then determined by considering all three of its decay channels, and consequently

$$\frac{1}{\tau_{\mathrm{SI}}} = r + w + p \left(1 + 2 \frac{[ISI]}{[SI]} \right) \tag{2.10}$$

through similar reasoning as above. Here the bracket term is the mean number of I-nodes the S-node of an active link is connected to. One analogously obtains $\tau_{\mathrm{SS}} = [SS] / (p \cdot [SSI])$ and $\tau_{\mathrm{II}} = 1 / (2 \cdot r)$ for the mean lifetimes of SS- and II-links, respectively, with all motif densities taken from the network in DE. All of these averages can also be obtained from the endemic steady states of Eqs. 2.2, with necessary triplet densities generated through the moment closure.

In Fig. 2.2, selected motif lifetimes in DE are plotted for various rewiring regimes. For MC simulations (described in Sec. 2.2), actual measured lifetimes and lifetimes computed via Eqs. 2.9 and 2.10 through motif densities match perfectly. Using in contrast motif densities computed in the PA via Eqs. 2.1 and 2.2, the approximate nature of the moment closure in the PA becomes apparent: While the lifetimes of SS-links are well-predicted (Fig. 2.2a), those of active links are captured less successfully (Fig. 2.2b). This is because the moment closure for $[ISI]$ is used explicitly in Eq. 2.10, underestimating the actual number of respective triplets for low rewiring and overestimating them for large ω.

[2]The reader shall be reminded that this null model of node-state correlations does not imply zero degree correlations, i.e. does not presuppose any underlying network topology.

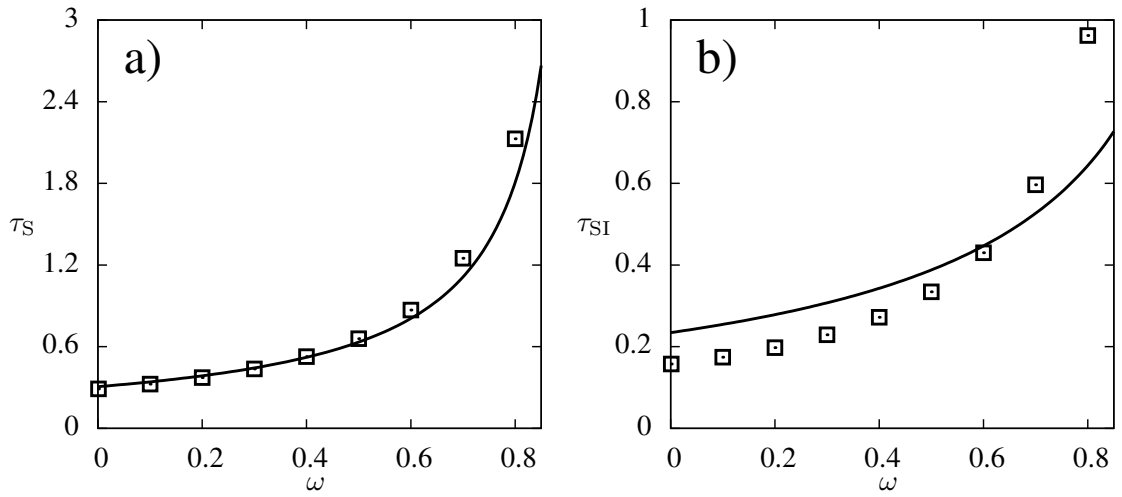

Figure 2.2: Motif lifetimes in DE taken from MC simulations (squares) and computed by the PA (solid lines). Lifetimes computed from MC motif densities exactly match actual lifetimes and are indistinguishable. **a)** Average lifetimes of S-nodes. **b)** Average lifetimes of SI-links. All simulations performed for $\rho = 0.6$ and $\langle k \rangle = 7$ from initial fraction 0.5 of randomly primed I-nodes in ER graph. All graphs recorded at $t = 5000$, with $N = 10^4$ nodes and averaged over 10^3 realizations.

2.2 The model in Monte-Carlo simulations

For individual-based MC simulations carried out in the remainder of this work, the Gillespie algorithm [66] is used. In general, this procedure exactly generates the distributions of the Master equation underlying the system. As mentioned above, the three processes of adaptive SIS act along active links (infection, rewiring) or on I-nodes (recovery). These two motifs are hence also called the reaction channels of the system, with their total number being $N \cdot ([SI] + [I])$. Once the system has been initialized, the algorithm then consists of the following steps that are iterated until either a predefined time limit is reached, or the system is irrevocably depleted of reaction channels:

1. At each time step, compute the number of all reaction channels and weight them with the rate of the respective process, i.e. $w \cdot [SI]$, $p \cdot [SI]$ and $r \cdot [I]$.

2. Randomly select a process with a probability equal to the fraction of its weighted reaction-channel number, e.g. rewiring would be selected for with probability $w \cdot [SI]/((w + p) \cdot [SI] + r \cdot [I])$. Randomly pick one reaction channel of chosen type and manipulate it according to the respective process.

3. Generate another random number and draw the length of the time step from a probability distribution of idle times between two processes. Use it to update system time.

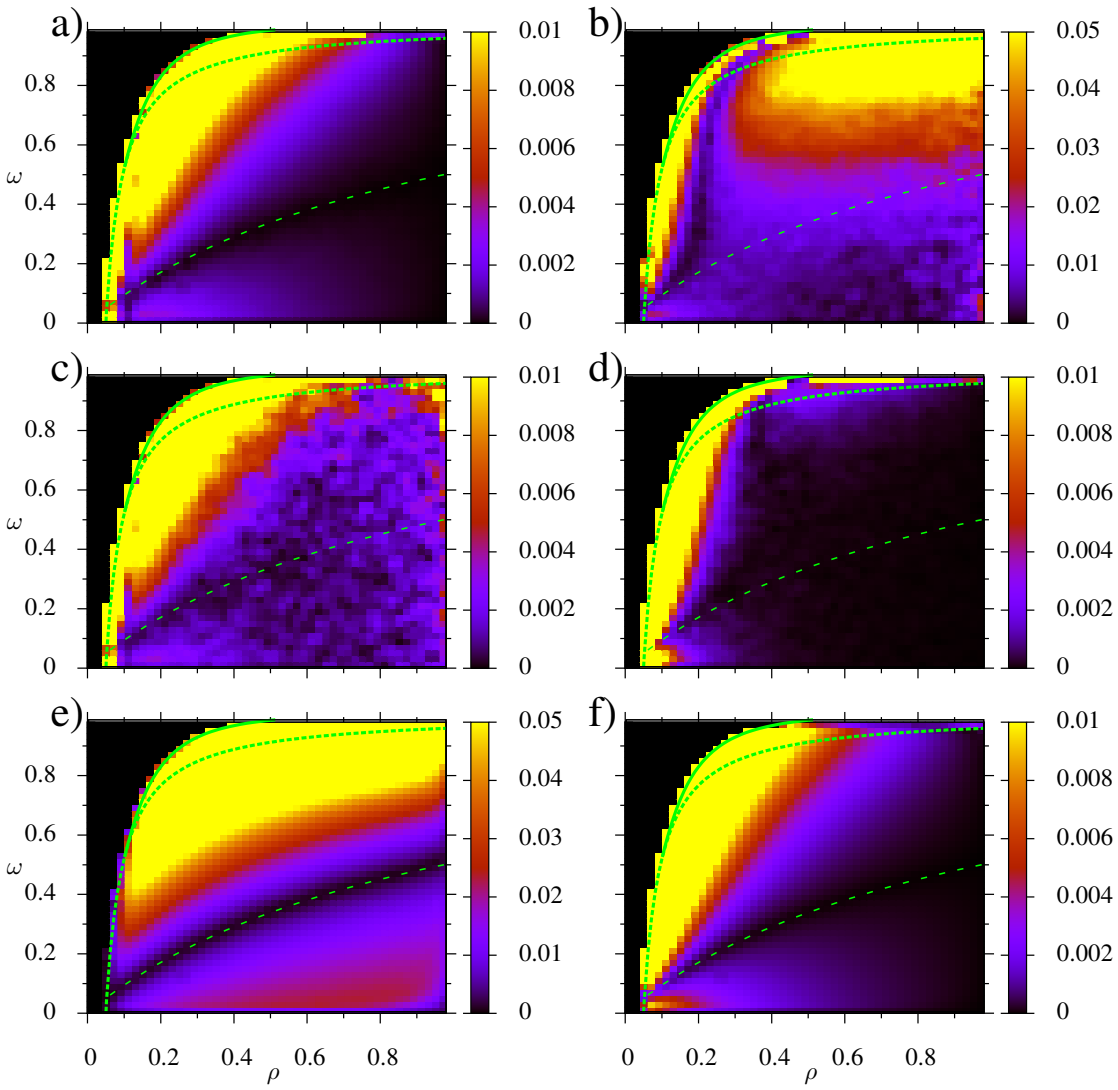

Figure 2.3: Relative error of steady-state motif densities and mean subensemble degrees between PA values and MC simulations, calculated with respect to predicted PA values. Solid lines mark fold bifurcations, dashed lines transcritical bifurcation and dotted lines $\langle k_S \rangle = \langle k_I \rangle$ in DE. **a)** $[I]$ **b)** $[SS]$ **c)** $[SI]$ **d)** $[II]$ **e)** $\langle k_S \rangle$ **f)** $\langle k_I \rangle$. Simulations from initial ER graphs with $N = 10^4$ and $\langle k \rangle = 20$, results recorded at $t = 3000$ and averaged over 10^3 runs.

In [42], the performance of the PA with $\eta = 1$ has been tentatively checked against the full system, with results being in line with the phase diagram Fig. 2.1. Comparing PA results with simulations of the full system, it becomes apparent that Eqs. 2.2 predict steady-state node and link densities rather well (Fig. 2.3). The larger deviations in $[SS]$ close to the transcritical bifurcation are due to the fact that inaccuracies in the moment closure[3] are amplified through the low

[3]For large ω, the moment closure is inaccurate due to longer-range state correlations and $\eta \neq 1$ for the underlying network [54].

number of susceptibles in the steady state for that particular region (Fig. 2.3b). For $w = p$ in the active phase, i.e. for equal mean subensemble degrees according to Eq. 2.7, the PA correctly predicts both the steady-state $[I]$ (Fig. 2.3a) and (equal) mean degrees of both subensembles (Fig. 2.3e-f), a phenomenon elaborated on in Sec. 2.3. In these and all further MC simulations, ER graphs mostly are chosen as initial topologies, as they conform with the choice of $\eta = 1$ in the PA (but see Fig. 2.5 for an exception).

Given a stable limit cycle in the PA for model parameters $(\omega, \rho, \langle k \rangle)$, it can be cumbersome to manually place initial conditions of the full system inside its basin of attraction. Instead, the full systen can be pumped into the oscillatory regime by the following procedure: Already fixing ρ and $\langle k \rangle$, choose a $\omega^* < \omega$ small enough to place the system inside the simple endemic phase (see Fig. 2.1). Now i) run a short simulational burst, making sure it yields a network in DE ii) set $\omega^* = (\omega^* + \Delta\omega)$ with $\Delta\omega \ll 1$ iii) repeat i)-ii) until $\omega^* = \omega$. This iteration relies a) on the fact that for active regimes of the PA, proximity in parameter space translates into respective DEs lying in each other's basins of attraction and b) on the assumption that a) can be generalized to networks in DE (made plausible further below).

Observing a steady-state topology

Individual-based simulations in the stationary active phase reveal that beyond the constant motif densities of the PA framework, network topology itself settles down to a dynamic equilibrium. Snapshots of the steady-state network convey a first impression of the system in DE: At low rewiring rates, S-nodes are homogeneously embedded in a sea of I-nodes with $\langle k_\mathrm{S} \rangle < \langle k_\mathrm{I} \rangle$ (Fig. 2.4b). For larger ω in the simple endemic phase, the S-ensemble increases its connectivity according to Eq. 2.7 (Fig. 2.4d), while for even higher rewiring rates in the bistable phase, a dense cluster of S-nodes is only loosely tied to an I-ensemble with sparse connectivity (Fig. 2.4f). Increasing ω even further, network fragmentation aggravates, diminishing the size of the sole giant component. For sufficiently large ω, active links are faster rewired than created by node-state dynamics, so that the system eventually ends up in the frozen phase with $[I] = 0$.

The steady-state topology that is produced and maintained through coevolving links and node states is characterized by various degree distributions. These DDs describe not only the global network, but also the subsets of S- and I-nodes, and are denoted as $P(k)$, $P_\mathrm{S}(k)$ and $P_\mathrm{I}(k)$, respectively(Figs. 2.4a, 2.4c and 2.4e). The DE extends to motif densities of arbitrarily high-order[4] as verified by MC simulations, and thus seems to be comprehensive.

[4]Within the bounds set by finite network sizes and feasibility in motif detection.

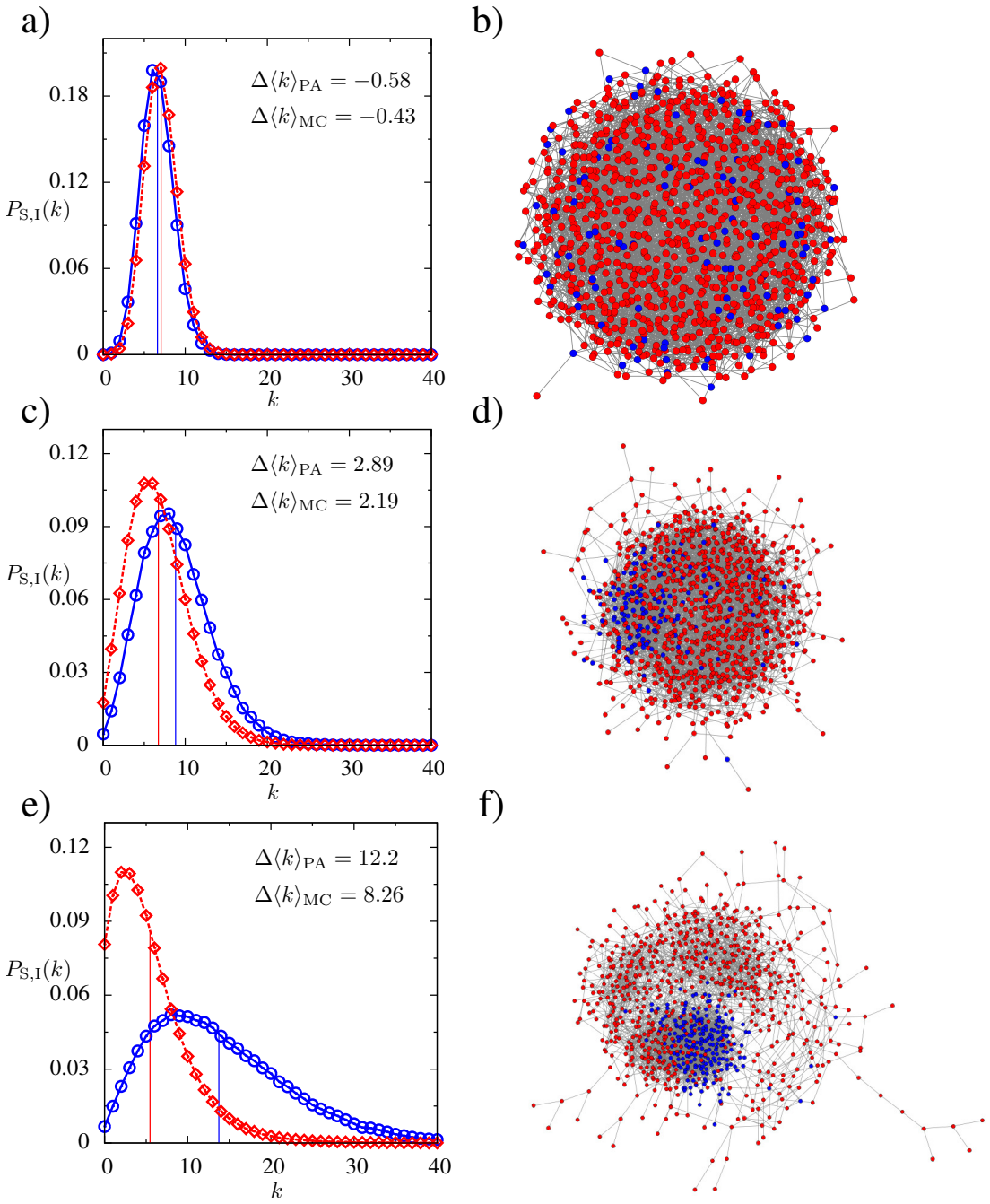

Figure 2.4: Adaptive SIS network in DE. Left column: Subensemble DDs of S-nodes (blue circles) and I-nodes (red diamonds). Vertical lines mark respective subensemble mean degrees, with $(\langle k_{\rm S}\rangle - \langle k_{\rm I}\rangle)$ taken from MC simulations ($\Delta\langle k\rangle_{\rm MC}$) and computed via Eq. 2.7 ($\Delta\langle k\rangle_{\rm PA}$). Right column: Snapshots of giant component with S-nodes (blue) and I-nodes (red). **a)-b)** $\omega = 0.1$ in simple endemic phase. **c)-d)** $\omega = 0.7$ in simple endemic phase. **e)-f)** $\omega = 0.88$ in bistable regime. All simulations with $\langle k\rangle = 7$, $\rho = 0.6$, from initial fraction 0.9 of randomly primed I-nodes on ER graph and ended at $t = 5000$. Simulations in a),c) and e) with $N = 10^4$ and averaged over 10^3 runs. Snapshots b), d) and f) taken for $N = 10^3$ and visualized with [67].

Moreover, for every DE reached in MC simulations, the steady-state topology is solely determined by model parameters, irrespective of initial network configurations (Fig. 2.5). This does however not rule out that for fixed model parameters close to the bistable or frozen phase of the PA, varying the initial topology can drive the system to the frozen state: Different η in Eqs. 2.2 distort phase boundaries or basins of attraction of competing fixed points, so that a DE reached for $\eta = 1$ may be unattainable for other values. From Eq. 2.7, it follows that in DE,

$$\langle k_\mathrm{S} \rangle = \langle k_\mathrm{I} \rangle = \langle k \rangle \Leftrightarrow w = p\,. \tag{2.11}$$

Remarkably, not only the average degrees of the two subensembles, but also their DDs in the full system coincide (Fig. 2.5b). Monte-Carlo simulations reveal that this equality occurs for rewiring rates slightly lower than p, but for all practical purposes, it can be assumed to hold at $w = p$ throughout parameter space. This symmetry however does not extend to the other subensemble distributions introduced in Sec. 3.2.

At $w = p$, steady-state distributions of subensemble degrees k are furthermore all given by $\langle k_\mathrm{S,I} \rangle^k \cdot e^{-\langle k_\mathrm{S,I} \rangle}/k!$ and thus are of the same type that also ER graphs feature [26]. While both node subensembles hence yield the same Poissonian DD along the dotted line in Fig. 2.1, the balance of subensemble *sizes* depends on the particular parameter values on the line, as $[I]$ in DE increases with p (Appendix A.1). The Poissonian shape of subensemble DDs combined with $\langle k_\mathrm{S} \rangle = \langle k_\mathrm{I} \rangle$ implies that the overall $P(k)$ is Poissonian for any fraction of ensemble sizes, too.

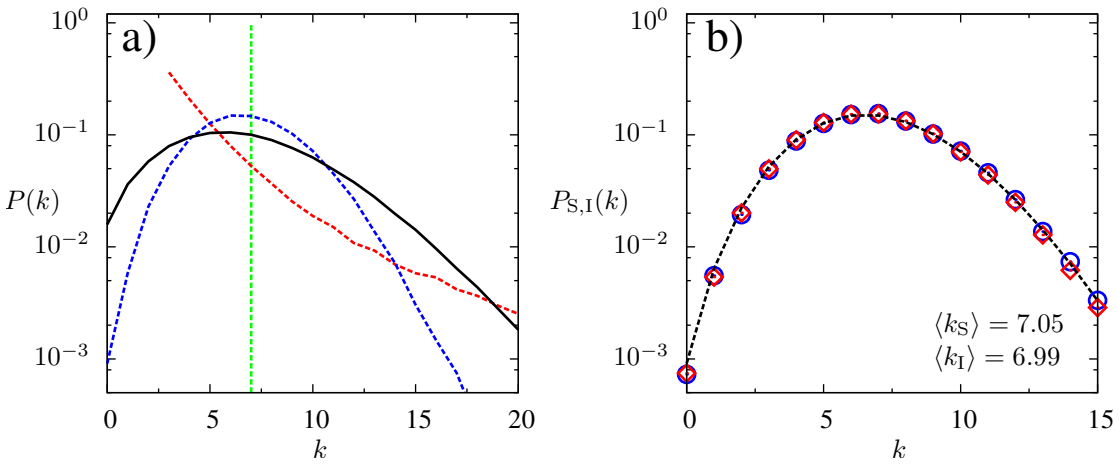

Figure 2.5: Uniqueness of and symmetry in DE in MC simulations. **a)** DDs of initial Barabási-Albert graph (dashed red line), ER graph (dashed blue line), regular random graph (dashed green bar), all settling down to the same DE for $\omega = 0.7$ (solid black line). **b)** Subensemble DDs of S-nodes (blue circles) and I-nodes (red diamonds) for $\omega = 0.375$ with mean degrees $\langle k_\mathrm{S,I} \rangle$, starting from regular random graph. The mean degree $\langle k \rangle = 7$ is fed into Poissonian distribution as first moment (dashed black line). All simulations with $\langle k \rangle = 7$ and $\rho = 0.6$ from initial fraction 0.5 of randomly primed I-nodes with $t = 10^3$. All graphs with $N = 10^4$ nodes and averaged over 10^3 realizations.

2.3 Generating degree distributions

Sections 2.1 and 2.2 demonstrated that although the PA is designed to model the time evolution of node-state correlations, it already yields a description of network topology in DE through a variety of averages. Due to the low number of degrees of freedom of the system, this description is necessarily coarse-grained: Nodes and links of same type are considered equivalent, and information about degree heterogeneity is only implicitly incorporated through the choice of η in the moment closure. Through simple considerations on the degree evolution of a SIS adaptive network, it is possible to obtain a more detailed account of steady-state topology, including the observed symmetry at $w = p$.

Recurrence relations

Let $\hat{P}_{\mathrm{A}}(k)$ be the fraction of nodes of state $A \in \{S, I\}$ and degree k in the network. Approximating the fraction of infected (susceptible) neighbors of a S-node (I-node) as $[SI]/([S]\cdot\langle k_{\mathrm{S}}\rangle)$ ($[SI]/([I]\cdot\langle k_{\mathrm{I}}\rangle)$), the degree-evolution equations of the adaptive SIS model are

$$\begin{aligned}\frac{\mathrm{d}\hat{P}_{\mathrm{I}}(k)}{\mathrm{d}t} &= p\frac{[SI]}{[S]\langle k_{\mathrm{S}}\rangle}k\hat{P}_{\mathrm{S}}(k) - r\hat{P}_{\mathrm{I}}(k) + w\frac{[SI]}{[I]\langle k_{\mathrm{I}}\rangle}\left((k+1)\,\hat{P}_{\mathrm{I}}(k+1) - k\hat{P}_{\mathrm{I}}(k)\right)\\ \frac{\mathrm{d}\hat{P}_{\mathrm{S}}(k)}{\mathrm{d}t} &= -p\frac{[SI]}{[S]\langle k_{\mathrm{S}}\rangle}k\hat{P}_{\mathrm{S}}(k) + r\hat{P}_{\mathrm{I}}(k) + \tilde{w}\left(\hat{P}_{\mathrm{S}}(k-1) - \hat{P}_{\mathrm{S}}(k)\right)\,. \end{aligned} \tag{2.12}$$

In both equations, the first, second and third term on the right-hand side describe infection, recovery and rewiring, respectively. In the second equation, the parameter $\tilde{w}$ quantifies the rate at which S-nodes are rewired to by other S-nodes. In a network of size N, there are $[SI]\cdot N$ links to be rewired to $[S]\cdot N$ S-nodes, and thus the rate of degree gain $\tilde{w}$ for a single S-node is $w\cdot[SI]/[S]$. Considering furthermore that $[SI] = r\cdot[I]/p$ in the first of Eqs. 2.2 in steady state, as well as $\hat{P}_{\mathrm{A}}(k) = [A]\cdot P_{\mathrm{A}}(k)$, Eqs. 2.12 in DE can be written as

$$\begin{aligned} 0 &= p\;k\frac{P_{\mathrm{S}}(k)}{\langle k_{\mathrm{S}}\rangle} - P_{\mathrm{I}}(k) + \frac{w}{p\langle k_{\mathrm{I}}\rangle}\left((k+1)\,P_{\mathrm{I}}(k+1) - k\;P_{\mathrm{I}}(k)\right)\\ 0 &= -p\;k\frac{P_{\mathrm{S}}(k)}{\langle k_{\mathrm{S}}\rangle} + P_{\mathrm{I}}(k) - \frac{w}{p}\left(P_{\mathrm{S}}(k-1) - P_{\mathrm{S}}(k)\right)\,. \end{aligned} \tag{2.13}$$

The network's mean degree

$$\langle k\rangle = (1-[I])\langle k_{\mathrm{S}}\rangle + [I]\langle k_{\mathrm{I}}\rangle \tag{2.14}$$

is known, so that for $w \neq 0$, Eqs. 2.13 are recurrence relations for the two subensemble DDs $P_{\mathrm{S,I}}(k)$ with two free parameters, for example $[I]$ and $\langle k_{\mathrm{S}}\rangle$. The

second of Eqs. 2.13 then reads as

$$P_{\mathrm{I}}(0) = \frac{w}{p} P_{\mathrm{S}}(0) \tag{2.15}$$

for $k = 0$, leaving an additional free parameter $P_{\mathrm{S}}(0)$. Apart from being generated by Eqs. 2.13, the two subensemble DDs must be normalized, so that Eqs. 2.13 and the two normalization conditions fully determine $\langle k_{\mathrm{S}} \rangle$ and $P_{\mathrm{S,I}}(k)$. Note that the only remaining free parameter is the steady-state $[I]$, and that the moment-closure assumption has not been resorted to, as the first of Eqs. 2.2 is a balance equation not involving triplet densities. It can furthermore be seen through Eq. 2.15 that $P_{\mathrm{S}}(k)$ and $P_{\mathrm{I}}(k)$ must be different whenever $w \neq p$.

In the case of $w = 0$ and $p \neq 0$, Eqs. 2.13 are not independent and only determine that

$$P_{\mathrm{I}}(k) = k \frac{P_{\mathrm{S}}(k)}{\langle k_{\mathrm{S}} \rangle} \,. \tag{2.16}$$

This seems to leave $P_{\mathrm{S}}(k)$ completely free, but the overall DD $P(k)$ is known and fixed, so that

$$\begin{aligned} P(k) &= (1 - [I]) P_{\mathrm{S}}(k) + [I] P_{\mathrm{I}}(k) \\ &= (1 - [I]) P_{\mathrm{S}}(k) + [I] k \frac{P_{\mathrm{S}}(k)}{\langle k_{\mathrm{S}} \rangle} \\ &= \left((1 - [I]) + k \frac{[I]}{\langle k_{\mathrm{S}} \rangle} \right) P_{\mathrm{S}}(k) \,. \end{aligned} \tag{2.17}$$

The normalization conditions for $P_{\mathrm{S,I}}(k)$, Eqs. 2.16 and 2.17 as well as the free parameter $[I]$ again fully determine $\langle k_{\mathrm{S}} \rangle$ and $P_{\mathrm{S,I}}(k)$.

Relating the moments

Besides recurrence relations for subensemble DDs, useful expressions involving the distributions' moments can be obtained. Multiplying either of Eqs. 2.13 with k and then summing over k yields

$$0 = \frac{\langle k_{\mathrm{S}}^2 \rangle}{\langle k_{\mathrm{S}} \rangle} - \langle k_{\mathrm{I}} \rangle - \frac{w}{p} \,, \tag{2.18}$$

which - with the variance $\sigma_S^2 = (\langle k_{\mathrm{S}}^2 \rangle - \langle k_{\mathrm{S}} \rangle^2)$ of $P_{\mathrm{S}}(k)$ - can be written as

$$\langle k_{\mathrm{S}} \rangle - \langle k_{\mathrm{I}} \rangle = \frac{w}{p} - \frac{\sigma_{\mathrm{S}}^2}{\langle k_{\mathrm{S}} \rangle} \,. \tag{2.19}$$

Comparing Eqs. 2.7 and 2.19 shows that the standard moment-closure assumption in the PA corresponds to setting $\sigma_{\mathrm{S}}^2 = \langle k_{\mathrm{S}} \rangle$ throughout the active phase, i.e. it is consistent with (yet does not imply) a Poissonian DD of the S-ensemble.

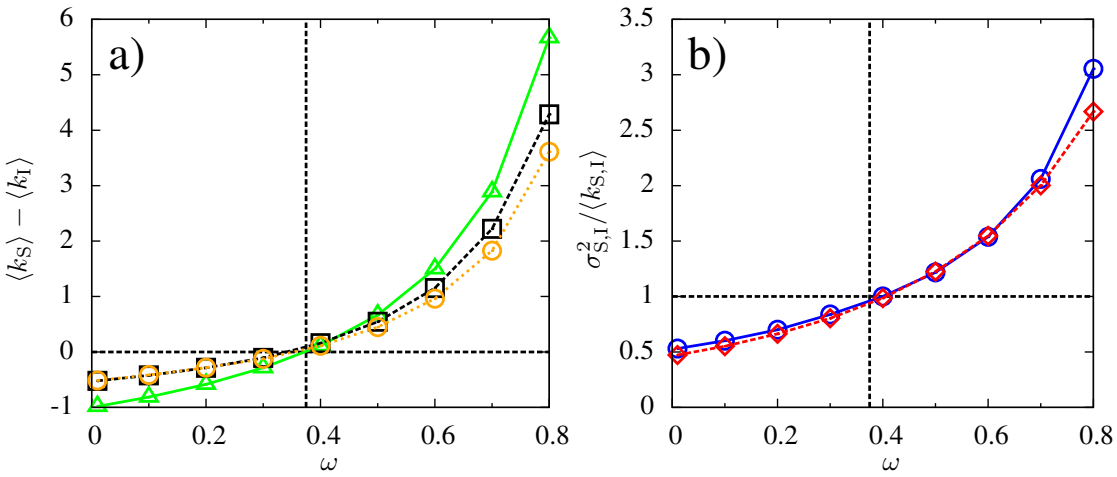

Figure 2.6: a) Differences in mean subensemble degrees as taken fom MC simulations (black squares), Eq. 2.7 (green triangles) and Eq. 2.19 (orange circles). **b)** Variance normalized by mean degree of S-ensemble DD (blue circles) and I-ensemble DD (red diamonds). Vertical dashed line signals $w = p$. Simulations from initial ER graphs with $N = 10^4$ and $\langle k\rangle = 5$ for $\rho = 0.6$, averaged over 10^3 runs.

In Fig. 2.6a, the predictions for steady-state $(\langle k_S\rangle - \langle k_I\rangle)$ of both the standard PA (Eq. 2.7) and Eq. 2.19 are shown as a function of $\omega \equiv w/(w + p + r)$ for constant $\rho \equiv p/(p + r)$. It can be seen that almost everywhere in the active phase, the standard PA values deviate from MC simulations, confirming that $P_S(k)$ is generally not Poissonian. Very close to $w = p$ however, the PA prediction becomes very accurate, thus indicating a Poissonian $P_S(k)$ while yielding equal mean subensemble degrees. Degree differences calculated from Eq. 2.19 on the other hand deviate from MC values only for high-rewiring regimes, where state-degree correlations diminish the accuracy of mean fields used in Eqs. 2.13. Figure 2.6b depicts the fraction of variances with mean degrees for both subensembles, again indicating that around $w = p$, both distributions become Poissonian (see also Fig. 2.5).

While the standard PA has been obtained by setting the moment-closure parameter η to 1 in Eqs. 2.2, leaving η undetermined and computing differences in steady-state subensemble degrees for various η is consistent with

$$\langle k_S\rangle - \langle k_I\rangle = \frac{1}{\eta}\frac{w}{p} - 1 + f(\eta)\,, \tag{2.20}$$

where

$$f(\eta) = \frac{\eta - 1}{2\eta}\left(1 - \langle k\rangle - \sqrt{(\langle k\rangle - 1)^2 p^2 + 4pr(1 + (\eta - 1)\langle k\rangle) - 4rw}\right) \tag{2.21}$$

(compare with Eq. 2.7). It follows that with Eqs. 2.19, 2.20 and 2.21, a more accurate moment closure can be achieved through computing η with σ^2_S.

Revisiting the recurrence relations

The standard PA in Sec. 2.1 has been shown to predict $w = p \Rightarrow \langle k_\mathrm{S}\rangle = \langle k_\mathrm{I}\rangle$ in DE, while considerations above on the subensemble DDs' first two moments yielded $\langle k_\mathrm{S}\rangle = \langle k_\mathrm{I}\rangle \Rightarrow \sigma_\mathrm{S}^2 = \langle k_\mathrm{S}\rangle$. This is consistent with observing identical Poissonian subensemble DDs at $w = p$ in Sec. 2.2, but to give this observation a stronger analytical support, Eqs. 2.12 need to be invoked again. For $w = p$, it is easy to verify that

$$P_\mathrm{S}(k) = \langle k_\mathrm{S}\rangle^k \frac{e^{-\langle k_\mathrm{S}\rangle}}{k!} = P_\mathrm{I}(k) \tag{2.22}$$

with $\langle k_\mathrm{S}\rangle = \langle k_\mathrm{I}\rangle = \langle k\rangle$ is *one* normalized solution of Eqs. 2.12, independently of the only free parameter $[I]$. Hence the recurrence relations are a self-sufficient framework in showing that at $w = p$, Poissonian subensemble DDs with equal mean degrees are one possible outcome of adaptive SIS dynamics. In contrast, actually generating steady-state subensemble DDs through Eqs. 2.12 still relies on feeding in $[I]$.

The reasoning underlying the recurrence relations also applies to other versions of the adaptive SIS model, in particular to the modified voter models proposed in Secs. 6.1 and 7.1. More precisely, Eqs. 2.12 are valid for that model family, leading to the prediction that also in these models, i) the stationary DDs depend only on $\langle k\rangle$, $[I]$ and w/p ii) the aforementioned subensemble symmetry holds at $w = p$ if the system is in DE.

2.4 Summary

Elaborating on the pair approximation of the adaptive contact process, an expression for the epidemic threshold is derived and a criterion for the onset of bistability formulated. Moreover, analytic expressions for several motif densities and average lifetimes are obtained for the system in dynamic equilibrium, as well as a coarse-grained description of network topology. In addition, the performance of the pair approximation in describing dynamic equilibria is checked against Monte-Carlo simulations and found to be satisfying for large regions of the active phase.

A particular parameter region is identified for which there exists a congruence of steady-state subensemble degree distributions of Poissonian shape. This symmetry is explained by degree-recurrence relations for the two subensembles. The recurrence relations yield an approximate description of the stationary degree distributions observed in simulations, depending only on node densities as additional input parameters. This additionally allows for a computation of more accurate moment closures than the standard pair approximation offers.

2.4. Summary

Yet unexplained is the *uniqueness* and *comprehensiveness* of dynamic equilibria, i.e. the fact that regardless of initial conditions and solely determined by model parameters, node states and network structure coevolve to yield not only constant and unique low-level motif densities, but generally a characteristic steady-state topology described by various stationary distributions. In addition, it is desirable to analytically generate observed subensemble degree distributions, as well as to widen the description of equilibrium statistics through i) deriving additional subensemble distributions ii) relating those to the familiar subensemble degree distributions. This will be the subject of Chapter 3.

3 THE NODE CYCLE

The adaptive contact process has been given a coarse-grained description in Sec. 2.1, and observed stationary degree distributions in MC simulations in Sec. 2.2 have been made plausible by an ansatz presented in Sec. 2.3. Yet in order to set up a self-sufficient framework showing the existence and uniqueness of steady-state topologies in the active phase, more refined building blocks than link densities and distributions in total degrees are needed.

3.1 Degree dynamics as a random walk

The active-neighborhood approach

With a node's joint degree (x, y) giving the numbers x and y of its susceptible and infected neighbors, respectively, the steady-state subensemble distributions $P_{\mathrm{S,I}}(x, y)$ in joint degrees provide a more detailed probabilistic account of a node's *active neighborhood* and are therefore aimed at by recent models [65, 68, 69]. Considering that

$$1 = \sum_{x,y=0}^{\infty} P_{\mathrm{S,I}}(x, y)\,, \tag{3.1}$$

one can retrieve all DE averages from these distributions that were computed with the PA in Chapter 2. Since $([S] \cdot \langle k_{\mathrm{S}} \rangle + [I] \cdot \langle k_{\mathrm{I}} \rangle) = \langle k \rangle$ with

$$\langle k_{\mathrm{S,I}} \rangle = \sum_{x,y=0}^{\infty} (x + y) P_{\mathrm{S,I}}(x, y)\,, \tag{3.2}$$

it follows straight from the distributions' first moments that

$$[I] = \frac{\langle k \rangle - \langle k_{\mathrm{S}} \rangle}{\langle k_{\mathrm{I}} \rangle - \langle k_{\mathrm{S}} \rangle} \tag{3.3}$$

for $\langle k_{\mathrm{S}} \rangle \neq \langle k_{\mathrm{I}} \rangle$. The density of active links is equal to the mean number of infected (susceptible) neighbors of S-nodes (I-nodes), weighted with the fraction

of the latter in the whole network. Therefore

$$\begin{aligned}[SI] &= [S] \sum_{x,y=0}^{\infty} y \; P_{\mathrm{S}}(x,y) \\ &= [I] \sum_{x,y=0}^{\infty} x \; P_{\mathrm{I}}(x,y) \end{aligned} \tag{3.4}$$

is exemplarily obtained for the density of active links. In the same manner, one moreover calculates

$$[ISI] = [S] \sum_{x,y=0}^{\infty} \frac{y(y-1)}{2} P_{\mathrm{S}}(x,y) \tag{3.5}$$

for the triplet density only approximated in Eq. 2.1. Along those lines, all motif densities up to the level of triplets can be computed, and from them mean liftetimes for all link and node types according to Sec. 2.1. As triplet densities do not need to be approximated as in the pairwise framework, extracted lifetimes are now exact.

In the active-neighborhood approach, nodes of equal state and joint degree are lumped into a single compartment with specific gain and loss rates for the member nodes' abundance. While the original framework in [65] will be briefly introduced in Sec. 4.3, the key idea of this work uses the active-neighborhood approach and will be laid out in Chapters 3 to 5: An analytic framework that generates joint DDs[1]. for both subensembles in DE, links them to a range of other characteristic probability distributions, and moreover addresses the existence and uniqueness of comprehensive DEs noted in Sec. 2.2.

Setting up Master equations

As a starting point, one can focus on the stochastic process that each node and its links follow as the former undergoes state change from susceptible to infected and back again, gaining (in the susceptible *S-stage*) or losing (in the infected *I-stage*) links. In each stage, the node's joint degree (x, y) is then kept track of. Due to infection, recovery and rewiring, the numbers x and y change at certain rates, defining a Markov process that can be described in each stage as a finite random walk on a degree grid spanned by x and y (Fig. 3.1). These time-continuous random walks performed in each stage are one-step processes in both coordinates. They are coupled by stage transitions, which take place at constant rate r from the node's infected I-stage to its susceptible S-stage, and at rate $p \cdot y$ from the S-stage to the I-stage. In the following, quantities computed in the random-walk scenario will be given an interpretation in terms of node-state and node-degree dynamics if deemed necessary.

[1] In this work, *DD* and *joint DD* will be used interchangeably, but distinguished if in order.

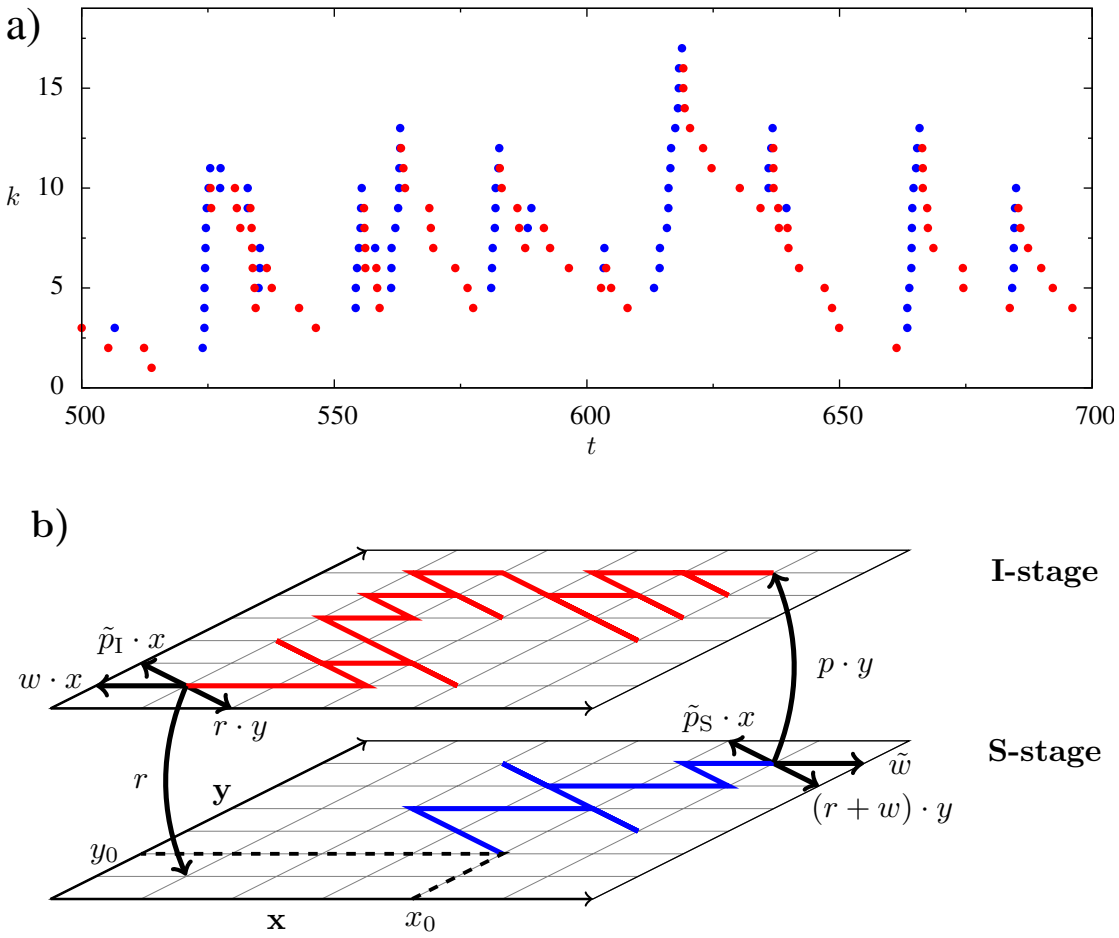

Figure 3.1: State and degree evolution of a node going through the S-stage (blue) and I-stage (red). **a)** Evolution of total degree for $\omega = 0.7$, $\rho = 0.7$ in MC simulations in DE. $N = 10^4$, $\langle k \rangle = 7$. **b)** Joint-degree evolution in one node cycle, starting with joint degree (x_0, y_0) in the S-stage. Bold arrows show all possible transitions and their rates. Simulations from initial ER graphs with a fraction 0.5 of randomly primed I-nodes.

The probability $[x, y] \equiv P_A(x, y, t|x_0, y_0)$ of a walker in stage $A \in \{S, I\}$ to be at coordinates (x, y) at time t when having started at coordinates (x_0, y_0), obeys the Master equation

$$\begin{aligned}\frac{\mathrm{d}[x,y]}{\mathrm{d}t} =&(w+r)\{(y+1)[x-1,y+1]-y[x,y]\}-py[x,y]\\ &+\tilde{w}([x-1,y]-[x,y])+\tilde{p}_S\{(x+1)\,[x+1,y-1]-x[x,y]\}\end{aligned} \tag{3.6}$$

in the S-stage and

$$\begin{aligned}\frac{\mathrm{d}[x,y]}{\mathrm{d}t} =&r\{(y+1)\,[x-1,y+1]-y[x,y]\}+w\{(x+1)[x+1,y]-x[x,y]\}\\ &-r[x,y]+\tilde{p}_I\{(x+1)\,[x+1,y-1]-x[x,y]\}\end{aligned} \tag{3.7}$$

in the I-stage, with boundary conditions $[-1, y] = [x, -1] = 0$ applying to both stages.

In Eq. 3.6 for the time evolution of a S-node's neighborhood, the first term on the right-hand side for instance takes into account the swapping of an infected neighbor with a susceptible neighbor due either to rewiring or to recovery of the infected neighbor. The second term on the right represents the transition to the I-stage and an overall probability mass loss as in the active phase as all susceptible nodes eventually are infected. The stochastic dynamics of the local random variables x and y is mediated through the set of model parameters $\mu = \{w, p, r\}$, and coupled to the global network dynamics through the set κ of three *correspondence parameters*: the total degree gain rate $\tilde{w}$ in the S-stage and the force of infection $\tilde{p}_{\mathrm{S,I}}$ that determines the infection rate of susceptible neighbors of the node in the respective stage. On the right-hand side of Eq. 3.6, these two transitions are represented by the third and fourth term, respectively. The correspondence parameters are assumed to be constant[2] and will be assigned values later on.

Solving the Master equations

The state and degree evolution of a single node in a network in DE is then given by a composite random walk described with Eq. 3.6 in the S-stage and Eq. 3.7 in the I-stage. If all correspondence parameters are set to zero, the network background does not exert any influence on single-node dynamics, corresponding to a frozen network configuration. For this choice of κ, the absorbing state of the random walk is any $[x, 0]$ ($x \in \mathbb{N}$) in the S-stage and corresponds to the system's disease-free equilibrium also described by Eqs. 2.2 of the PA.

Using the generating-function formalism, the Master equations 3.6 and 3.7 can be solved for either stage $A \in \{S, I\}$ [58]. After being transformed into a linear first-order PDE for the probability generating function

$$F_{\mathrm{A}} \equiv F_{\mathrm{A}}(\chi, \gamma, t|x_0, y_0) \equiv \sum_{x,y=0}^{\infty} \chi^x \gamma^y P_{\mathrm{A}}(x, y, t|x_0, y_0)\,, \tag{3.8}$$

employing the method of characteristics yields

$$\begin{aligned} F_{\mathrm{S}}(\chi, \gamma, t|x_0, y_0) = {} & (c_1(t)\,\chi + c_2(t)\,\gamma)^{x_0}\,(c_3(t)\,\chi + c_4(t)\,\gamma)^{y_0} \\ & c_8(x_0, y_0)\, e^{c_5(t)\chi + c_6(t)\gamma + c_7(t, x_0, y_0)} \end{aligned} \tag{3.9}$$

for the S-stage and a similar expression for the I-stage (Appendix A.2). Here $c_j(t)$ with $j \in \{1 \ldots 7\}$ consist of linear combinations of exponential functions of time, $c_7(t, x_0, y_0)$ depends linearly on time and initial coordinates, whereas $c_8(x_0, y_0)$

[2] This will be justified in Sec. 5.2.

is an exponential function of the initial coordinates. According to Eq. 3.8, the probability densities can then be extracted from the generating function as

$$P_{\mathrm{A}}(x,y,t|x_0,y_0) = \frac{1}{x!y!}\frac{\partial^{x+y}}{\partial\chi^x\partial\gamma^y}F_{\mathrm{A}}(\chi,\gamma,t|x_0,y_0)\bigg|_{\chi=\gamma=0}, \tag{3.10}$$

yielding the time-dependent probability densities in either node stage. These closed-form expressions are the solutions to Eqs. 3.6 and 3.7, and distributions may be extracted from them to characterize the random walk in each stage.

3.2 Characterizing the random walk

Probability generating functions handily encapsulate the probabilistic description of stochastic processes, so that retrieving probability densities via Eq. 3.10 is not always needed. In our case of the random walk in stage A with starting coordinates (x_0, y_0) for instance, it immediately follows from Eq. 3.8 that

$$F_{\mathrm{A}}(1,1,t|x_0,y_0) = \sum_{x,y=0}^{\infty} P_{\mathrm{A}}(x,y,t|x_0,y_0) \tag{3.11}$$

is the remaining probability mass[3] at time t, with

$$\begin{aligned} F_{\mathrm{A}}(1,1,0|x,y) &= 1 \\ \lim_{t\to\infty} F_{\mathrm{A}}(1,1,t|x,y) &= 0 \end{aligned} \tag{3.12}$$

for any coordinate pair (x, y). Once a closed-form expression for $F_{\mathrm{A}}(1,1,t|x_0,y_0)$ has been found, normalization of probabilistic measures for the respective node stage is hence simplified (see below).

Extracting conditional quantities

One can use Eq. 3.10 to compute the Taylor expansion of Eq. 3.9 up to arbitrary order. That yields an expression for $P_{\mathrm{S}}(x,y,t|x_0,y_0)$ that is a finite sum of exponentials (Appendix A.3). The (overall) conditional probability mass of the random walker in the S-stage at (x, y), having started at (x_0, y_0), reads as

$$P_{\mathrm{S}}(x,y|x_0,y_0) = \int_0^{\infty} P_{\mathrm{S}}(x,y,t|x_0,y_0)\,\mathrm{d}t\,. \tag{3.13}$$

[3]Keep in mind that each stage is continuously losing probability mass due to nonzero transition rates to the next stage.

Given that the rate of reinfection of a S-node with y infected neighbors is $p \cdot y$, the probability of switching to the I-stage at coordinates (x, y) in the time interval $[t, t + \mathrm{d}t]$ is $p \cdot y \cdot P_{\mathrm{S}}(x, y, t|x_0, y_0) \cdot \mathrm{d}t$. One subsequently calculates

$$\begin{aligned}\Phi_{\mathrm{S}}(x, y|x_0, y_0) &= p\ y\ \int_0^\infty P_{\mathrm{S}}(x, y, t|x_0, y_0)\ \mathrm{d}t \\ &= p\ y\ P_{\mathrm{S}}(x, y|x_0, y_0)\end{aligned} \tag{3.14}$$

to obtain the probability of, having started at (x_0, y_0), ending the walk in the S-stage at (x, y).

In a similar fashion, closed-form expressions for the generating function, the conditional probability mass $P_{\mathrm{I}}(x, y|x_0, y_0)$ and conditional stage-transition probabilities

$$\Phi_{\mathrm{I}}(x, y|x_0, y_0) = r\ P_{\mathrm{I}}(x, y|x_0, y_0) \tag{3.15}$$

are obtained for the I-stage (Appendix A.2 and A.3). Since

$$F_{\mathrm{I}}(1, 1, t|x_0, y_0) = e^{-rt}\ , \tag{3.16}$$

the random walk in the I-stage loses probability mass with constant rate r, as one would expect for the degree-independent recovery of I-nodes. By definition

$$\sum_{x,y=0}^{\infty} \Phi_{\mathrm{S,I}}(x, y|x_0, y_0) = 1 \tag{3.17}$$

holds, since a random walker eventually switches stages.

Distributions of total probability mass

The time-independent conditional quantities $\Phi_{\mathrm{S,I}}(x, y|x_0, y_0)$ and $P_{\mathrm{S,I}}(x, y|x_0, y_0)$ introduced above can be represented by matrices (Appendix A.4). They encode the dynamics of the random walk in stage $A \in \{S, I\}$. To define an actual stochastic process, one has to feed in vectors that represent joint probability distributions in starting coordinates (x_0, y_0) (this mapping onto vectors also follows along the lines of Appendix A.4). If these starting coordinates are distributed as $\Phi^*_{\mathrm{S}}(x_0, y_0)$ in the S-stage and $\Phi^*_{\mathrm{I}}(x_0, y_0)$ in the I-stage, one can weight the conditional quantities with these initial coordinate distributions (ICD) and compute *stage distributions* that characterize the ensuing random walk in each node stage[4].

[4]Matrices and vectors will be denoted by their entries and vice versa. Furthermore, all distributions extracted from the random walk will be given an asterisk to distinguish them from ensemble distributions they will be compared to in Chapters 4 and 5.

The normalized total probability mass at coordinates (x, y) in stage $A \in \{S, I\}$ is obtained as

$$P_{\mathrm{A}}^*(x,y) = \frac{\sum_{x_0,y_0=0}^{\infty} P_{\mathrm{A}}(x,y|x_0,y_0)\ \Phi_{\mathrm{A}}^*(x_0,y_0)}{\sum_{x',y'=0}^{\infty}\sum_{x_0,y_0=0}^{\infty} P_{\mathrm{A}}(x',y'|x_0,y_0)\ \Phi_{\mathrm{A}}^*(x_0,y_0)}$$
$$= \frac{\sum_{x_0,y_0=0}^{\infty} P_{\mathrm{A}}(x,y|x_0,y_0)\ \Phi_{\mathrm{A}}^*(x_0,y_0)}{\sum_{x_0,y_0=0}^{\infty} \Phi_{\mathrm{A}}^*(x_0,y_0) \int_{t=0}^{\infty} F_{\mathrm{A}}(1,1,t|x_0,y_0)\ \mathrm{d}t}\,. \tag{3.18}$$

Note that unlike $\Phi_{\mathrm{A}}(x, y|x_0, y_0)$, $P_{\mathrm{A}}(x, y|x_0, y_0)$ are not conditional probabilities. To normalize the computed total probability mass, it is therefore paramount to weight $P_{\mathrm{A}}(x, y|x_0, y_0)$ with the respective ICD *before* normalization. This results in distribution $P_{\mathrm{A}}^*(x, y)$, giving the probability that in stage A, the random walker will be encountered at (x, y) at a randomly picked point of time. The respective mean $\langle k_{\mathrm{A}}\rangle^*$ is calculated as in Eq. 3.2 and, in the scheme of single-node dynamics, is just the mean degree of the node in stage A.

Survival functions and lifetime distributions

The survival function $L_{\mathrm{A}}^*(t, x, y)$ of a random walker in stage $A \in \{S, I\}$ with starting coordinates (x, y) is simply given by

$$L_{\mathrm{A}}^*(t) = F_{\mathrm{A}}(1, 1, t|x, y)\,, \tag{3.19}$$

delivering the probability that the random walker is still in the respective stage at time t. This implies

$$L_{\mathrm{A}}^*(t) = \sum_{x,y=0}^{\infty} \Phi_{\mathrm{A}}^*(x,y) F_{\mathrm{A}}(1,1,t|x,y) \tag{3.20}$$

as the survival function for walkers with the known ICD $\Phi_{\mathrm{A}}^*(x, y)$. Hence in the I-stage,

$$L_{\mathrm{I}}^*(t, x, y) = L_{\mathrm{I}}^*(t) = e^{-r\ t} \tag{3.21}$$

according to Eq. 3.16, underlining that the random walker exits the stage independently from its starting coordinates.

For the the lifetime distributions $T_{\mathrm{A}}^*(t, x, y)$ of random walkers with initial coordinates (x, y),

$$F_{\mathrm{A}}(1, 1, t|x, y) = 1 - \int_0^t T_{\mathrm{A}}^*(t', x, y)\ \mathrm{d}t' \tag{3.22}$$

holds. Weighting with the respective ICD yields

$$T_{\mathrm{A}}^{*}(t) = -\frac{\mathrm{d}}{\mathrm{d}t}\sum_{x,y=0}^{\infty}\Phi_{\mathrm{A}}^{*}(x,y)F_{\mathrm{A}}(1,1,t|x,y) \tag{3.23}$$

as the lifetime distribution of random walkers in stage $A \in \{S, I\}$. The latter is a probability distribution, whereas the survival function is its tail distribution according to

$$L_{\mathrm{A}}^{*}(t,x,y) = 1 - \int_{0}^{t} T_{\mathrm{A}}^{*}(t',x,y)\ \mathrm{d}t'\,, \tag{3.24}$$

so that in particular

$$T_{\mathrm{I}}^{*}(t,x,y) = T_{\mathrm{I}}^{*}(t) = r\ e^{-r\ t} \tag{3.25}$$

through Eq. 3.21.

Average lifetimes

The average duration of each stage $A \in \{S, I\}$ is given by

$$\begin{aligned}
\tau_{\mathrm{A}}^{*} &= \int_{0}^{\infty} t\ T_{\mathrm{A}}^{*}(t)\ \mathrm{d}t \\
&= -\sum_{x,y=0}^{\infty}\Phi_{\mathrm{A}}^{*}(x,y)\int_{0}^{\infty} t\frac{\mathrm{d}}{\mathrm{d}t}F_{\mathrm{A}}(1,1,t|x,y)\ \mathrm{d}t \\
&= \sum_{x,y=0}^{\infty}\Phi_{\mathrm{A}}^{*}(x,y)\left(\int_{0}^{\infty} F_{\mathrm{A}}(1,1,t|x,y)\ \mathrm{d}t - t\ F_{\mathrm{A}}(1,1,t|x,y)\big|_{0}^{\infty}\right) \\
&= \sum_{x,y=0}^{\infty}\Phi_{\mathrm{A}}^{*}(x,y)\int_{0}^{\infty} F_{\mathrm{A}}(1,1,t|x,y)\ \mathrm{d}t \\
&= \int_{0}^{\infty} L_{\mathrm{A}}^{*}(t)\ \mathrm{d}t\,.
\end{aligned} \tag{3.26}$$

Here the second equality holds because of Eq. 3.23, while the fourth does due to Eqs. 3.12 and the fact that for sufficiently large t, the remaining probability mass $F_{\mathrm{A}}(1,1,t|x,y)$ in stage A falls off exponentially with time (Appendix A.2). It furthermore follows from Eqs. 3.16 and 3.26 that

$$\tau_{\mathrm{I}}^{*} = \frac{1}{r} \tag{3.27}$$

as expected, as random walkers exit the I-stage at a coordinate-independent constant rate r.

According to Eq. 3.26, the mean stage lifetimes $\tau^*_{\mathrm{S,I}}$ yield the (constant) denominator of the right-hand side of Eq. 3.18. Since $\tau^*_{\mathrm{I}} = 1/r$, $P^*_{\mathrm{I}}(x, y)$ in Eq. 3.18 can be computed symbolically. In contrast, the time integral in the denominator of $P^*_{\mathrm{S}}(x, y)$ in Eq. 3.18 does not need to be calculated numerically, as the distribution can be normalized by the sum over its numerator.

It follows that all stage distributions considered here are not only closed-form expressions that characterize the respective random walk, but can be computed symbolically. The node stages have been considered separately so far, but since the long-term behavior of a node is a sequence of alternating S- and I-stages, their random walks ought to be coupled to fully capture single-node dynamics.

3.3 Iterating the random walk

The stage transition matrix $\Phi_{\mathrm{A}}(x, y|x_0, y_0)$ maps the random walker's ICD in stage A onto the ICD of the subsequent stage according to

$$\Phi^*_{\mathrm{I,S}}(x, y) = \sum_{x_0,y_0=0}^{\infty} \Phi_{\mathrm{S,I}}(x, y|x_0, y_0)\ \Phi^*_{\mathrm{S,I}}(x_0, y_0)\,. \tag{3.28}$$

With this relation at hand, two important equalities can be readily computed - one for the average lifetime in the S-stage, another for the ICD of the same stage. Weighting both sides of Eq. 3.14 with $\Phi^*_{\mathrm{S}}(x, y)$, using Eq. 3.28 on the left-hand side and inserting Eqs. 3.18 as well 3.26 on the right-hand-side, one obtains

$$\Phi^*_{\mathrm{I}}(x, y) = p\ y\ P^*_{\mathrm{S}}(x, y)\ \tau^*_S\,, \tag{3.29}$$

and therefore normalizing over $\Phi^*_{\mathrm{I}}(x, y)$ implies

$$\tau^*_S = \left(p \sum_{x',y'=0}^{\infty} y\ P^*_{\mathrm{S}}(x, y) \right)^{-1}. \tag{3.30}$$

In the scheme of single-node dynamics, the summation term in the last equation translates into the mean number of infected neighbors of a S-node, regardless with which distribution in joint degrees it starts its stage.

If Eq. 3.15 is weighted with $\Phi^*_{\mathrm{I}}(x, y)$ and then one procedes as in the previous case,

$$\Phi^*_{\mathrm{S}}(x, y) = P^*_{\mathrm{I}}(x, y) \tag{3.31}$$

is calculated. This means that regardless of the shape of the ICD, sampling the position of the random walker in the I-stage at arbitrary times yields the same

distribution as sampling its exit coordinates to the S-stage (at the end of the I-stage). Considering the overall drift towards $x = y = 0$ in that stage (rewiring causes a net loss of total degree in I-nodes), this may seem counterintuitive, but is just a consequence of the exponential lifetime distribution of walkers in the I-stage.

Existence and uniqueness of the stationary regime

Having related the ICDs through Eq. 3.28, two iterations of the equation yield a *node cycle* (NC), i.e. the sequence of two random walks in the S- and the subsequent I-stage. Then the ICD of the S-stage changes as

$$\Phi_{\mathrm{S}}^{*'}(x,y) = \sum_{x_0,y_0=0}^{\infty} \Phi(x,y|x_0,y_0)\,\Phi_{\mathrm{S}}^{*}(x_0,y_0)\ , \tag{3.32}$$

where $\Phi(x,y|x_0,y_0)$ is given by the Chapman-Kolmogorov identity

$$\Phi(x,y|x_0,y_0) \equiv \sum_{x',y'=0}^{\infty} \Phi_{\mathrm{I}}(x,y|x',y')\Phi_{\mathrm{S}}(x',y'|x_0,y_0)\ . \tag{3.33}$$

The latter equation defines a composite stage transition (CST) matrix that in Eq. 3.32 maps the ICD of the S-stage onto itself. The matrix entries $\Phi(x,y|x_0,y_0)$ are the conditional probabilities that, given a random walk starts the S-stage at coordinates (x_0,y_0), it re-enters the S-stage at (x,y) after one iteration of the node cycle.

If a cutoff for the maximum considered total degree k_{M} is set, $\Phi(x,y|x_0,y_0)$ can be represented by a stochastic matrix that encodes a finite Markov chain. According to Appendix A.2 and A.3, $\Phi_{\mathrm{S}}(x,y|x_0,y_0)$ ($\Phi_{\mathrm{I}}(x,y|x_0,y_0)$) is nonzero if and only if $(x+y) \geq (x_0+y_0)$ ($x+y \leq x_0+y_0$). This simply reflects the fact that in the S-stage (I-stage), the net degree gain (degree loss) can lead to any final joint degree (x,y) compatible with aforementioned restrictions. It then follows through Eq. 3.33 that $\Phi_{\mathrm{I}}(x,y|x_0,y_0) > 0$ for all considered coordinates. Hence every state (x,y) can be reached from any state (x_0,y_0) with just one NC iteration, and the Perron-Frobenius theorem [70] then states that matrix $\Phi(x,y|x_0,y_0)$ has the eigenvalue 1 with the largest absolute value of the matrix' spectrum. The associated right eigenvector is moreover unique and the only right eigenvector of $\Phi(x,y|x_0,y_0)$ with non-negative entries.

It follows that an arbitrary ICD in the S-stage will converge upon iteration of the node cycle to the unique stationary distribution $\Phi_{\mathrm{S}}^{*}(x,y)$ given by that eigenvector[5], and it does so for any choice of nonzero model and correspondence parameters. This power iteration, i.e. iterating Eq. 3.32 through repeated multiplication

[5] In the following, the asterisk implies stationarity of NC distributions.

of the CST-matrix with an arbitrary ICD, yields $\Phi^*_{\mathrm{S}}(x, y)$ with arbitrary precision [70]. As will be argued in Sec. 5.2, it also enables one to attain an approximate understanding of the system's transient towards DE.

The eigenvector $\Phi^*_{\mathrm{S}}(x_0, y_0)$ is a central pillar of the NC framework and can be easily computed with various software libraries, avoiding convergence considerations that arise during power iteration. In the node cycle given by the iteration of Eq. 3.32, $\Phi^*_{\mathrm{S}}(x_0, y_0)$ is identified as the unique stationary ICD of the S-stage. Equivalently, it is the stationary distribution in exit coordinates of random walks in the I-stage. More importantly, it provides the weighting to conditional quantities with which all previously-mentioned stage distributions are generated. The latter inherit both stationarity as well as uniqueness from that ICD and broaden the description of the stationary NC.

Figure 3.2 depicts the relations between all eight stage distributions. As laid out previously, they are tied to one another by linear mappings. While most distributions are obtained from the two ICDs, the latter can reversely be arrived at from the distributed probability mass through Eqs. 3.14 and 3.29. Given the expressions for the transformations, it is noteworthy that neither the mean network degree $\langle k \rangle$ nor motif densities in the network seem to be relevant for dynamics in the NC. They will however gain significance later on when formulating constraints that tie single-node dynamics to the rest of the network in DE.

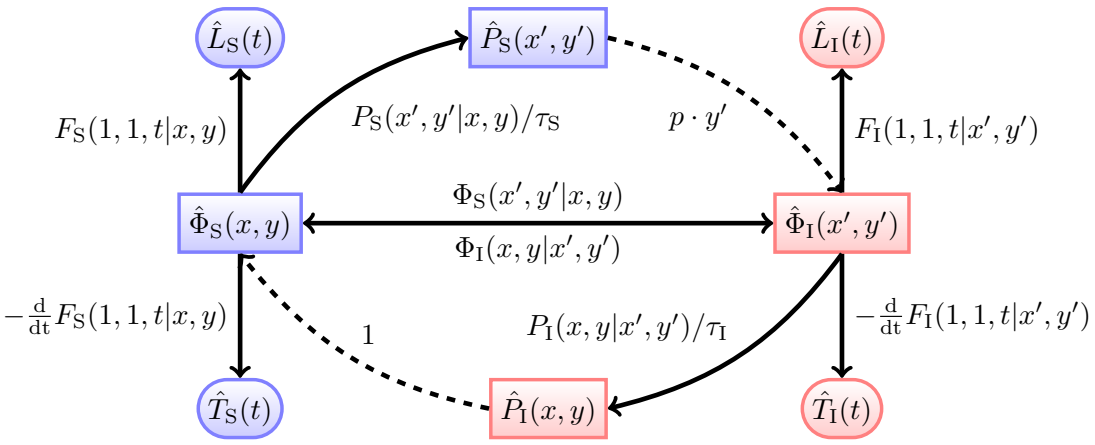

Figure 3.2: Interdependency of ensemble distributions in the S-stage (blue boxes) and I-stage (red boxes) which are distributions in degrees (sharp edges) and lifetimes (rounded corners). Solid arrows signify a linear transformation through summing over all variables common to the initial distribution and the mediating matrix of the same index. Dashed arrows symbolize multiplication of the initial distribution with the arrow label.

The duration of one node cycle

According to Sec. 3.2, the probability for a random walker in the S-stage - having started at coordinates (x_0, y_0) - to switch to the I-stage at (x, y) in the time interval $[t, t+\mathrm{d}t]$ is $p \cdot y \cdot P_{\mathrm{S}}(x, y, t|x_0, y_0) \cdot \mathrm{d}t$. Then the average time a random walker needs to pass through the sequence of S- and I-stage, given that it started at coordinates (x_0, y_0) in the S-stage and switched to the I-stage at (x, y) in the time interval $[t, t + \mathrm{d}t]$, is

$$\tau^*(x_0, y_0, x, y, t)\mathrm{d}t = p\ y\ P_{\mathrm{S}}(x, y, t|x_0, y_0)\mathrm{d}t \int_0^\infty (t' + t) T_{\mathrm{I}}^*(t', x, y)\mathrm{d}t' \,. \tag{3.34}$$

The average duration τ^* of one node cycle $S \to I \to S$ (the sequence of a S-stage followed by an I-stage) is, for any given ICD $\Phi_{\mathrm{S}}^*(x_0, y_0)$, obviously

$$\begin{aligned}
\tau^* &= \sum_{x_0,y_0=0}^{\infty} \Phi_{\mathrm{S}}^*(x_0, y_0) \sum_{x,y=0}^{\infty} \int_0^\infty \tau^*(x_0, y_0, x, y, t)\ \mathrm{d}t \\
&= \sum_{x_0,y_0=0}^{\infty} \Phi_{\mathrm{S}}^*(x_0, y_0) \sum_{x,y=0}^{\infty} \int_0^\infty \int_0^\infty p\ y\ P_{\mathrm{S}}(x, y, t|x_0, y_0)(t' + t) T_{\mathrm{I}}^*(t', x, y)\mathrm{d}t'\ \mathrm{d}t \\
&= \sum_{x_0,y_0=0}^{\infty} \Phi_{\mathrm{S}}^*(x_0, y_0) \sum_{x,y=0}^{\infty} \int_0^\infty p\ y\ P_{\mathrm{S}}(x, y, t|x_0, y_0)(\tau_{\mathrm{I}}^* + t)\mathrm{d}t \\
&= \tau_{\mathrm{I}}^* + \sum_{x_0,y_0=0}^{\infty} \Phi_{\mathrm{S}}^*(x_0, y_0) \int_0^\infty t \sum_{x,y=0}^{\infty} p\ y\ P_{\mathrm{S}}(x, y, t|x_0, y_0)\mathrm{d}t \,.
\end{aligned} \tag{3.35}$$

The third equality stems from integrating $(t + t') \cdot T_{\mathrm{I}}^*(t', x, y)$ over t' and using Eq. 3.25 as well as $\tau_{\mathrm{I}}^* = 1/r$, while the last is obtained through inserting Eq. 3.14. Following Sec. 3.2, the inner sum of the second term of the last equality is the total probability mass exiting the S-stage in the time interval $[t, t + \mathrm{d}t]$. Consequently

$$\sum_{x,y=0}^{\infty} p\ y\ P_{\mathrm{S}}(x, y, t|x_0, y_0) = -\frac{\mathrm{d}}{\mathrm{d}t} F_{\mathrm{S}}(1, 1, t|x_0, y_0) \,, \tag{3.36}$$

and inserting Eq. 3.36 into Eq. 3.35 finally yields

$$\tau^* = \tau_{\mathrm{I}}^* + \tau_{\mathrm{S}}^* \tag{3.37}$$

through Eq. 3.23. Hence the average duration of a full node cycle is the sum of the average stage lifetimes, even in non-stationary NC regimes. This is a consequence of the coordinate-independent recovery of I-nodes in adaptive SIS dynamics, and does not necessarily hold for adaptive networks without such a simple stage-transition rule.

3.4 Summary

The state and degree evolution of a typical node in a network in dynamic equilibrium is treated as a composite random walk. For each stage, this random walk - guided by sets of model and correspondence parameters - is solved exactly, with closed-form expressions for a variety of characteristic distributions being extracted. These stage distributions are related through linear transformations, and several equalities for the (not necessarily stationary) network process are retrieved.

Iterating the composite random walk yields a *node cycle* in both state and degree evolution, featuring a stationary regime in the long-term limit and for any choice of parameters. This regime is characterized by a unique set of stage distributions whose shapes are solely determined by the two parameter sets. Additionally, the average length of one node-cycle iteration is elaborated on.

The set of correspondence parameters, encapsulating the influence of the network background on local node dynamics, needs yet to be specified so as to relate single-node and network dynamics. Then the existence and uniqueness of steady-state stage distributions in the node cycle are inherited to the respective ensemble distributions in the network process, so that the existence of unique and comprehensive[6] dynamic equilibria observed in Monte-Carlo simulations can be given an analytic foundation. Chapter 4 will take this final step.

[6] In the sense of a variety of stationary ensemble distributions.

4 LINKING THE NODE CYCLE TO NETWORK DYNAMICS

In Chapter 3, the (iterated) node cycle was solved as the long-term state and degree evolution of a single node in a network in DE. The network in DE was so far considered to be an abstract background in the active phase, as correspondence parameters were not specified. For any choice of nonzero correspondence and model parameters, the NC was shown to yield a unique stationary regime statistically described by a set of stage distributions. But under which conditions do stage distributions become subensemble distributions, i.e. when does the long-term single-node behavior encode equilibrium statistics for the node ensemble?

4.1 Preliminary considerations

The best the NC framework in its current form can - by design - aim for is a description of the network DE on the compartmental level, that is, through joint subensemble DDs and node-state densities with no further correlations between nodes assumed. To be able to extract ensemble statistics from the NC iteration, the evolution of node in its state and its immediate neighborhood should consequently look the same as seen from any node in the network in DE. Hence for a given set μ of model parameters and mean network degree $\langle k \rangle$, the long-term state and degree evolution as described by the NC should be captured by the same set κ of correspondence parameters for any node of the network. For now it suffices to remark that the rewiring process ensures this by picking an arbitrary active link and a random susceptible rewiring partner. Indeed, simulations of the steady state of the network model reveal that recording ensemble statistics yields the same distributions as sampling a single node over a sufficiently long time. These ergodic properties of the network process will be elaborated on in Sec. 5.2.

Selecting μ and $\langle k \rangle$ to settle on particular node dynamics and their topological background, κ must then be chosen so as to fulfill any desired global properties on the network the NC is unable to account for, such as for instance the specific value for $\langle k \rangle$. Moreover, averages generated by the stationary NC through

its stage distributions ought to be made consistent with the network background acting upon the NC, imposing additional independent constraints on κ. With the optimal choice for κ, the NC becomes a fully self-contained analytical framework for which the long-term dynamics of a single node is made consistent with a given network background in DE. Once this has been ensured, it is labeled *correspondence* between single-node and network dynamics. Then the stationary NC distributions $\Phi^*_{\mathrm{A}}(x,y)$, $P^*_{\mathrm{A}}(x,y)$, $T^*_{\mathrm{A}}(t)$ and $L^*_{\mathrm{A}}(t)$ become distributions $\Phi_{\mathrm{A}}(x,y)$, $P_{\mathrm{A}}(x,y)$, $T_{\mathrm{A}}(t)$ and $L_{\mathrm{A}}(t)$ describing node-ensemble statistics in the respective DE, and can be compared to the output of MC simulations.

Extracting identities

In DE, node densities must be equal to the fraction of the time a node typically spends in the respective stage, so that $[S]/[I] = \tau^*_{\mathrm{S}}/\tau^*_{\mathrm{I}}$ and therefore

$$\begin{aligned} [S]^* &= \frac{\tau^*_{\mathrm{S}}}{\tau^*_{\mathrm{S}} + \tau^*_{\mathrm{I}}} \\ [I]^* &= \frac{\tau^*_{\mathrm{I}}}{\tau^*_{\mathrm{S}} + \tau^*_{\mathrm{I}}} \end{aligned} \tag{4.1}$$

when correspondence holds[1]. With the node densities at hand, motif densities of higher order can be extracted from the stage distributions $P^*_{\mathrm{S,I}}(x,y)$ as in Sec. 3.1. Given those motif densities, constraints on κ can subsequently be formulated to enforce correspondence in Sec. 4.2. But even before assigning values to optimal κ, it is possible to retrieve important identities from the NC.

Inserting stage distributions $P^*_{\mathrm{S,I}}(x,y)$ and Eq. 3.30 into Eqs. 3.4, one obtains

$$\tau^*_{\mathrm{S}} = \frac{[S]^*}{p\ [SI]^*}\,, \tag{4.2}$$

the NC counterpart to Eq. 2.9. Through Eq. 3.30, this equality even holds in non-stationary NC regimes.

In the stationary NC and for any κ, the average degree gain in the S-stage is equal to the average degree loss in the I-stage, as otherwise there would not be a stationary ICD $\Phi^*_{\mathrm{S}}(x,y)$. It follows that

$$\tau^*_{\mathrm{S}}\ \tilde{w} = \tau^*_{\mathrm{I}}\ w\ \sum_{x,y=0}^{\infty} x\ P^*_{\mathrm{I}}(x,y)\,. \tag{4.3}$$

[1] In the following, all NC averages are taken from the stationary NC and, like all stage distributions, assigned an asterisk.

With Eq. 4.2 and $\tau_{\mathrm{S}}^*/\tau_{\mathrm{I}}^* = [S]^*/[I]^*$ (from Eqs. 4.1) at hand,

$$\frac{[S]^*}{p\ [SI]^*} = \tau_{\mathrm{I}}^*\ \frac{[S]^*}{[I]^*} \tag{4.4}$$

and finally

$$p\ [SI]^* = r\ [I]^* \tag{4.5}$$

are derived. The last equality is a balance equation for the two node ensembles in steady state - its PA counterpart being the root of the first of Eqs. 2.2.

4.2 Formulating and optimizing constraints

In the previous section, several identities have been shown to arise from the NC even without imposing correspondence through a set of optimal κ. For correspondence between the NC and network dynamics, one however needs to establish constraints for the values that $\langle k \rangle$ and κ can assume in single-node dynamics.

Equalities through one constraint

When extracting motif densities from Eq. 4.1, one should exercise caution in the case of the density $[SI]^*$ of active links. While according to Eqs. 3.4 it does not matter in the network domain which of the two node stages the link count is based on, it generally does when counting in the NC if no correspondence has been established yet. Demanding that S- and I-stages in the NC shall represent nodes that are each other's neighbors, computing $[SI]^*$ with distributions $P_{\mathrm{S,I}}^*(x,y)$ through Eqs. 3.4 should yield the same (but otherwise not specified) value in both stages. Through Eqs. 4.1, one calculates

$$\tau_{\mathrm{S}}^* \sum_{x,y=0}^{\infty} y\ P_{\mathrm{S}}^*(x,y) = \tau_{\mathrm{I}}^* \sum_{x,y=0}^{\infty} x\ P_{\mathrm{I}}^*(x,y)\,. \tag{4.6}$$

With that constraint at hand, several equalities can be set up relating to the average number of connections in each stage. Inserting Eqs. 3.27 and 3.30 into Eq. 4.6 yields

$$\frac{r}{p} = \sum_{x,y=0}^{\infty} x\ P_{\mathrm{I}}^*(x,y) \tag{4.7}$$

for the mean number of susceptible neighbors (the mean susceptible degree) of an I-node. Combining moreover Eq. 4.3 and 4.7 results in

$$\tilde{w} = \frac{w}{p\ \tau_{\mathrm{S}}^*}\,, \tag{4.8}$$

so that w/p is the average degree gain in the S-stage. Since according to Eq. 3.31, the mean degree in the beginning of the S-stage is equal to the mean degree in the I-stage $\langle k_\mathrm{I}\rangle^*$,

$$\langle k_\mathrm{I}\rangle^* + \frac{w}{p} = \sum_{x,y=0}^{\infty} (x+y)\Phi_\mathrm{I}^*(x,y) \tag{4.9}$$

is calculated as the mean degree of newly infected I-nodes.

Setting up the cost function

Fully tying the NC to network dynamics requires multiple constraints on the choice of κ. The adaptive contact process features link conservation, so that a constant mean degree $\langle k\rangle$ needs to be imposed via

$$\langle k\rangle = \frac{\tau_\mathrm{S}^*\langle k_\mathrm{S}\rangle^* + \tau_\mathrm{I}^*\langle k_\mathrm{I}\rangle^*}{\tau_\mathrm{S}^* + \tau_\mathrm{I}^*}\,. \tag{4.10}$$

Consequently

$$C_k(\langle k\rangle,\kappa) = \left(1 - \frac{\left(\tau_\mathrm{S}^*\langle k_\mathrm{S}\rangle^* + \tau_\mathrm{I}^*\langle k_\mathrm{I}\rangle^*\right)/\left(\tau_\mathrm{S}^* + \tau_\mathrm{I}^*\right)}{\langle k\rangle}\right)^2\,, \tag{4.11}$$

with $C_k(\langle k\rangle,\kappa) = 0$, should hold to embed the NC into a network of constant mean degree $\langle k\rangle$. The dependency of the cost function $C_k(\langle k\rangle,\kappa)$ on the correspondence parameters is given implicitly through the stationary NC averages on the right-hand side of Eq. 4.11.

For a choice of κ that ensures correspondence between NC and network dynamics in DE, the three correspondence parameters introduced in Sec. 3.1 are similar in nature, in that they describe the number of infected neighbors of S-nodes, either without additional conditions or given that the latter are attached to another particular node type: In Eqs. 2.12, rate $\tilde{w}$ was already introduced and shown to be proportional to $[SI]/[S]$, the average number of infected neighbors of a S-node. The correspondence parameter $\tilde{p}_\mathrm{A}$ on the other hand yields the force of infection on a susceptible neighbor in stage $A \in \{S, I\}$, so that $\tilde{p}_\mathrm{A}/p$ gives the mean number of infected neighbors of a S-node conditional on being connected to a node in state A. Therefore, using motif densities generated by the NC,

$$\begin{aligned}
\frac{\tilde{w}}{w} &= \frac{[SI]^*}{[S]^*}\\
\frac{\tilde{p}_\mathrm{S}}{p} &= \frac{[SSI]^*}{2[SS]^*}\\
\frac{\tilde{p}_\mathrm{I}}{p} &= \frac{2[ISI]^*}{[SI]^*} + 1
\end{aligned} \tag{4.12}$$

should hold. Here the first equation yields the same constraint as Eq. 4.6, as one notices when plugging Eq. 4.2 into Eq. 4.8. The right-hand side of the last equality of Eq. 4.12 is for instance composed of the mean number of additional infected neighbors of the S-node of an active link, plus the I-node at the other link end.

It follows that in the network description, each of the three correspondence parameters can be expressed by a mean field composed of low-order motif densities. At exact correspondence, those densities should also be given by the corresponding NC averages. This results in three self-consistency relations that should hold regardless of imposed mean degree, and they are constraints on κ that can be combined into a cost function as

$$C_c(\kappa) = \left(1 - \frac{[SI]^*/[S]^*}{\tilde{w}/w}\right)^2 + \left(1 - \frac{[SSI]^*/2/[SS]^*}{\tilde{p}_\mathrm{S}/p}\right)^2 + \left(1 - \frac{2[ISI]^*/[SI]^* + 1}{\tilde{p}_\mathrm{I}/p}\right)^2 . \tag{4.13}$$

As described above, the constraints that $C_c(\kappa)$ encodes are state and degree correlations, and are fulfilled if and only if $C_c(\kappa) = 0$.

The NC averages in Eqs. 4.10 and 4.12 are convoluted functions of μ and κ evaluated within the NC. For a given adaptive network with fixed μ and $\langle k \rangle$, $C_k(\langle k \rangle, \kappa)$ and $C_c(\kappa)$ are cost functions in κ defined by the respective constraints. It has to be kept in mind that the number of constraints exceeds the number of correspondence parameters, so that the system of equations made up by the four constraints is generally overdetermined.

Because deciding for constant $\tilde{p}_{\mathrm{S,I}}$ may only approximate the interaction of a node's neighborhood with the rest of the network (Sec. 5.2), the four constraints in Eqs. 4.10 and 4.12 may not admit a solution in κ at all. Hence establishing correspondence with network dynamics in DE is achieved through identifying *optimal* κ that minimize $C_k(\langle k \rangle, \kappa)$ and $C_c(\kappa)$. Due to the different nature of constraints imposed via Eq. 4.10 on the one hand and Eqs. 4.12 on the other hand, it is instructive to first compute the set of κ minimizing $C_k(\langle k \rangle, \kappa)$ and of those κ minimizing $C_c(\kappa)$ separately. Since candidates for optimal correspondence parameters should ensure minimization of both cost functions, one then has to identify overlaps of those two sets. Each overlap constitutes a region of correspondence, and its coordinates κ can be fed into the NC to describe the respective DE.

With that at hand, one can now address the comprehensiveness and uniqueness of DEs remarked on in Sec. 2.2: If node, link and triplet densities in the adaptive network settle down to a steady state, the correspondence parameters of the NC also do through the self-consistency relations Eqs. 4.12 that are formulated with these low-order densities. This in turn lets the Perron-Frobenius theorem apply in the NC (see Sec 3.3), generating a unique set of stationary stage distributions (subensemble distributions at correspondence). Hence the NC shows that

stationary averages imply unique stationary distributions they arise from, most prominently - but not exclusively - steady-state degree distributions. The comprehensiveness of DEs is then given by the variety of steady-state subensemble distributions related through the NC (see Fig. 3.2).

Minimizing the cost function

In a random network and in the absence of degree and node-state correlations, the cost function $C_c(\kappa)$ would be minimal along $\tilde{w}/w = \tilde{p}_\mathrm{S}/p = (\tilde{p}_\mathrm{I}/p - 1)$. This is because without any such correlations, the average excess joint degree of any node type in a network with a Poissonian degree distribution equals the average joint degree [71]. In case of the expected number of infected neighbors of a S-node, MC simulations in DE indeed confirm that $[SI]/[S] \approx [SSI]/(2 \cdot [SS])$ for a wide range of μ. Thus the cost functions shall be visualized on the $(\tilde{w}/w = \tilde{p}_\mathrm{S}/p)$-plane in three-dimensional search space (Fig. 4.1). Standard minimization routines like the conjugate-gradient method [72] operate in full search space and are used to obtain optimal correspondence parameters.

To compactify search space and enhance optimization, the correspondence parameters are rescaled in a manner similar to PA parameters in Eqs. 2.4, so that

$$\frac{\tilde{w}/w}{\tilde{w}/w+1}, \frac{\tilde{p}_\mathrm{S}/p}{\tilde{p}_\mathrm{S}/p+1}, \text{ and } \frac{\tilde{p}_\mathrm{I}/p-1}{\tilde{p}_\mathrm{I}/p} \in [0,1)$$

are used as new parameters for

$$\frac{\tilde{w}}{w}, \frac{\tilde{p}_\mathrm{S}}{p}, \text{ and } \left(\frac{\tilde{p}_\mathrm{I}}{p} - 1\right) \in [0,\infty)\,.$$

As in fact there are degree and node-state correlations to be expected in a network in DE, $C_c(\kappa)$ is minimized slightly off the $(\tilde{w}/w = \tilde{p}_\mathrm{S}/p)$-plane (Fig. 4.1a).

Fixing μ and changing the imposed mean degree allows for detecting the system's phases (as defined by different numbers of overlap regions) by computing NC densities for search space only once. Varying $\langle k \rangle$ then leaves the region of minima of $C_c(\kappa)$ unchanged, whereas that of $C_k(\langle k \rangle, \kappa)$ shifts according to Eq. 4.11 (Fig. 4.1b-d). The absence of any region of overlap indicates that the NC cannot be matched to a network in DE, and corresponds to parameter values μ and $\langle k \rangle$ for which the network is in the frozen phase (Fig. 4.1b), small $\langle k \rangle$). One overlap region corresponds to the existence of one DE, detecting a simple endemic phase (Fig. 4.1d, large $\langle k \rangle$). Two regions of overlap are associated with a bistable phase (Fig. 4.1c, intermediate $\langle k \rangle$): The κ with larger components represents the stable DE of the active branch, whereas the one with smaller components is associated with the *unstable* DE of the hysteresis loop leading to bistability in Eqs. 2.2.

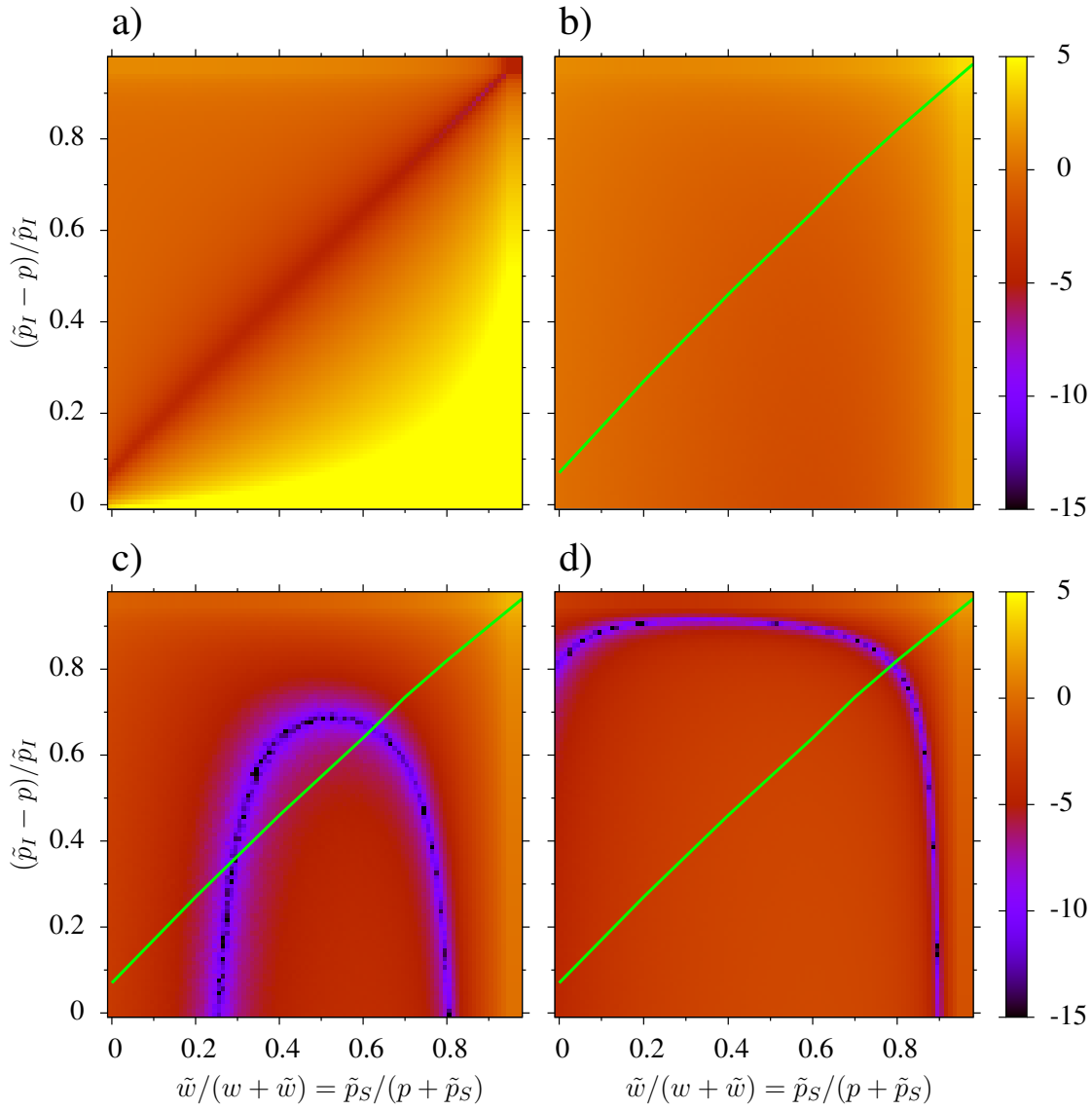

Figure 4.1: Logarithmic color-coded plots of cost functions on $(\tilde{w}/w = \tilde{p}_S/p)$-plane with axes rescaled to unit length. Coordinates for low cost function values ($\leq 10^{-5}$) are κ ensuring good correspondence for the respective constraint. **a)** $C_c(\kappa)$, with optimizing κ close to, but not on $\tilde{w}/w = \tilde{p}_S/p$. **b)-d)** $C_k(\langle k\rangle, \kappa)$, with green solid lines representing κ that minimize $C_c(\kappa)$ as in a). **b)** $\langle k\rangle = 3$. **c)** $\langle k\rangle = 5$. **d)** $\langle k\rangle = 7$. Model parameters $w = 0.05$, $p = 0.008$, $r = 0.005$ and maximum cutoff degree $k_M = 50$. Simulations from initial ER graphs with a fraction 0.5 of randomly primed I-nodes. Statistics recorded at $t = 3000$ for 10^3 network realizations.

The mean degrees $\langle k\rangle$ triggering a change in the number of overlap regions coincide with the values of $\langle k\rangle$ observed at corresponding phase transitions in simulations (also leaving μ fixed). Furthermore this number is equal to the number of stable and unstable DEs predicted by Eqs. 2.2 for the corresponding phase in the PA. The

supercritical Hopf bifurcation in Eqs. 2.2, giving rise to a small stable oscillatory regime in the bistable phase in Fig. 2.1, leaves the number of DEs unchanged. Consequently, no indications for that phase transition are found in the NC, as the framework cannot distinguish between the bistable phase's active steady state and its oscillatory regime. Concurrently, the NC is insensitive to the stability of its detected DEs. Yet it strongly hints that unstable DEs are physical and not mere model artefacts, and offers an extensive description of them.

Alternatively, one could browse the system's phases analogously to Sec. 2.2, where model parameters were varied for a constant $\langle k \rangle$. This however would imply that for each move in parameter space μ, the motif densities used in the two cost functions had to be re-calculated with the NC for all of search space κ. While possible, that would imply a considerable computational effort, so that the aforementioned method is preferable, requiring only one computation of NC densities for the entire search space.

Through Eqs. 4.12, optimal κ can be calculated for a given set of motif densities of a network in DE. Taking the latter from either MC simulations or the PA[2], the coordinates of optimal κ in every overlap region can be cross-checked. For DEs of a variety of μ and imposed $\langle k \rangle$, these predicted coordinates very well match those obtained with optimization algorithms. In the example of the bistable phase's unstable DE in Fig. 4.1c, the PA delivers steady-state motif densities $[I] = 0.46$, $[II] = 0.35$ and $[SS] = 1.86$, which translate into coordinates

$$\frac{\tilde{w}}{\tilde{w} + w} = \frac{\tilde{p}_{\mathrm{S}}}{\tilde{p}_{\mathrm{S}} + p} = \frac{\tilde{p}_{\mathrm{I}} - p}{\tilde{p}_{\mathrm{I}}} = 0.35\,. \tag{4.14}$$

This yields a good estimate for the coordinates of the respective overlap region and underlines the validity of the NC approach. Deviations to NC coordinates are due to the approximate nature of the moment closure employed in the PA, whereas the equality of the three PA coordinates stems from choosing $\eta = 1$ in Eqs. 2.2 and the fact that through the absence of degree correlations in the PA, the constraints in Eqs. 4.12 are equivalent.

Running the node cycle

Once correspondence has been established, stage distributions characterize node subensembles. To better visualize the bivariate distributions computed with the NC and obtained from MC simulations, the distributions over the sum of their variables are considered, so that for instance for the S-ensemble,

$$P_{\mathrm{S}}(k) \equiv \sum_{x+y=k}^{\infty} (x + y) P_{\mathrm{S}}(x, y)\,. \tag{4.15}$$

[2]The necessary triplet densities in the PA are approximated through its moment closure.

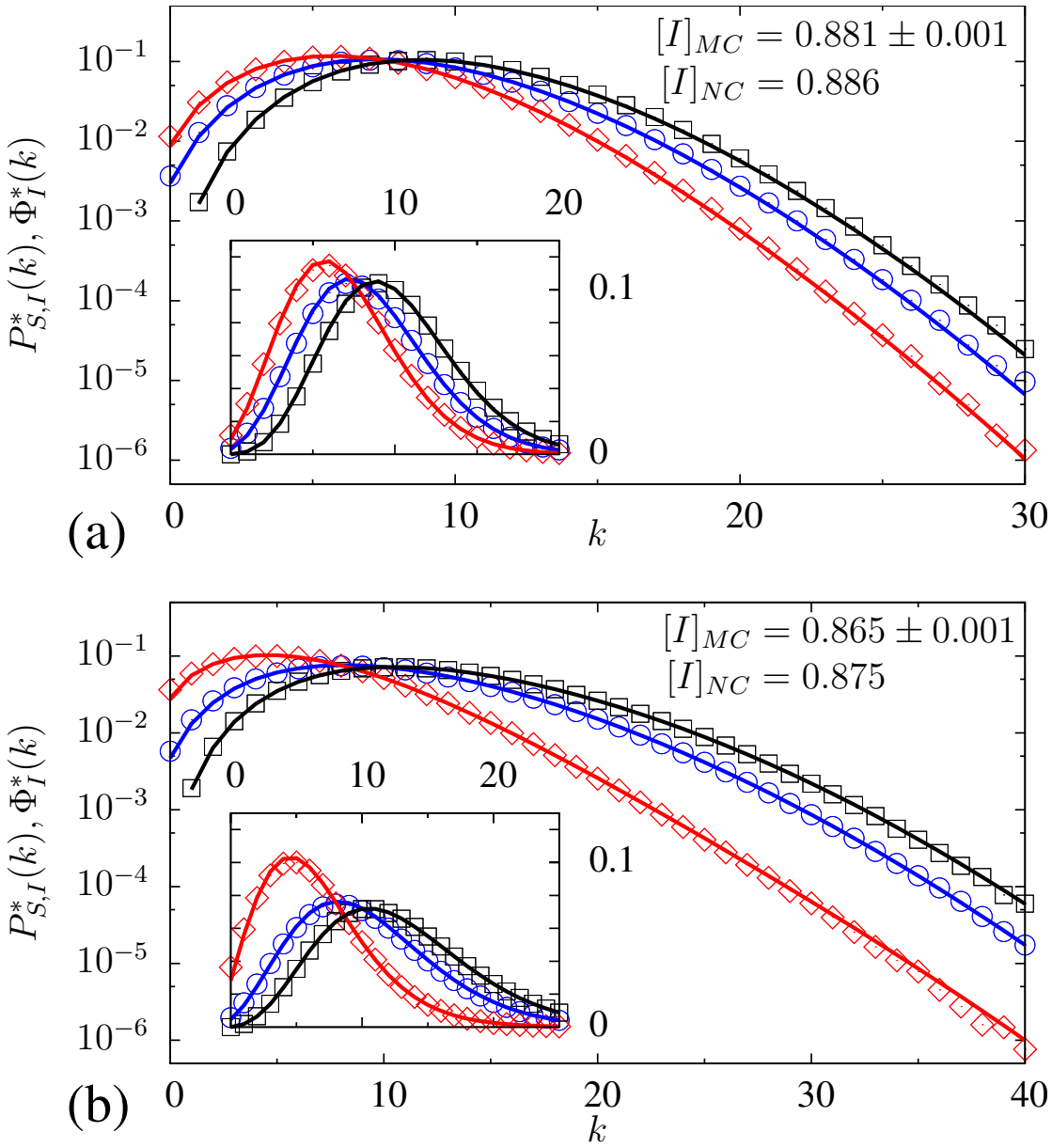

Figure 4.2: Subensemble degree distributions for two different rewiring regimes taken from MC simulations for susceptibles (blue circles), infected (red diamonds) as well as the steady-state ICD for the I-stage (black squares). Solid lines are NC predictions. Insets: Linear plots of the distributions in their dominating degree range; comparison of steady-state prevalence $[I]_{MC}$ taken from MC simulations and $[I]_{NC}$ computed by the NC framework. Parameters $p = 0.008$, $r = 0.005$. **a)** $w = 0.025$, $\tilde{w} = 0.12$, $\tilde{p}_{\mathrm{S}} = 0.044$, $\tilde{p}_{\mathrm{I}} = 0.049$. **b)** $w = 0.050$, $\tilde{w} = 0.22$, $\tilde{p}_{\mathrm{S}} = 0.042$, $\tilde{p}_{\mathrm{I}} = 0.045$. Cutoff for overall degree in NC matrices is $k_{\max} = 80$. MC simulations with $N = 5 \cdot 10^4$ nodes, $\langle k \rangle = 7$, initial ER graphs and initial prevalence $[I] = 0.6$. Statistics recorded at $t = 3000$ for 10^3 network realizations.

In the following, all bivariate stage and subensemble distributions will be contracted to distributions of just one variable in that manner. Results for a low- and high-rewiring regime in a network of average degree $\langle k \rangle = 7$ are presented in Fig. 4.2, with optimal correspondence parameters obtained from the conjugate-gradient method. For different choices of w, r and p in the stationary active phase, the NC stage distributions show very good quantitative agreement with subensemble distributions obtained from MC simulations. Higher rewiring rates in Fig. 4.2b clearly increase degree heterogeneity in comparison with Fig.4.2a.

Both figures underline the difference between subensemble DDs and ICDs: The former are compiled through sampling degrees at any stage of the node evolution, whereas for the latter, only newborn nodes are considered. The subensemble DD of I-nodes and the ICD of the S-ensemble match exactly as given by Eq. 3.31, so that only the former is plotted. In contrast, the ICD $\Phi_{\mathrm{I}}(k)$ of the I-ensemble is considerably skewed towards larger degrees, as becoming an infected node marks the turning point from gaining to losing links. From Eq. 3.29 it moreover follows that $\Phi^*_{\mathrm{I}}(0) = \Phi_{\mathrm{I}}(0) = 0$: Each newborn I-node has to have at least one neighbor, which is the I-node it got infected by.

As already shown for node and link densities in Fig. 2.3, the PA yields a good description of low-order motif densities in steady state for large parts of the active phase. This is also reflected by the accuracy of the moment closure for the relevant triplet densities in Eqs. 2.2 (Table 4.1).

	Pair Approximation	Node Cycle	Monte-Carlo Simulations
$[ISI]$	1.43 (1.32)	1.43 (1.31)	1.43 (1.30)
$[SSI]$	2.09 (3.80)	2.07 (3.72)	2.07 (3.72)

Table 4.1: Selected steady-state triplet densities as computed by the PA, NC and in MC simulations for parameter values in Fig. 4.2a (Fig. 4.2b).

4.3 Comparison of rewiring mechanisms

Two modifications of the original SIS rewiring mechanism are presented here to showcase the applicability of the NC. The first, media-driven rewiring (MR) introduced in [73], relates disease awareness to instantaneous knowledge of the *prevalence* $\tilde{i}$ (the fraction of I-nodes) through a rewiring rate $w \cdot \tilde{i}$ (w = constant). Hence in MR, a global time-dependent quantity is fed back to the rate of a semi-local rewiring mechanism[3]. The second modification, proposed in [74], suggests that S-nodes rewire links with a constant rate to a randomly selected node, regardless

[3]It would be fully local if the S-node that is rewired to was picked sufficiently "close" to the respective active link, as defined by the shortest path from either of the link's end nodes.

of the state of the latter. This blind rewiring (BR) is an antipode to the selective rewiring (SR) that was put forward in the original model in Sec. 2.1, with parametrizations interpolating between those two limiting cases acknowledging partial knowledge of other individuals' disease status in a population.

To model MR in the NC, the additional correspondence parameter $\tilde{i}$ has to be introduced, and all rewiring terms in Eqs. 3.6 and 3.7 must be rescaled by a factor $\tilde{i}$. The new parameter is also needed to properly describe an additional mean field necessary for BR. Since there an active link is rewired to an I-node with probability $\tilde{i}$, both rewiring terms in Eq. 3.6 for the S-stage need to be rescaled by a factor $\left(1-\tilde{i}\right)$ to represent "successful" rewiring to another S-node. In Eq. 3.7 for the I-stage, no such rescaling takes place, but its existing rewiring term ought to be complemented by adding $\tilde{w}\cdot\left(1-\tilde{i}\right)\cdot([x-1,y]-[x,y])$. This is because an I-node is assigned new susceptible neighbors with rate $w\cdot\tilde{i}\cdot[SI]/[I]$ due to "erroneous" rewiring, which at correspondence reads as $\tilde{w}\cdot\left(1-\tilde{i}\right)$ according to $\tilde{i}=[I]$ and the first of Eqs. 4.12.

Setting up cost functions

With $C_k(\langle k\rangle,\kappa)$ and $C_c(\kappa)$ (Eqs. 4.11 and 4.13) from Sec. 4.2 still being a valid set of cost functions for both MR and BR, $\tilde{i}=[I]^*$ should hold[4], which with Eq. 4.1 results in the additional cost function

$$C_i(\kappa)=\left(1-\frac{\tau_I^*/\left(\tau_S^*+\tau_I^*\right)}{\tilde{i}}\right)^2 \tag{4.16}$$

to be minimized. As previously discussed, the mean lifetimes in Eq. 4.16 are convoluted functions of model parameters $\mu=\{w,p,r\}$ and correspondence parameters $\kappa=\{\tilde{w},\tilde{p_S},\tilde{p_I},\tilde{i}\}$ evaluated entirely within the NC. Therefore in the two modified rewiring scenarios, the cost functions $C_k(\langle k\rangle,\kappa)$, $C_c(\kappa)$ and $C_i(\kappa)$ ought to be minimized to establish correspondence between the NC and the respective network model in DE. Taking Eqs. 4.1 however shows that at exact correspondence,

$$\frac{1-[I]^*}{[I]^*}=\frac{\tau_{\mathrm{S}}^*}{\tau_{\mathrm{I}}^*}=r\frac{1-[I]^*}{p\ [SI]^*}=\frac{r\ w}{p\ \tilde{w}} \tag{4.17}$$

where the second equality stems from Eqs. 3.4 and 3.30, while the third is derived from the first of Eqs. 4.12. Setting $\tilde{i}=[I]^*$ finally yields

$$\tilde{i}=\frac{1}{wr/\left(\tilde{w}p\right)+1} \tag{4.18}$$

so that for every optimal κ, $\tilde{i}$ is completely determined by the other correspondence and model parameters. This is assumed to also be approximately true at optimal[5]

[4]The reader is reminded that asterisks mark stationary NC distributions and averages that have been computed with unspecified correspondence parameters.

[5]The possibility of exact correspondence is discussed in Sec. 5.2.

κ, so that the search space for any optimization algorithm aimed at minimizing cost functions $C_k(\langle k\rangle, \kappa)$, $C_c(\kappa)$ and $C_i(\kappa)$ remains three-dimensional in both MR and BR. Evaluation of $C_i(\kappa)$ for $\tilde{i}$ given by Eq. 4.17 at optimal κ shows that this assumption is justified.

Comparing distributions

With a given set of model parameters and the mean degree specifying an adaptive network, the NC identifies the DEs and the corresponding sets of optimal correspondence parameters. For the three rewiring mechanisms, one can then extract the various probability distributions and averages described in Sec. 3.2, and compare them to the output of MC simulations (Fig. 4.3). Due to recovery being neighborhood-independent and happening at a constant rate in all three scenarios, Eq. 3.31 still holds, so that $P_{\mathrm{I}}(x, y) = \Phi_{\mathrm{S}}(x, y)$ also in BR and MR.

Since the iterative nature of the optimization procedure outlined in Chapter 4 makes the latter computionally expensive (see also Sec. 5.1), a relatively small cutoff of total degree k_{M} in NC transition matrices is convenient to identify DEs. However, properly modeling the degree evolution of a node with Eqs. 3.6 and 3.7 requires setting a sufficiently large k_{M}. Consequently, optimal κ obtained for low degree cutoffs may provide a slightly blurred correspondence between the NC framework and an adaptive network in DE, resulting in small deviations in distributions and averages as observed in Fig. 4.3.

For the model parameters and mean degree used in Fig. 4.3, both SR and BR are in the bistable phase [42, 74], with the respective DE chosen to be in the stable active branch. In contrast, MR is in its simple endemic phase for the same choice of parameters [73]. There, MR is equivalent to SR with the rewiring rate rescaled by a factor $[I]$. It follows that degree distributions and survival functions of those two rewiring mechanisms resemble each other (Figs. 4.3a-d), with the higher rewiring rate $w > w\cdot[I]$ in SR prolonging the S-stage, lowering overall prevalence and letting both subensembles sample large degrees in comparison with MR. The higher the overall steady-state prevalence, the more similar are those two rewiring scenarios.

For the same model parameters and mean degree, the DE in BR must feature an even higher prevalence than in the DE of SR, owing to the generally lower rate $w \cdot (1 - [I])$ of successful rewiring of S-nodes from infected neighbors. Under large $[I]$, successful rewiring happens on a much slower time scale than disease dynamics governed by model parameters p and r. Hence stage lifetimes are too short to let the typical node sample a wide range of degrees, so that ensuing subensemble distributions i) display smaller tails than their SR and MR counterparts ii) almost coincide.

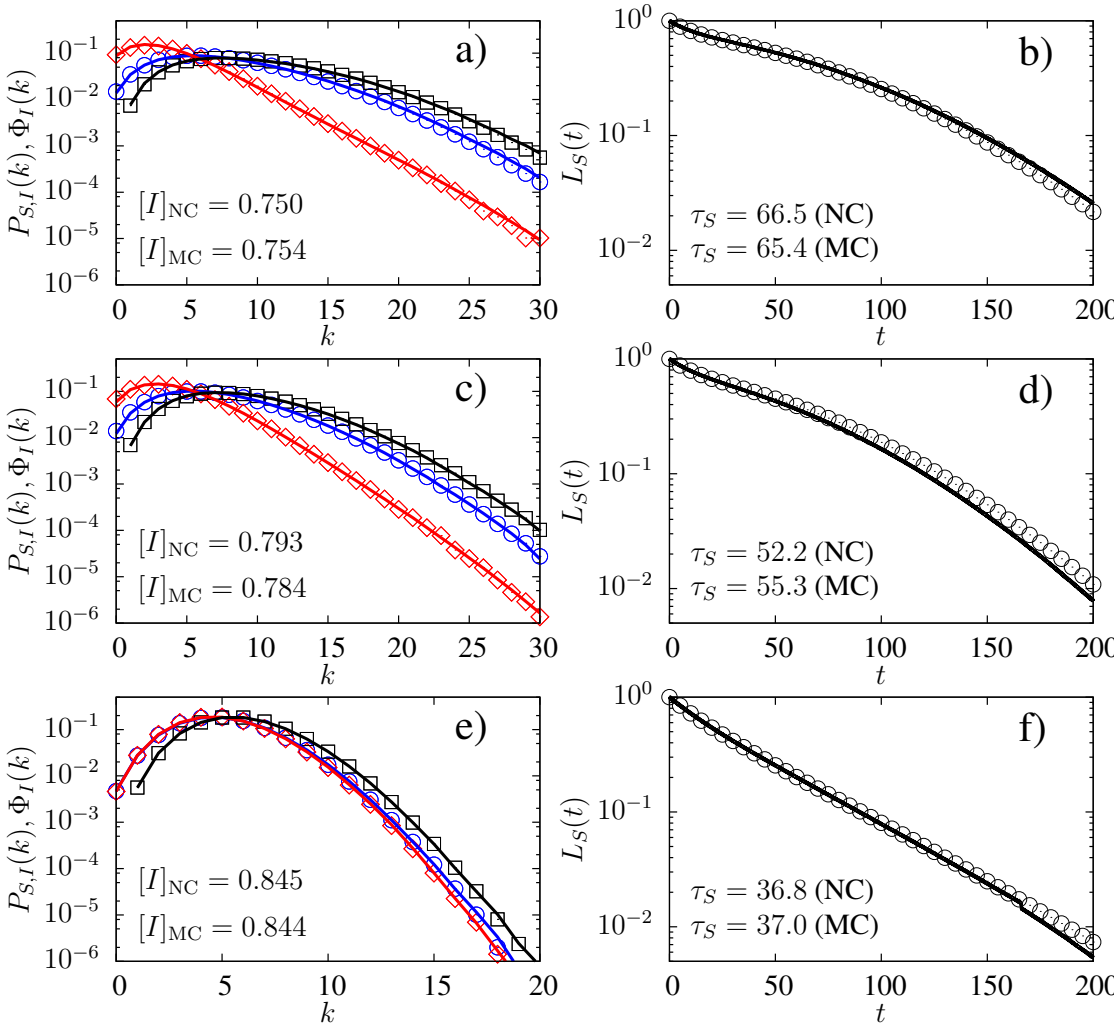

Figure 4.3: Characteristic distributions of a network in DE for SR (a)-b)), MR (c)-d)) and BR (e)-f)). Left column: Degree distributions for S-nodes (blue circles), I-nodes (red diamonds), as well as of initial degrees of I-nodes (black squares). Right column: Plots of survival functions of S-nodes. Solid lines are predictions by the NC. Insets: Comparison of prevalence $[I]_{\mathrm{MC}}$ taken from MC simulations and $[I]_{\mathrm{NC}}$ computed by in the NC (left column), and of mean S-lifetimes obtained from MC simulations and the NC (right column). $w = 0.05$, $p = 0.008$, $r = 0.005$; $\langle k \rangle = 5$, $k_{\mathrm{M}} = 80$. **a)-b)**: SR (stable active branch of bistable phase) with $\tilde{w} = 0.095$, $\tilde{p}_{\mathrm{S}} = 0.017$, $\tilde{p}_{\mathrm{I}} = 0.027$. **c)-d)**: MR (simple endemic phase) with $\tilde{w} = 0.12$, $\tilde{p}_{\mathrm{S}} = 0.022$, $\tilde{p}_{\mathrm{I}} = 0.031$. **e)-f)**: BR (stable active branch bistable phase) with $\tilde{w} = 0.17$, $\tilde{p}_{\mathrm{S}} = 0.026$, $\tilde{p}_{\mathrm{I}} = 0.035$. MC simulations with $N = 5 \cdot 10^4$ nodes, initial ER graphs and initial prevalence $[I] = 0.6$. Statistics recorded at $t = 3000$ for 10^4 network realizations.

As shown in Sec. 3.2, the subensemble survival functions (and the closely related lifetime distributions) provide an additional means to characterize a network in DE. While $L_{\mathrm{I}}(t) = e^{-r \cdot t}$ follows trivially from the constant recovery rate of I-nodes

in all three rewiring mechanisms, the exponential $L_S(t)$ in BR sets the S-ensemble apart from that of SR and MR (Fig. 4.3f). It implies an exponential lifetime distribution $T_S(t)$, indicating that the force of infection on a S-node in DE, and thus its number of infected neighbors, is approximately constant along its lifetime. Of the three processes that influence that number, both recovery and successful rewiring happen at very low rates compared to a S-node's lifetime (due to the large prevalence[6] $[I]$ in the case of rewiring). The contribution of the third process - conversion of susceptible into infected neighbors - is also small due to the small number of susceptible neighbors of a typical node: Neither in its S-stage (due to erroneous rewiring and slow recovery of infected neighbors) nor in the preceding I-stage (due to again a modest recovery rate and a large number of competing I-nodes at the receiving end of erroneous rewiring) can the node agglomorate a large fraction of susceptible neighbors. It follows that the change in the number of infected neighbors of S-nodes happens at a considerably slower time scale than infection of the S-node, and hence its neighborhood exerts an almost constant force of infection, explaining the exponential shape of $L_S(t)$ in BR.

4.4 Summary

Even without imposing correspondence between single-node and network dynamics in the adaptive contact process, some equalities that characterize ensemble behavior are extracted from the node-cycle framework. To eventually ensure correspondence in dynamic equilibrium, constraints for the choice of correspondence parameters are formulated. In the course of that, the existence and uniqueness of stationary ensemble distributions is tied to the mere occurrence of a few steady-state ensemble averages, a result valid for a wide class of adaptive networks.

Through the numerical evaluation of the cost function stemming from imposed constraints, single-node dynamics in the node cycle are made consistent with the network process, and all stable as well as unstable dynamic equilibria for given model parameters are detected. In addition, phase transitions are predicted, and the node-cycle framework is applied to two sets of model parameters, yielding a very good agreement with results from Monte-Carlo simulations.

Lastly, three different rewiring schemes in the adaptive contact process are considered and given an extensive node-cycle description. Computing steady-state degree distributions and lifetime profiles, the results derived from the node-cycle method are again found to match those taken from simulations. Differences between the dynamic equilibria of the different rewiring scenarios are made plausible within the node-cycle framework.

[6] The average lifetime of infected neighbors is $1/r = 200$ in Fig. 4.3f compared to $\tau_S \approx 37$.

5 ELABORATIONS ON THE NODE CYCLE

The node-cycle framework has been laid out in detail in Chapters 3 and 4, with other ansatzes occasionally mentioned, but not elaborated on. To fully place the NC in context with the research field of adaptive networks, crosslinks to other existing frameworks ought to be established and areas of competence identified. To facilitate this quest, a reformulation of the original framework shall be searched for to shed light on some of its previously overlooked aspects.

5.1 An alternative formulation

Instead of considering the random walk in each node stage separately as in Sec. 3.1, one can write down the Master equation for the composite random walk through all node stages. In the case of the adaptive SIS model, Eqs. 3.6 and 3.7 need to be given an extra term quantifying the inflow of probability mass from the respective other stage[1]. The ensuing coupled equations read as

$$\begin{aligned}\frac{\mathrm{d}[x,y]_\mathrm{S}}{\mathrm{d}t} =&(w+r)\{(y+1)\,[x-1,y+1]_\mathrm{S} - y[x,y]_\mathrm{S}\}\boxed{+r[x,y]_\mathrm{I}}\\ &- p\; y[x,y]_\mathrm{S} + \tilde{w}\,([x-1,y]_\mathrm{S} - [x,y]_\mathrm{S})\\ &+ \tilde{p}_\mathrm{S}\{(x+1)\,[x+1,y-1]_\mathrm{S} - x[x,y]_\mathrm{S}\} \end{aligned} \tag{5.1}$$

in the S-stage and in the I stage as

$$\begin{aligned}\frac{\mathrm{d}[x,y]_\mathrm{I}}{\mathrm{d}t} =&r\{(y+1)\,[x-1,y+1]_\mathrm{I} - y[x,y]_\mathrm{I}\}\boxed{+py[x,y]_\mathrm{S}}\\ &+ w\{(x+1)\,[x+1,y]_\mathrm{I} - x[x,y]_\mathrm{I}\} - r[x,y]_\mathrm{I}\\ &+ \tilde{p}_\mathrm{I}\{(x+1)\,[x+1,y-1]_\mathrm{I} - x[x,y]_\mathrm{I}\}\,, \end{aligned} \tag{5.2}$$

[1]The loss of probability mass is already considered in the original formulation of the NC.

with the influx term in each stage boxed and

$$\sum_{x,y=0}^{\infty} [x,y]_{\mathrm{S}} = 1 - [I]$$
$$\sum_{x,y=0}^{\infty} [x,y]_{\mathrm{I}} = [I]\,. \tag{5.3}$$

The bracket notation $[x,y]_{\mathrm{A}}$ defines the time-dependent probability of the random walker being at coordinates (x,y) and in stage $A \in \{S,I\}$. Note that in contrast to the conventional NC, the two subensemble DDs are not normalized anymore, but instead their sum is (Eq. 3.1 versus Eqs. 5.3).

Proceeding as in Appendix A.2, Eqs. 5.1 and 5.2 can be transformed into two coupled linear first-order PDEs of the respective generating functions that are very similar to the two PDEs of the NC. More precisely, Eq. 5.1 transforms into Eq. A.9 plus an influx term $r \cdot F_{\mathrm{I}}$, and Eq. 5.2 into Eq. A.18 plus $p \cdot \gamma \cdot \partial F_{\mathrm{S}}/\partial\gamma$. If this formalism is applied to the original coevolutionary voter model in [38], the coupled linear first-order PDEs can be disentangled by setting the inflow of probability mass into one stage equal to the outflow, something made possible by the symmetry of the model [75]. Consequently, the system can be analytically solved in the spirit of Appendix A.3. In the asymmetric adaptive SIS model however, the PDEs are decoupled only at the cost of obtaining two nonlinear second-order PDEs.

Solving a coupled system of linear first-oder or nonlinear second-order PDEs usually relies on numerical techniques, ruling out the occasional epiphanies of analytical solutions as in [75]. Obtained probability densities in the two stages yield the evolution of the full system from any given initial configuration, i.e. the full and subensemble DDs at any given time. One should keep in mind that these time-dependent probability densities differ from those defined in Eqs. 3.6 and 3.7 for the NC: The latter equations characterize different random walks for which the time scale only coincides with that in the full network if stationarity and correspondence are given.

The comprehensiveness of the solution of Eqs. 5.1 and 5.2 in the time domain comes with the drawback of the DE (if existent) only being described by the asymptotic shape of the subensemble DDs. As a consequence, the transformations in Fig. 3.2 still need to be employed to gain a more detailed account through the various stage distributions.

A second route

A variation on the approach above is to rewrite Eqs. 5.1 and 5.2 as

$$\frac{\mathrm{d}}{\mathrm{d}t}\begin{pmatrix}[x,y]_{\mathrm{S}}\\ [x,y]_{\mathrm{I}}\end{pmatrix} = \Lambda(x,y|x',y')\begin{pmatrix}[x',y']_{\mathrm{S}}\\ [x',y']_{\mathrm{I}}\end{pmatrix}. \tag{5.4}$$

Stationary states of the system consequently span the null space of the matrix[2] $\Lambda(x,y|x',y')$ that can be readily computed, since according to Eqs. 5.1 and 5.2, the entries of $\Lambda(x,y|x',y')$ are linear in model parameters as well as in its row and column indices x, y, x' and y'. Since Eq. 5.4 describes the same system as the original Eqs. 3.6 and 3.7, the existence and uniqueness of stage distributions in the NC imply the null space of $\Lambda(x,y|x',y')$ being one-dimensional. It yields the unique stationary distribution and thus the subensemble DDs.

The different strategies through which distributions are arrived at in the NC and in this ansatz are mirrored by the matrices used: In Eq. 5.4, $\Lambda(x,y|x',y')$ mediates the time evolution of the system, whereas in contrast the CST-matrix $\Phi(x,y|x',y')$ in Eq. 3.32 maps ICDs onto each other, also giving a very coarse-grained understanding of the system's temporal evolution (Sec. 5.2).

A deterministic interpretation

Besides giving a probabilistic account of a single node's state and degree evolution, Eq. 5.4 can also be interpreted deterministically to describe the node ensemble: The equations then yield the time evolution of the *abundance* of nodes in a given compartment $[X,Y]_{\mathrm{S,I}}$, the latter of which contains nodes of equal state and joint degree. The assumed equivalence of all nodes in the same compartment is the ensemble counterpart of assuming ergodicity in the node-state and degree evolution of a single node. Transitions between compartments in this deterministic interpretation are mediated by the same model and correspondence parameters as in the NC[3] (with κ again approximated by the mean fields given through Eqs. 4.12). In Sec. 5.2, this model correspondence will be elaborated on.

It is worth remarking that the deterministic interpretation is very similar to the so-called compartmental model of [65]. The only difference between these two frameworks is that in the compartmental approach, the mean fields in κ are now represented by time-dependent correspondence parameters that are computed en route from motif densities encoded in $[X,Y]_{\mathrm{S,I}}$, generally preventing an analytic treatment of the system.

[2] As before and according to Appendix A.4, order-four tensors and matrices are assumed to be encoded in matrices and vectors, respectively.

[3] Conversely, the NC is a stochastic interpretation of the deterministic model through letting single-node dynamics sample ensemble behavior.

The roadmap to the node cycle

In Chapters 3 and 4, the cornerstones of the NC were laid out. But inevitably, the actual research route included considerable meandering into yet unmentioned territory: Many ansatzes were either too approximate or flawed altogether. Following those additional research lines nonetheless guided the quest for feasible solutions and was instructive in its own right, deserving a honorable mention.

Setting up degree-class equations similar to [63] for SIS dynamics, recurrence relations for the subensemble DD's moments were obtained up to arbitrary order, with the respective DDs being extracted from them. In contrast to the ansatz in Sec. 2.3, these equations included certain motif densities whose (necessary) approximation was dependent on the age of involved S- and I-nodes, letting the notion of a node's lifetime arise for the first time [76].

While this hybrid approach combining ensemble and single-node statistics yielded unsatisfying results, it lead to focusing on a node's joint degree evolution in each of its stages. To enhance analytic treatment, the I-stage was further divided into two substages characterizing different regimes of degree loss of an I-node, and processes where neglected according to the substage type. Soon discarding this simplification, the time evolution of both the average number of susceptible and infected neighbors in each stage was written as two coupled ODEs, and solved exactly using matrix exponentials [77]. Closed-form solutions were obtained that depended on initial joint degrees as well as on processes exerted by the network background, the latter of which gave rise to the concept of correspondence parameters of Chapter 3 [76].

Trying to reproduce MC time series of a node's stage-dependent joint degree evolution, initial average joint degrees for both stages (the initial conditions for aforementioned closed-form solutions) were determined by considering a sequence of a S- and I-stage - a node cycle. Solving the ensuing self-consistency relations (and tuning the correspondence parameters by hand) again did not generate sufficiently accurate predictions. As a result, this fully deterministic model of a node's joint degree evolution was made partially stochastic i) through considering *distributions* in initial joint degrees (the ICDs in Chapter 3) and ii) later on by additionally allowing for the stage lifetime to be a random variable through heuristic expressions of lifetime distribution of each stage. Consequently an ICD of one stage was mapped onto the ICD of the subsequent stage through still deterministic degree evolution equations, with more elaborate self-consistency relations allowing for the computation of stationary ICDs. The subensemble DDs were related to the times the degree trajectories spent in each degree compartment, establishing a linear map of ICDs to DDs.

Not quite matching the ICDs generated by MC simulations, a fully stochastic process was decided on by modeling a node's degree evolution between two ICDs

as a random walk. The ensuing Master equations were transformed into Fokker-Planck equations with the step-operator formalism of [58], but the form of the latter equation did not allow for analytic treatment. By using the generating-function formalism of [58] instead, the NC framework was arrived at in its current form (as laid out in Chapters 3 and 4).

Furthermore, the computation of stationary DDs in the adaptive SIS model was carried out according to the spectral method presented in [78]. This method performs a change of random variables in a given Master equation, resulting in a system of equations that generally facilitates an iterative computation of stationary solutions with a subsequent back-transformation to the initial random variables. The particular structure of Eqs. 5.1 and 5.2 however ruled out a significant speed gain through that method.

5.2 Questions & answers

Chapters 3 and 4 introduced and applied the NC framework, and in Sec. 5.1, reformulations were presented. To ensure a proper understanding of the NC, more of its aspects are quickly highlighted in the following.

How can the NC be generalized?

To account for correlations beyond immediate network neighbors, the pairwise model from [42] can in principle be extended to a moment closure at the level of higher-order network motifs, at the expense of analytical tractability due to an increasing number of nonlinear ODEs involved. Similarly, the accuracy of the NC can be improved: Apart from modeling dynamics of a node's neighborhood, one could additionally keep track of i) the set of nodes whose shortest distance to said central node is 2 (its secondary neighborhood) or ii) the neighbors' neighbors. Note that ansatzes i) and ii) coincide only if there are no closed node triplets (i.e. triangles) in the network. In either case, computation times would drastically increase, as the number of entries of stage transition matrices reached k_{M}^8 entries in models with binary node space (Sec. 5.1).

Moreover, the NC can be applied to cyclic dynamics

$$S_1 \to S_2 \to ... \to S_{\mathrm{n}} \to S_1$$

with any number n of node stages and the increasing computational effort laid out above. A nontrivial extension of the framework is however needed to describe processes that are not strictly cyclic, e.g.

$$S_1 \rightleftarrows S_2 \to S_3 \to S_1 \,.$$

Nevertheless, such dynamics still can display DEs - the prerequisite for the emergence of DEs is merely that probability mass cannot get stuck in any node stage. Stage transition matrices would have to be set up differently to account for the outflow of probability mass from one stage to multiple others, and the CST-matrix mapping an ICD onto itself would not just be a product of the stage transition matrices .

Is it possible to describe transients?

Given optimal correspondence parameters κ, one can iterate the NC through taking an initial ICD and mapping it onto itself through repeated multiplication with the CST-matrix (Sec. 3.3). Through the number of iterations needed to reach a stationary ICD, combined with the knowledge of average stage lifetimes, transient times can be computed. This provides a description of the transients at a very coarse-grained level. An exact description is however not possible due to the following restrictions:

1. During the transient, the set κ in the entries of the CST-matrix refers to a network already in DE, and certainly assumes different values before reaching steady state. Hence the system is described with distorted correspondence. Yet this distortion is minor, because generally the network settles down much faster to conditions satisfying given κ than overall network topology does. Hence in that regard, it is possible to describe the topological evolution with constant correspondence parameter of already optimal value.

2. The system is by definition not stationary. Hence there is no ergodicity in node-state and node-degree evolution, and thus no valid description of the network domain within the NC domain.

3. The ICDs at the beginning and end of the transient generally cannot be assigned a network state (which is rather characterized by degree distributions): A DD yields a network snapshot at a certain instant in time, whereas an ICD does not, as it samples the starting degree of a certain node stage that is gone through asynchronously by the node ensemble. Consequently, one needs to compute DDs from initial and final ICDs according to the transformations in Fig. 3.2, each of which is again associated with an additional time interval in the full system.

4. Computing the transient behavior as above requires browsing κ-space and locating the DE that the NC will eventually settle down to. If however there are coexisting (stable) DEs, the transient modeling is further complicated by i) not knowing which set of optimal κ to use (if the final DE is unknown) and ii) not being able to quantify how the basins of attraction of the other DEs influence the transient of the system (see [79] for a recent treatment).

Can cost-function minimization be sped up?

In the case of large cutoff degrees k_{M} in the CST-matrix or a large number n of possible node states, the NC procedures laid out in Chapters 3 and 4 are computationally expensive: For each of the n node stages, the Master equation for the respective joint degree evolution is set up and solved for arbitrary μ and κ. For every κ considered, one subsequently computes n dense stage transition matrices with $\sim k_{\mathrm{M}}^4$ nontrivial entries each. A composite random walk through the n stages is described by the CST-matrix, i.e. the product of all stage transition matrices. The unique positive eigenvector of the CST-matrix yields a stationary probability distribution ($\Phi_{\mathrm{S}}^*(x,y)$ in the adaptive SIS model) and, among others, degree distributions in all stages. From those degree distributions, steady-state averages are extracted and fed into the cost function's evaluation at κ, allowing for function minimization and ultimately identifying optimal correspondence parameters for the system in DE.

The ansatz in Eq. 5.4 on the other hand delivers the essential degree distributions straightaway. The matrix $\Lambda(x,y|x',y')$ has $\sim n^2 \cdot k_{\mathrm{M}}^4$ entries, but is sparse unlike the CST-matrix $\Phi(x,y|x',y')$. Moreover, its nonzero entries are linear combinations of model and correspondence parameters, whereas its NC counterpart features elaborate expressions as in Appendix A.3. Therefore, cost function evaluation in the quest of optimal κ is sped up considerably when using Eq. 5.4. Once correspondence has been established, the stationary degree distributions can be transformed into ICDs and lifetime distributions according to Fig. 3.2.

Establishing correspondence between the NC and the network domain can still be cumbersome, involving the numerical minimization of a convoluted cost function to detect DEs. The search space spanned by the set κ of correspondence parameters can be prohibitively large, so that optimization techniques like gradient descent or the conjugate-gradient method may still converge slowly. On the other hand, Sec. 4.2 demonstrated that by classifying constraints into multiple sets and assigning a particular cost function to each of them, one can reduce the dimension of search space. Moreover, the resulting constraint-specific cost functions are less convoluted than the global one, and their roots can occasionally be given an approximate closed-form expression. An obvious aim is to find such expressions for the roots of all involved cost functions, so that then i) the need for numerical minimization is eliminated or greatly reduced and ii) the NC becomes a genuinely analytic framework.

Must correspondence parameters necessarily be constant?

The NC in its current form assumes that in each node stage in a network in DE, constant correspondence parameters κ are able to capture the interaction of

the network background with a typical node's neighborhood. The random-walk scenario outlined in Sec. 3.1 could in principle be formulated with coordinate- and time-dependent correspondence parameters. The time dependence of κ does not affect the transformation of the Master equations into PDEs of generating functions. Coordinate dependence on the other hand does, and if a PDE can nevertheless be obtained for each stage, it will then generally be of higher order and nonlinear. Analytically solving such a PDE with time-dependent coefficients is generally not possible. The CST-matrix $\Phi(x,..,z|x_0,..,z_0)$ will however still encode a time-homogeneous Markov chain that is ergodic, securing the existence and uniqueness of stage distributions extracted from an eigenvector calculation.

How important is a time-dependence of κ?

It has become clear in Sec. 5.1 that Eq. 5.4 can be interpreted as yielding the time evolution of node abundancies in compartments $[X,Y]_{\mathrm{S,I}}$. Due to its identical syntax, showing for the NC that time-independent κ can capture the DE network background translates into demonstrating that they do in the deterministic interpretation of Eqs. 5.4. As there is no external forcing of the network dynamics, any time-dependent κ can in principle be rewritten as a function of model parameters and motif densities up to the highest possible order[4], so that the explicit time dependence is turned into an implicit one (with Eqs. 4.13 being just low-order approximations). It will be made plausible further below that for a wide class of adaptive networks, DEs are all-encompassing, in that densities of motifs of any order settle down to a steady state. It follows that the reformulated correspondence parameters do, too - in the deterministic interpretation of Eqs. 5.4 and thus also in the NC. This argument also makes use of the equivalence of nodes in the same compartment, assuming that processes mediated by κ do not distinguish between them.

How relevant is a coordinate-dependence of κ?

While above it was argued that time-independent correspondence parameters can be assumed for a wide class of models, coordinate-dependent correspondence parameters are plausible: A node's neigborhood usually influences the set of secondary neighbors, which - encapsulated as correspondence parameters - in turn act back on the node's neighborhood. For all adaptive networks and parameter regions investigated, assuming coordinate-independence in κ already yielded an excellent description of network DEs. This indicates that for those networks in DE, degree and state correlations between nodes more than two links apart are either minuscule or insignificant for modeling the time evolution of joint DDs.

[4]Bounded by the finite size of the network under consideration.

How realistic is a variable κ during NC iteration?

Another scenario, related to the transient modeling discussed above, is that correspondence parameters could also be made dependent on the current count $m \in \mathbb{N}$ of an ongoing NC iteration. This would enable one to account for the changing network background experienced by a typical node during the transient, and result in a time-inhomogeneous Markov chain $\Phi_{\mathrm{m}}(x, .., z|x_0, .., z_0)$. The existence and uniqueness of stationary stage distributions would then have to be judged on from the particular form of the CST-matrix.

Is the NC applicable to dynamics on static networks?

If $w = \tilde{w} = 0$, a random walker in both stages of Fig. 3.1 is confined to paths with $(x + y) = k =$ constant. This is because now there is no typical node that samples the range of total degrees k, as those are fixed for every node. It follows that the CST-matrix is not irreducible anymore, the Markov chain it encodes not ergodic, and thus all following considerations in Chapter 3 on the NC break down. Similarly, the alternative NC formulation in terms of Eq. 5.4 becomes defunct, as the matrix' null space is not one-dimensional anymore.

Does the NC capture the ensemble symmetry in adaptive SIS?

In Secs. 2.2 and 2.3, the particular consequences of setting $w = p$ in the active phase of the adaptive SIS model were identified as i) the equality $P_{\mathrm{S}}(k) = P_{\mathrm{I}}(k)$ of subensemble distributions in *total* degree k ii) their Poissonian shape iii) the correct prediction of steady-state prevalence and mean subensemble degrees by the PA. The symmetry in i) is shown by MC simulations to be partial, as it does not extend to joint DDs, ICDs or lifetime distributions of the subensembles. Hence the degree-balance ansatz put forward in Sec. 2.3 is sufficient to capture the essence of i) and ii), while doing so within the NC framework seems highly nontrivial. A promising direction is to alter the generating functions in Eq. 3.8 to describe random walks in the contracted variable $k = (x+y)$, and to subsequently reformulate the NC to yield the observed symmetry at $w = p$.

What stochastic properties does the node cycle possess?

Through the Chapman-Kolmogorov identity in Eq. 3.33, the description of the composite random walk given by Eqs. 3.6 and 3.7 is simplified to just two coordinates in Eq. 3.32. This procedure is similar to introducing Poincaré maps for

flows in phase space [15], and enables one to easily confirm the stationarity of the reformulated stochastic process through considering the Perron-Frobenius vector of the mediating CST-matrix $\Phi(x, y|x_0, y_0)$ (see Sec. 3.3). Given $\Phi(x, y|x_0, y_0)$, the underlying stationary stochastic process could be investigated more thoroughly, judging on properties like detailed balance [58] to deepen the understanding of the node cycle.

What ergodic properties of the network process does the NC rely on?

In Sec. 4.1, two necessary conditions for the applicability of the NC were established. A rather technical one concerned cost-function optimization and was extensively dealt with in the subsequent chapter. The more fundamental condition was only briefly touched: To anchor the NC method on solid ground, every node in a network in DE should go through the same history of i) status change and ii) degree evolution. Infection and recovery ensure i) on every connected subgraph in DE, while random rewiring extends ii) to the whole network by eventually reconnecting any isolated subgraph in finite time. Since fulfilling i) implies that in DE every node undergoes perpetual state change, the random rewiring rule acts on every node in any state, ensuring ii)[5].

How comprehensive is a DE?

In Chapters 3 and 4 it was shown that for a wide class of adaptive networks in DE, steady-state node and link densities imply stationary joint-degree distributions, so that node-state and node-degree dynamics are the same for any node in the network. Given the nature of infection, recovery and rewiring in the adaptive SIS model, it is in fact reasonable to assume that no matter which node one picks to observe surrounding DE dynamics from, the entire network will be seen to evolve the same way. This is corroborated by MC simulations in which also higher-order motif densities reach stationary values in DE. Hence all ensemble measures seemingly settle down to a steady state - the DE is *maximally comprehensive*.

A more thorough investigation of DE comprehensiveness could involve the *graphicality* of motif sequences imposed on a network (as already applied in [80] in another context). Given a stationary distribution of motifs of a certain order[6], is it realizable, i.e. are there any network configurations compatible with that

[5]Interestingly, property i) does not extend to *link-type* dynamics in DE, i.e. generally $\tau_{\mathrm{AB}}/\sum_{(\mathrm{I,J})}\tau_{\mathrm{IJ}} \neq 2\cdot[AB]/\langle k\rangle$, with index duplets (I, J) summing over all link types.

[6]In the particular case of the configuration model, a sequence of star motifs is imposed - the familiar degree distribution.

motif sequence? If so, how many? Surely increasing the motif order in imposed sequences drastically reduces the number of compatible network configurations, especially when prohibiting self- and double-connections of nodes. The decreasing number of possible network realizations would hence increasingly constrain the shape of even higher-order motif distributions the network can possess, making a plausible case for a maximally comprehensive DE if the stationarity of motif distributions of sufficiently high order has been established.

5.3 Comparison to other frameworks

Adaptive networks in the active phase have been treated analytically when time scales of node dynamics and topology evolution are separable [81, 82, 83]. For fast network dynamics in the context of evolutionary games, it was shown that the node states evolve according to an effective pay-off matrix that takes into account the equilibrium network properties [81, 82]. For the more general case that permits similar time scales, two equation-based frameworks taking the contact process as the underlying dynamics have so far been put forward apart from the NC.

One is the familiar pairwise formalism of [42] and related frameworks [43, 84, 74], where the time evolution of network motif densities is modeled up to the level of pairs, with description of highest-order motifs relying on the standard pair approximation moment closure assumption. As shown in Chapter 2, this yields a low-dimensional set of ODEs that allows for analytic treatment, predicting system phases and pair densities in transients and DE with an accuracy limited by moment closure validity. Approximate phase diagrams are also derived in the scope of even simpler effective mean-field descriptions [74]. While this type of models gives a global account of the network in DE through averages that characterize steady-state dynamics, their low number of degrees of freedom precludes any detailed description of the network's topology. The PA approach for the contact process in Sec. 2.1 was extended to a three-state model (the Susceptible-Infected-Recovered-Susceptible cycle) describing more realistic infection dynamics [85]. This model, too, displays a stationary active phase, and simulations in DE also converge to well-defined overall and state-specific degree distributions. In [85], an attempt is laid out to describe the topology of the network by translating the pairwise dynamics of [42] to a degree-class formulation similarly to the ansatz in [63]. This approach yields a self-contained method to determine the degree distributions of all three node types, but fails to reproduce the observed output of MC simulations. Given however the infected degree distribution extracted from simulations, the two remaining distributions are accurately described.

The second class of analytic frameworks previously put forward to tackle DEs in adaptive networks is the compartmental model. Elaborating on a state- and

degree-based compartmental formulation developed earlier [68], Marceau et al. in [65] modeled the time evolution of fractions of nodes with the same state and joint degree (see Sec. 5.1). In the spirit of the moment closure in the PA ansatz, infection dynamics beyond a node's immediate neighborhood are approximated by a mean field that is computed en route and assumes no correlations beyond the level of next neighbors. A large set of coupled nonlinear ODEs ensues that defies analytic treatment. Instead, numerical integration yields the time evolution of the joint degree distribution, as well as of low-order network motif densities derived from it. This approach provides an alternative to stochastic simulations on networks for the description of the DE, with the same limitations due to transient's length and the additional loss of accuracy involved in the mean field approximation.

A third, semianalytic approach goes back to the original formulation of Eqs. 2.2. It avoids any moment-closure approximation in the numerical integration of the ODEs by computing the triplet densities at each integration step through short bursts of MC simulations on networks [73]. Much like [85], this hybrid approach gives a more precise ODE-based description of the system than its purely deterministic counterpart. It accurately reproduces the time evolution of the network's node and pair densities, and hence also the global phase diagram, but it brings no improvement regarding the analysis of the steady-state degree distributions.

The DE's comprehensiveness observed in the adaptive SIS model extends to MC simulations of various adaptive networks in DE, showing that apart from global averages and degree-related probability distributions, a wide range of other topological measures settle down to an equilibrium. The most comprehensive description of DEs in frameworks like the compartmental model or the NC is at the level of configuration model networks, implying that only the topology measures determined by the joint degree distributions can be derived. To this point, a more extensive account of steady-state topology has to resort to modeling the time evolution of the network's adjacency matrix or a related construct [86]. In [87] however, the steady-state community structure of a general class of adaptive networks in DE was characterized by a simple ODE.

Identifying areas of competence

By construction, the pairwise model introduced in Sec. 2.1 is too coarse-grained to distinguish between some vital differences in rewiring mechanisms, whereas more local frameworks like the compartmental model or the NC can accommodate those changes that do alter the ensuing steady-state topology. This can be illustrated with the different rewiring mechanisms of the adaptive SIS model presented in Sec. 4.3: If an active link has been cut in the original SR scenario, adding it between two randomly selected susceptibles instead of classically rewiring it to just one implies a different random walk in the NC than Eqs. 3.6 and 3.7 give,

and hence altered degree distributions extracted from them. The equations of the pairwise model however cannot account for this change in rewiring mechanism and remain equal to those describing the SR scenario. Likewise, BR reduces like MR to a rescaled SR in Eqs. 2.2, whereas in the NC and the compartmental model, that structural difference between BR and SR is correctly accounted for.

Conversely, the NC in its current form is, unlike the two ODE-based models, not designed to capture active phase dynamics other than DEs. In its essence, it lets the long-term behavior of a single node self-consistently generate node-ensemble statistics, so that oscillatory or more complicated non-stationary regimes in the network domain are averaged out in the NC domain and cannot manifest themselves in stage distributions. But similar to the pairwise model, the NC can indicate a global frozen phase for given model parameters μ: When its different cost functions do not display overlapping minima, no self-consistent embedding of single-node dynamics in a network in DE exists, so that either a more complicated regime in the active phase or a frozen phase is at hand (see Fig. 4.1b).

	Pairwise Model	**Compartmental Model**	**Node Cycle**
subtle changes in elementary processes	insensitive	sensitive	sensitive
transient modeling	numerical	numerical	-
DE uniqueness	explained	-	explained
DE comprehensiveness	-	-	explained
DE detection	analytical	(numerical)	(analytical)
DE description	$[A]$, $[AB]$, $[ABC]$, τ_{A}, τ_{AB}	$[A]$, $P_{\mathrm{A}}(x,y)$	$[A]$, $P_{\mathrm{A}}(x,y)$, $T_{\mathrm{A}}(t)$, $\Phi_{\mathrm{A}}(x,y)$
DE stability	stable/unstable DEs detected, described, distinguished	stable DEs detected, described	stable/unstable DEs detected, described

Table 5.1: Comparison of frameworks capturing DEs in adaptive networks. Node-state densities $[A]$ and subensemble joint degree distributions $P_A(x,y)$ encode link densities $[AB]$, higher-order star motif densities as well as mean node-state and link lifetimes, with A and B assuming any value in node-state space. For every node stage A, $T_A^*(t)$ and $\Phi_A^*(x,y)$ are the stage lifetime distribution and joint distribution of initial degrees, respectively. Identifying DEs with the compartmental model is subject to the usual limitations of numerical integration, whereas for the NC, cost functions are computed analytically and minimized with standard optimization techniques.

Table 5.1 contrasts the three main modeling frameworks analytically dealing with dynamic equilibria in adaptive networks. As the ansatz [75] briefly presented in Sec. 5.1 is essentially contained in the NC framework, and its closed-form solution just obtainable for symmetric coevolutionary dynamics, it is left out of consideration.

5.4 Summary

An alternative, faster route is laid out to obtain steady-state characteristics of adaptive networks. This is achieved through a reformulation of the original node-cycle ansatz, bearing resemblance to a deterministic description of node-ensemble dynamics.

Secondly, the presentation of the node-cycle framework is rounded up by shedding light on its limitations and possible modifications.

Lastly, several frameworks of the same aim are introduced. The node cycle's scope of description of dynamic equilibria is compared with that of both the compartmental and the pairwise model, and areas of competence for each of the descriptions are identified. Moreover, the overall research route towards the current formulation of the node cycle is presented in a condensed form.

6 ASYMMETRIC COEVOLUTIONARY OPINION DYNAMICS

The adaptive contact process dealt with in Chapters 2 to 5 has some appealing properties, making it a fitting testing ground for formalisms of coevolutionary dynamics: i) A binary node-state space and three parameters that already yield various dynamical regimes. ii) A large metastability of DEs in simulations, as there is just one absorbing state stochastic fluctuations can drive the system to. Consequently DEs can be reliably sampled in already moderate system sizes. iii) An asymmetric rewiring mechanism that generally induces degree heterogeneity and node-state clustering in the network, accounting for strong correlations that let the DE deviate considerably from respective null models.

Another simple example of an adaptive network is the coevolutionary variant [38] of the classic voter model [88], mimicking the spreading of two opinions in a population whose members strive for homophilic interactions. Its dynamics feed entirely on active links connecting the two competing node types[1], and can be implemented in the following ways:

In the node-update scheme of the model, at every time step a node A and one of its neighbours B are randomly picked. If the link connecting them is active, then in the direct (reverse) node-update, node A (node B) rewires it with probability ω to another randomly selected node of the same type or adopts the state of node B (node A) with probability $(1-\omega)$. If however the link is inert, i.e. connects two nodes of the same type, nothing happens.

For the coevolutionary voter model with link update, a random link is picked. If it is inert, nothing happens. If it is active, one of its two end nodes is randomly chosen. Then, this node rewires that link with probability ω to an arbitrarily picked node of the same type or adopts the state of the node at the other end of the link with probability $(1-\omega)$.

[1] In the adaptive SIS model on the other hand, only infection and rewiring operate on active links, while the recovery rule acts on nodes.

The ensuing dynamics are completely symmetric in node states, with the update schemes yielding similar outcomes [54], yet with one major difference: For link update, the average network magnetization - the difference in the two fractions of nodes types - is conserved. In contrast, it is just conserved under node update if the network's degree distribution is sufficiently homogeneous, while it is not otherwise [89].

There exist numerous variations of the adaptive voter model, including blind rewiring as introduced in Sec. 4.3 [90] and update rules acting globally instead of just in a node's neigborhood [39]. In the following, the symmetry of the coevolutionary voter model (referred to as *symmetric model*) will be broken by assigning different update schemes to different node ensembles and moreover by introducing a bias for the rewiring rule. The idea is that the two opposing opinions are associated with different social attitudes, which translate into different strategies to promote consensus in their holders' local environment.

6.1 The model and its asymptotic states

The asymmetric coevolutionary voter model

Denoting the fraction of I-nodes by x, three elementary processes shall give rise to asymmetric adaptive opinion dynamics. Rewiring and infection (now referred to as transmission in the context of opinion dynamics) are employed and parameterized as in the adaptive SIS model, so that the S-ensemble engages in the same dynamics as laid out in Sec. 2.1. Equivalently, the S-nodes undergo the coevolutionary voter dynamics of [38] under a link-update scheme.

The third process in contrast describes opinion adoption in the I-ensemble and is based on the node-update scheme: In relaxation, randomly selected I-nodes shall relax to S-nodes with rate $(1-\omega)(1-\rho)(1+a\cdot m)$. This resembles the recovery rule in Sec. 2.1, but now the factor $(1+a\cdot m)$ lets the network magnetization $m \equiv (1-2\cdot x)$ ($m \in [-1,1]$) steer the rate of the process, with $a \in [0,1]$ quantifying the coupling of relaxation to m. Hence the relaxation of I-nodes is boosted by a strong (global) presence of S-nodes, whereas it is diminished by a dominance of I-nodes. Consequently, opinion adoption among I-nodes also resembles classic voter dynamics with (direct) node update, with the difference being that it is guided by overall network magnetization, not the magnetization of the neighbourhood of the respective I-node. It can therefore be seen as a mean-field description of the latter process.

These three processes set up an interplay of link-update coevolutionary voter dynamics with mean-field node-update voter dynamics by tying each to a specific node ensemble and letting those compete. The ensemble-specific update schemes

shall reflect two competing spreading strategies in a population: Segregationist S-nodes are orthodox opinion holders that spread their opinion via social pressure and strive for local consensus by seeking to interact with their peers. Proselytic I-nodes engage with and convert S-nodes in personal interactions, and their heterodox opinion relaxes to the S-ground state at a rate that reflects the overall dominance of that opinion. While biased voter dynamics have been put forward through different rates of opinion adoption [91] or interactions along directed links [92, 93], the asymmetric dynamics outlined above are a result of differing adoption strategies, their differing rates, as well as the biased rewiring rule described above. The dynamics are moverover reminiscent of the adaptive SIS model, in that in the latter I-nodes relax with a constant rate (retrieved through setting $a = 0$), while transmission and rewiring are as described above.

The PA description

As in Sec. 2.1, a coarse-grained description of the network process is achieved by its pairwise approximation, again featuring the parameter η that encapsulates the width of the underlying network's degree distribution (see [54] for a review). For the asymmetric opinion dynamics introduced above, the relevant link densities y and z refer to II-links SI-links, respectively[2]. Like in the adaptive SIS model, rewiring ensures link-number conservation, so that the density of SS-links is given by $(\langle k\rangle/2 - y - z)$ for $0 \leq (y + z) \leq \langle k\rangle/2$ and fixed mean degree $\langle k\rangle$. The PA of the process then yields

$$\begin{aligned}
\frac{\mathrm{d}x}{\mathrm{d}t} &= (1-\omega)\left(\rho z - (1-\rho)\boxed{r_\mathrm{a}}x\right)\\
\frac{\mathrm{d}y}{\mathrm{d}t} &= (1-\omega)\left(\rho z\left(\eta\frac{z}{1-x}+1\right) - 2(1-\rho)\boxed{r_\mathrm{a}}y\right)\\
\frac{\mathrm{d}z}{\mathrm{d}t} &= -z\left(\omega + (1-\omega)\left(\rho + (1-\rho)\boxed{r_\mathrm{a}}\right)\right) - (1-\omega)\rho\eta\frac{z^2}{1-x}\\
&\quad + 2(1-\omega)(1-\rho)\boxed{r_\mathrm{a}}y + 2(1-\omega)\rho\eta\frac{(\langle k\rangle - y - z)\,z}{1-x}
\end{aligned} \tag{6.1}$$

with $r_\mathrm{a} = 1 + a(1 - 2\cdot x)$, similar to Eqs. 2.2 for the adaptive SIS model. The last term of the time evolution of z in Eqs. 6.1 for instance describes the gain in SI-links through the infection of either end of an SS-link. In that case, the crucial density of the relevant triplet motif (consisting of a central S-node connected to both a S- and an I-node) is approximated using the densities of the aforementioned link types and of S-nodes, analogously to Eq. 2.1.

As in the adaptive SIS model, link aquisition and opinion adoption are tailored to specific node ensembles, so that highly-skewed degree distributions can ensue for

[2]In the following, this compact notation will prove helpful when analytically investigating the dynamics of the model.

a wide range of parameters (see Sec. 4.3). For that reason, instead of the regular random graphs taken in [38, 94], initial ER graphs in MC simulations and $\eta = 1$ in the PA are again decided for. As will become apparent, the PA sufficiently captures the corresponding network process with that choice of η.

Choosing $0 < a < 1$, i.e. an intermediate coupling of relaxation to network magnetization, the same system phases as in the adaptive SIS model ensue (Fig. 6.1). The simple endemic phase however shrinks considerably, while the simple bistable and stable oscillatory regimes are widened significantly.

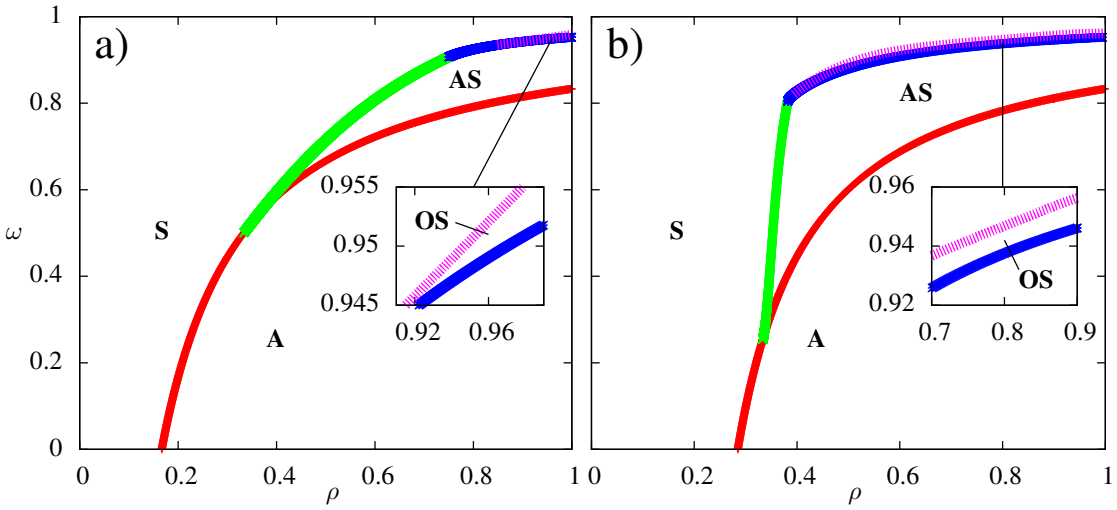

Figure 6.1: Phase diagram of **a)** adaptive SIS **b)** asymmetric coevolutionary opinion dynamics with $a = 0.99$. Transcritical bifurcations (red line), fold bifurcations (green line), Andronov-Hopf bifurcations (blue line) and cycle-fold bifurcations (purple line) mark the following phases: S-consensus (**S**), simple active phase (**A**), simple bistable phase (**AS**), oscillatory bistable phase (**OS**, insets). Mean degree $\langle k \rangle = 5$, compiled with [61].

Since within $0 \leq a < 1$ system dynamics is qualitatively the same as in the adaptive SIS model, $a = 1$ for all further discussions to fully couple the relaxation of I-individuals to the composition of the population. Any reference to Eqs. 6.1 will also imply the choice $a = 1$ and labeled *asymmetric model*. Moreover, the long-term behavior of the dynamics will be focused on and compared to the asymptotic scenarios of the symmetric model.

Asymptotic states in the PA

Denoting the state vector of Eqs. 6.1 as (x, y, z) with $x \in [0, 1]$, $y \in [0, \langle k \rangle/2]$ and $z \in [0, \langle k \rangle/2 - y]$ yields the two (frozen) S- and I-consensus states $(0, 0, 0)$ and $(1, \langle k \rangle/2, 0)$, respectively. It is straightforward to check that these are equilibria

for Eqs. 6.1. A linear stability analysis of the PA in Appendix A.5 reveals that S-consensus is stable for

$$\rho \leq \frac{2-\omega}{(2+\langle k\rangle)\,(1-\omega)}\,. \tag{6.2}$$

As the PA equations are singular at $(1, \langle k\rangle/2, 0)$, one needs to resort to regularization techniques to obtain

$$\rho > \min\left(\frac{2}{1+\langle k\rangle}, \frac{2-3\omega}{1-\omega}\right) \tag{6.3}$$

as the parameter region for stable I-consensus (see Appendix A.5). Note that if $0 \leq a < 1$, I-consensus is not an absorbing state.

Apart from a frozen phase, the PA yields a DE for a small parameter region

$$\frac{2-\omega}{(2+\langle k\rangle)\,(1-\omega)} \leq \rho \leq \frac{2}{1+\langle k\rangle} \tag{6.4}$$

bordering the two consensus states. In this region of intermediate ρ and small ω, relaxation and transmission balance out, with the small rewiring rate allowing for the continued existence of a nonzero density of active links and a steady-state fraction of I-nodes of

$$x_{\mathrm{A}} = \frac{2-(2+\langle k\rangle)\rho(1-\omega)-\omega}{\omega-\rho(1-\omega)}\,. \tag{6.5}$$

The system's only active phase ensues, whose size in the phase diagram shown in Fig 6.2a decreases for increasing mean degree $\langle k\rangle$. For $x_{\mathrm{A}} = 1/2$ (the dashed line in Fig. 6.2a), the magnetization of the system in steady state is zero while still in the active phase, so that I-nodes relax with constant rate r and the PA describes the DE of the adaptive SIS model at the respective parameters.

The triple point T in Fig. 6.2a at

$$\begin{aligned}\rho &= \frac{2}{1+\langle k\rangle} \equiv \rho_{\mathrm{T}}\\ \omega &= \frac{2}{3+\langle k\rangle} \equiv \omega_{\mathrm{T}}\end{aligned} \tag{6.6}$$

lies at the confluence of the active and the two absorbing phases. It marks the end of the active phase and the advent of a bistable regime of coexisting consensus states for faster rewiring, with ρ tuning the competition of the latter's basins of attraction.

The subensemble mean degrees in DE are given by the PA as

$$\begin{aligned}\langle k_{\mathrm{S}}\rangle &= \frac{2-2\rho(1-\omega)-\omega)}{\rho(1-\omega)}\\ \langle k_{\mathrm{I}}\rangle &= \frac{2}{\rho}-1\,,\end{aligned} \tag{6.7}$$

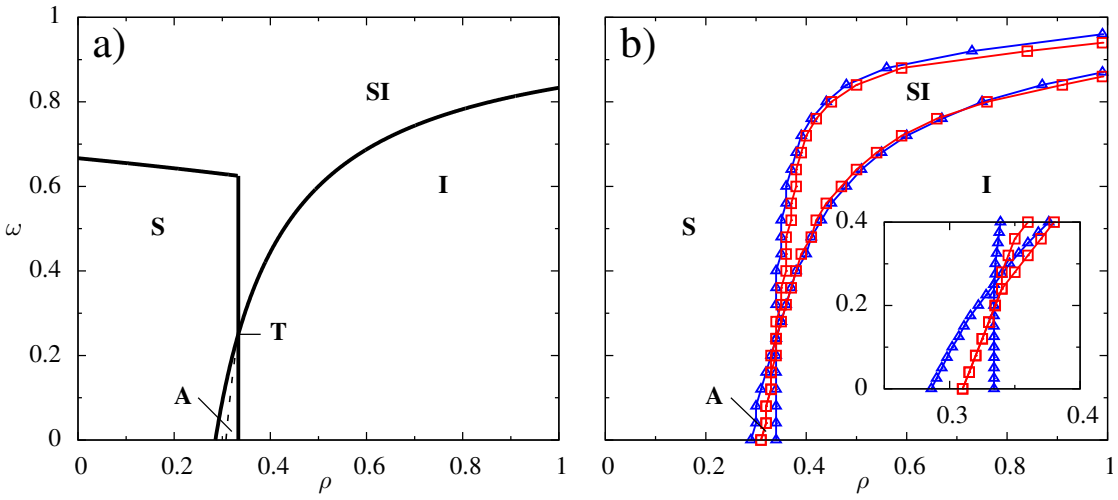

Figure 6.2: **a)** Phase diagram with steady states S-consensus (**S**), I-consensus (**I**) and the active phase (**A**), as well as the triple point **T**, bounded by solid lines. A sequence of symbols indicates the coexistence of respective attractors. The dashed line $x_A = 1/2$ yields DEs of adaptive SIS for respective parameter values. **b)** Change of asymptotic behavior in the PA with initial conditions $(0.1, 0.025, 0.45)$, $(0.5, 0.625, 1.25)$ and $(0.9, 1.025, 0.45)$ (numerical integration of PA, blue triangles) and initially connected ER graphs with fractions 0.1, 0.5 and 0.9 of randomly assigned I-states (MC simulations, red squares). Regions of equal asymptotic behavior are marked by the same sequence of symbols as in a). For sufficiently long simulation runs, stochastic fluctuations in the metastable state drive the full system into S- or I-consensus (inset of b)). Mean degree $\langle k \rangle = 5$, MC simulations with $N = 5000$ nodes and results averaged over 100 realizations.

with Eq. 2.7 from the adaptive SIS model also applying here. Throughout the active phase, $\rho \leq \omega/(1-\omega)$ holds, with the equality fulfilled only at the triple point. It follows that in steady state, the mean degree of the S-ensemble is not larger than that of the I-ensemble, despite the rewiring bias towards S-nodes.

Comparison to the stochastic network process

To properly compare the PA with MC simulations, one has to faithfully translate network configurations into PA state vectors. An ER graph with a fraction x_0 of randomly primed I-nodes is captured by the PA as

$$(x, y, z) = (x_0, \langle k \rangle x_0^2/2, \langle k \rangle (1 - x_0) x_0) \,.$$

Initial conditions in all MC runs are set this way and translated into the PA formalism accordingly. To let the PA capture the finite size of networks with N nodes and $N \cdot \langle k \rangle/2$ links, integration of Eqs. 6.1 is stopped as soon as $x < 1/N$ or $1 - 1/N < x$, emulating the two possible frozen consensus states in a network.

Furthermore, it is important to identify "pathological" network configurations and avoid them altogether. If for instance MC simulations without rewiring ran on networks with isolated S-subgraphs (consisting of only S-nodes), I-consensus could not be reached, as these subgraphs would be left untouched by network dynamics. This would moreover add a constant offset to the network's magnetization that distorted relaxation. Consequently, "natural" system dynamics without rewiring can only unfold when taking place on a connected network. For consistency reasons, procedures ought to be implemented that avoid fragmentation of initial random networks for all ω, without ruling out later fragmentation in the course of coevolutionary dynamics.

Since $\langle k \rangle < \log(N)$ for mean degrees $\langle k \rangle$ and system sizes N used in MC simulations here, an initial ER graph is almost surely fragmented [26]. Its isolated subgraphs need to be linked through i) linking two randomly selected nodes from separate subgraphs ii) randomly picking a node that emanates links of the same type added in i), randomly choosing and deleting one of them iii) repeating i)-ii) until the graph is connected. Because the initial ER graph has a Poissonian degree distribution, a lower limit on its number of disconnected components can be given through $e^{-\langle k \rangle} \cdot N$, where $e^{-\langle k \rangle}$ is the average fraction of isolated nodes. For the values of $\langle k \rangle$ and N used, this lower limit approximates the actual number of initially disconnected subgraphs very well. Thus the fraction of nodes involved in this linking procedure is very small. The procedure neither introduces correlations in node state nor degree, so that apart from the vanishing isolated nodes, the main characteristics of an ER network are preserved. All initial networks used in the following MC simulations are connected this way.

The possible coexistence of asymptotic states necessitates taking into account their competing basins of attraction. Selecting a sufficiently large set of initial conditions and monitoring the resulting asymptotic behavior of the system allows for the detection of all basins of attraction, both in integration of Eqs. 6.1 and MC simulations. Browsing parameter space with this procedure would lead to a comparison of the phase boundaries of Fig. 6.2a with their MC analogue. Instead, regions in parameter space are identified for which a given small set of initial conditions lets dynamics drive the PA and the full system into the same set of asymptotic states. Comparing such parameter regions resulting from integration of Eqs. 6.1 to those obtained from MC simulations allows for a quantitative comparison of PA dynamics and the corresponding network process without having to verify phase boundaries of Fig. 6.2a.

This coarse-grained browsing of initial conditions over the whole parameter space yields a good agreement between numerical integration of the PA and MC simulations (Fig. 6.2b), so that for initial (connected) ER graphs, the PA faithfully models the actual dynamics. A SI-parameter region in that context means that either S- or I-consensus can be reached from the set of initial conditions, whereas

regions S, I and A signal a uniform asymptotic behavior leading to S-consensus, I-consensus and a DE, respectively. In MC simulations, a metastable DE is observed for parameter values of the PA's active phase. In it, stochastic fluctuations eventually drive the system into one of the two consensus states. A more thorough PA description of the active phase, as well as a stochastic modeling of the corresponding metastable DE in the network process, will be given in Sec. 6.2.

6.2 Metastability in the active phase

For Eqs. 6.1 in the active phase, transient dynamics are reminiscent of what is reported from the symmetric model [38], in that the deterministic system quickly relaxes to a parabola-shaped curve M_D. Yet in contrast to [38], M_D is generally not a line of equilibria, but spanned by two heteroclinics connecting the stable node (the DE) with the saddles that represent the unstable consensus states. Once driven to M_D, the system slowly advances along the respective heteroclinic towards the DE (Fig. 6.3a). Strictly speaking, M_D is not a slow manifold, as the latter is associated with a degenerate eigenvalue of the linearized flow, while the DE is linearly stable throughout the active phase (except at the triple point). In the following, the definition is widened to any set of trajectories that the flow quickly relaxes to and then slowly proceeds along towards an attracting fixed point.

The "slow manifold" M_D is well-approximated by a curve M_A given by

$$M_\mathrm{A} = \begin{pmatrix} x \\ y_\mathrm{A}\{x\} \\ z_\mathrm{A}\{x\} \end{pmatrix} = \begin{pmatrix} x \\ x\frac{2x(x-\langle k\rangle)-2+\omega(1+(3+2\langle k\rangle-4x)x)}{2(\omega+\omega x-2)} \\ 2(1-x)x\frac{\langle k\rangle(\omega-1)+\omega+x-2\omega x}{\omega+\omega x-2} \end{pmatrix} , \tag{6.8}$$

with $y_\mathrm{A}\{x\}$ and $z_\mathrm{A}\{x\}$ being the equilibrium values of link densities y and z for a steady-state x. It follows that M_A is the set of all DEs that, for fixed $\langle k\rangle$ and $\omega < \omega_\mathrm{T}$, are generated by all ρ for which the system is in the active phase (given by the interval in Eq. 6.4). Thus the shape of M_A does not depend on ρ.

As ρ enters this interval from smaller values that lead to S-consensus, a transcritical bifurcation turns the stable node in $(0,0,0)$ into a saddle, emanating a stable DE that is moving along M_A. It reaches $(1,\langle k\rangle/2,0)$ at $\rho = \rho_\mathrm{T}$ and, in another transcritical bifurcation, vanishes while turning the saddle into a stable node representing I-consensus.

For $M_\mathrm{A} = M_\mathrm{D}$, the PA vector field along M_A must be tangent to M_A. Thus

$$\left[\left\|\begin{pmatrix}\dot{x}\\ \dot{y}\\ \dot{z}\end{pmatrix}\right\|^{-1}\begin{pmatrix}\dot{x}\\ \dot{y}\\ \dot{z}\end{pmatrix}\right]_{\substack{y=y_\mathrm{A}\{x\}\\ z=z_\mathrm{A}\{x\}}} = \pm\left\|\begin{pmatrix}1\\ \partial y_\mathrm{A}\{x\}/\partial x\\ \partial z_\mathrm{A}\{x\}/\partial x\end{pmatrix}\right\|^{-1}\begin{pmatrix}1\\ \partial y_\mathrm{A}\{x\}/\partial x\\ \partial z_\mathrm{A}\{x\}\partial x\end{pmatrix} \tag{6.9}$$

for $x \in [0, 1]$ according to Eqs. 6.1. Since in the active phase, the fixed point at coordinates $(x_\mathrm{A}, y_\mathrm{A}, z_\mathrm{A})$ is stable, the plus sign on the right-hand side should hold for all $x < x_\mathrm{A}$, and the minus sign otherwise. In general, Eq. 6.9 is not fulfilled, and hence M_A is not a trajectory of the system. It is however straightforward to show that this matching improves for increasing $\langle k \rangle$ and ω, while it is already very good for the low mean degrees and rewiring rates considered here. As a first approximation, the description of the latter stages of system evolution towards the DE can, as in [38, 94], consequently be collapsed to one variable x, constraining the remaining two to yield a path along M_A.

At the triple point T, i.e. for the highest rewiring rate still allowed in the active phase, the range of ρ for which there is an active phase shrinks to the single value $\rho = \rho_\mathrm{T}$ (Eq. 6.4 and Fig. 6.2a). It can be shown that then M_A and M_D exactly coincide, with the PA yielding a continuum of transversally stable stationary states given by Eq. 6.8. A more thorough description of the model phenomenology at T will be given in Sec. 6.3.

The active phase in the full system

The onset of the metastable DE in MC simulations is characterized by vastly increasing convergence times needed to reach a consensus state, particularly for zero rewiring (Fig. 6.3b). Projecting the network's time evolution onto the reduced phase space spanned by (x, y, z), the resulting random walk (RW) of the stochastic system follows closely the trajectory of its PA description along a curve M_S (Fig. 6.3a), but with three fundamental differences:

1. The exact shape of M_S depends on the system size N and approaches M_D (the slow manifold of the PA) as N increases.

2. For various starting conditions well apart from M_S, the RW does not immediately relax to M_S. Instead, the network undergoes a sequence of distinct configurations (corners of green trajectory in Fig. 6.3a) before its reduced description realigns with that given by M_A. These intermediate network configurations are dependent on initial conditions and partition the RW into several segments.

3. Stochastic fluctuations drive the system along M_S from the DE towards one of the two consensus states. Unlike in the stochastic process in the symmetric model, the type of this final consensus state in network dynamics is, for sufficiently large system sizes, predetermined by the system's parameters and independent of initial conditions (see below).

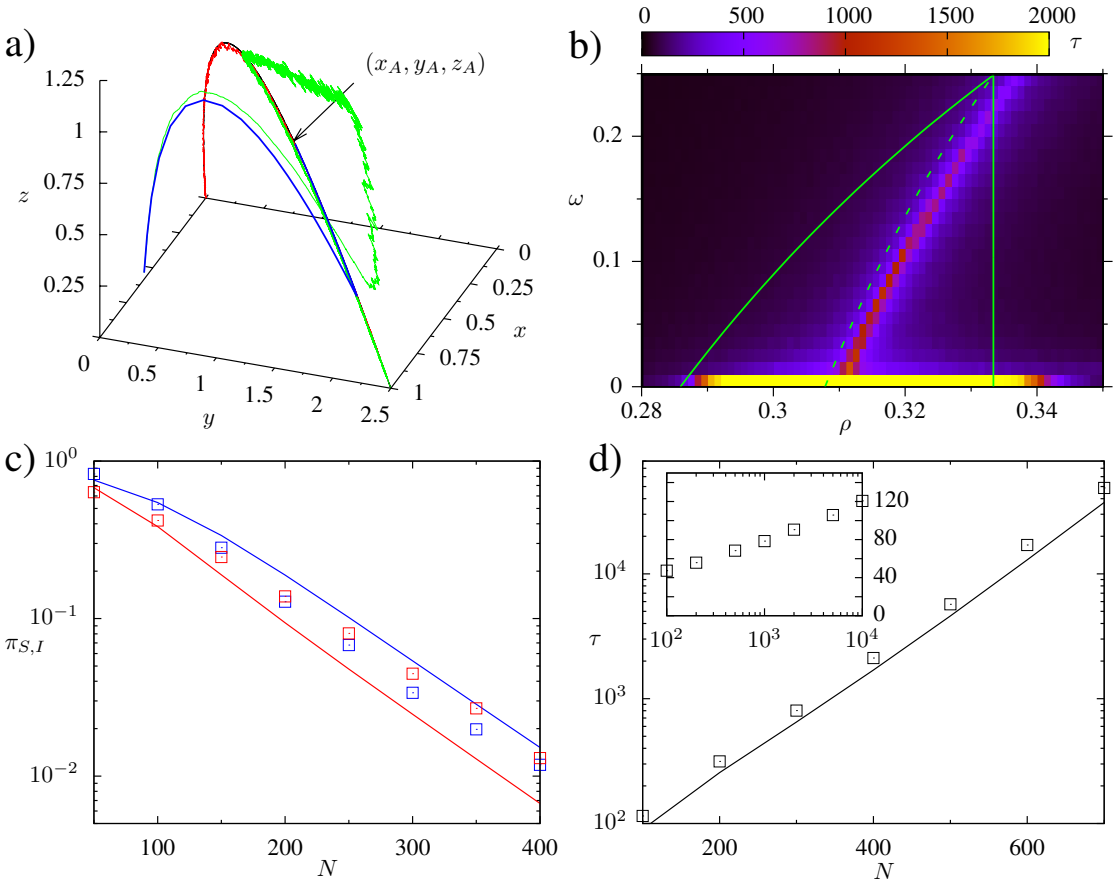

Figure 6.3: The active phase in the asymmetric model. **a)** Time evolution of state variables x, y and z for $\omega = 0.05$ and $\rho = 0.32$ along $M_{\rm A}$ (black line) that approximates $M_{\rm D}$. All MC trajectories end up in I-consensus, starting from $(0.01, 0.00025, 0.0495)$ (initial ER graph, red line) and $(0.8, 0.2, 0.2)$ (maximally random graph with respect to initial conditions, green line). The latter initial network is obtained through **i)** generating two separate random S- and I-subgraphs compatible with given x, y and $(\langle k\rangle/2 - y - z)$ and **ii)** connecting them through $N \cdot z$ randomly assigned active links. Numerical integration from $(0.8, 0.2, 0.2)$ (blue line) ends up in DE $(x_{\rm A}, y_{\rm A}, z_{\rm A})$. Network size $N = 10^4$ in MC run. **b)** Color-coded convergence times τ in MC simulations within DE phase boundaries obtained from PA (solid green lines); maximum τ are expected at $x_{\rm A} = 1/2$ (dashed green line). MC simulations with $N = 5000$, averaged over 100 runs. **c)** System-size dependent splitting probabilities for $\omega = 0$ computed through Eq. 6.12 (solid lines) and fixation probabilities taken from MC simulations (squares). $\pi_{\rm I}$ computed for $\rho = 0.305$ (starting from $x_0 = 0.9$, blue symbols), $\pi_{\rm S}$ computed for $\rho = 0.315$ (starting from $x_0 = 0.1$, red symbols). **d)** Convergence times in MC simulations (squares) and from Eq. 6.16 (solid lines) as a function of system size for $\omega = 0$ and $\rho = 0.3$. Inset MC simulations for $\omega = 0.05$. Results averaged over 10^4 runs ($10^2 \leq N < 10^3$) and 10^3 runs ($10^3 \leq N < 10^4$). Mean degree $\langle k\rangle = 5$ in all figures. MC simulations in b)-d) from initially connected ER graphs, in b) and d) with $x_0 = 0.5$. Error bars in c) and d) are smaller than markers.

Modeling dynamics along the slow manifold

Fast-slow dynamics in a system like Eqs. 6.1 often enable one to separate time scales, identifying a set of fast variables that quickly relax to quasi-stationary values, the latter of which change on a considerably slower time scale as functions of the slow variables. The slow manifold then needs to be determined and system dynamics projected onto it to simplify the system description through the ensuing reduction in degrees of freedom [19]. Following the approach successfully carried out for the classic and coevolutionary voter model [38, 94], the description of the full system to a RW along M_{S} is explored while considering the simplest case of zero rewiring. Lacking an analytic expression both for M_{S} and M_{D}, the RW is assumed to take place along the approximate slow manifold M_{A} given by Eq. 6.8, yielding a one-step process in the total number X of I-nodes with the Master equation

$$\begin{aligned}\frac{\partial[X]}{\partial t} =&\rho Z_{\mathrm{A}}\{X-1\}[X-1] + 2(1-\rho)(N-(X+1))\frac{X+1}{N}[X+1] \\ &- \rho Z_{\mathrm{A}}\{X\} - 2(1-\rho)(N-X)\frac{X}{N}[X]. \end{aligned} \tag{6.10}$$

Here $[X]$ is the time-dependent probability to find $X = N \cdot x$ I-nodes in a network of size N, and $Z_{\mathrm{A}}\{X\} = N z_{\mathrm{A}}\{X/N\}$ is the total number of active links computed from the respective link density at $\omega = 0$ in Eq. 6.8.

The consensus states $X = 0$ and $X = N$ are absorbing boundaries of the RW with starting point $X_0 \in [0, N]$, so that the eventual termination of the metastable state in the full system corresponds to a first-passage scenario. One is interested in the splitting probability $\pi_{\mathrm{I}}\{X_0, N\}$ ($\pi_{\mathrm{S}}\{X_0, N\}$) for the RW to end up at $X = N$ ($X = 0$), i.e. in the probability that the asymmetric RW first hits one of the two consensus states, given that it starts at $X = X_0$. These splitting probabilities approximate the fixation probabilities for the consensus states in the full system. Setting r_i as the number of relaxation events and g_i as the number of transmission events at coordinate $X = j$ yields

$$\begin{aligned} r_i &\equiv 2(1-\omega)(1-\rho)(1-i/N)i \\ g_i &\equiv (1-\omega)\rho Z_{\mathrm{A}}\{i\}\,. \end{aligned} \tag{6.11}$$

With Eq. 6.10 and following [58],

$$\pi_{\mathrm{I}}\{X_0, N\} = \left(1 + \frac{\sum_{i=X_0}^{N-1}\prod_{j=1}^{i} r_j/g_j}{1+\sum_{i=1}^{X_0-1}\prod_{j=1}^{i} r_j/g_j}\right)^{-1} \tag{6.12}$$

and $\pi_{\mathrm{S}}\{X_0, N\} = 1 - \pi_{\mathrm{I}}\{X_0, N\}$ are then obtained for dynamics with $\omega = 0$ (Appendix A.6). For a line of equilibria, i.e. where transmission events balance

out relaxation events according to $r_i = g_i$ at all $1 \leq i \leq N$, Eq. 6.12 yields $\pi_{\mathrm{I}}\{X_0, N\} = X_0/N$ as in the symmetric model.

Along similar lines, one can derive the expression for

$$\nu_{\mathrm{S,I}}\{X_0, N\} \equiv \pi_{\mathrm{S,I}}\{X_0, N\}\tau_{\mathrm{S,I}}\{X_0, N\}\,, \tag{6.13}$$

where $\tau_{\mathrm{S,I}}\{X_0, N\}$ are the mean first-passage times for the process in Eq. 6.10 to hit either S- or I-consensus when starting at X_0. Following Appendix A.6, one arrives at

$$\begin{aligned}\nu_{\mathrm{I}}\{X_0, N\} =&\pi_{\mathrm{I}}\{X_0, N\} \sum_{i=X_0}^{N-1} \sum_{j=1}^{i} \frac{\pi_{\mathrm{I}}\{j, N\}}{r_j} \prod_{k=j}^{i} \frac{r_k}{g_k} \\ &- (1 - \pi_{\mathrm{I}}\{X_0, N\}) \sum_{i=1}^{X_0-1} \sum_{j=1}^{i} \frac{\pi_{\mathrm{I}}\{j, N\}}{r_j} \prod_{k=j}^{i} \frac{r_k}{g_k}\end{aligned} \tag{6.14}$$

and

$$\begin{aligned}\nu_{\mathrm{S}}\{X_0, N\} =&(1 - \pi_{\mathrm{I}}\{X_0, N\}) \sum_{i=N-X_0}^{N-1} \sum_{j=1}^{i} \frac{1 - \pi_{\mathrm{I}}\{N-j, N\}}{g_{N-j}} \prod_{k=j}^{i} \frac{g_{N-k}}{r_{N-k}} \\ &- \pi_{\mathrm{I}}\{X_0, N\} \sum_{i=1}^{N-X_0-1} \sum_{j=1}^{i} \frac{1 - \pi_{\mathrm{I}}\{N-j, N\}}{g_{N-j}} \prod_{k=j}^{i} \frac{g_{N-k}}{r_{N-k}}\,.\end{aligned} \tag{6.15}$$

With Eqs. 6.14 and 6.15 giving the weighted mean first-passage times for both absorbing states, it follows that

$$\tau\{X_0, N\} = \nu_{\mathrm{S}}\{X_0, N\} + \nu_{\mathrm{I}}\{X_0, N\} \tag{6.16}$$

serves as an approximation for observed convergence times in MC simulations.

Capturing the stochastic route to consensus

The increasing predetermination of the consensus type for large N is depicted in Fig. 6.3c for both the full system and its reduced description along M_{A}. With Eq. 6.12, one verifies the earlier observation in MC simulations that for fixed X_0 and increasing system sizes, fixation probabilities in the metastable regime converge to 0 or 1, indicating one intermediate ρ-value that would yield non-integer values throughout. Furthermore, Eq. 6.12 reveals that for sufficiently large N, the final consensus type does not depend on X_0, but just on the position $x_{\mathrm{A}}\{\omega, \rho, \langle k\rangle\}$ of the DE on the slow manifold (in Fig. 6.3c, X_0 is chosen to be close to the respective disfavored consensus state). This is plausible considering that for sufficiently large N, the system can be seen as initially drifting towards

the DE, and from there diffusing to consensus. That also applies to $\omega > 0$, so that en route to the thermodynamic limit, stochastic fluctuations generally drive the system from the metastable to a consensus state whose type is increasingly independent of initial conditions. The fixation probabilities for the disfavored consensus states are observed to be proportional to $e^{-c \cdot N}$ (with a constant $c > 0$) for large enough N, a scaling confirmed by Eq. 6.12 (Fig. 6.3c).

The preferred consensus for large N shall be determined by whether its distance to the DE, to be bridged in X by stochastic fluctuations, is smaller than $N/2$. This heuristic rule is corroborated by Eq. 6.12 which, in the exemplary case of $\langle k \rangle = 5$ and $\omega = 0$ in Fig. 6.3b, yields $\rho = 0.308$ as the value for which preferred and disfavored consensus states switch when varying ρ ($x_{\mathrm{A}}\{0, 0.308, 5\} = 0.509$. For $x_{\mathrm{A}} = 1/2$ then, i.e. when the PA describes the adaptive SIS model in steady state, one would conversely expect maximum first passage times for the RW along the slow manifold, and therefore also maximum convergence times τ for the full system. Indeed this assumption yields a good estimate for maximum τ for both the non-rewiring case and dynamics with topology change. The line of maximum convergence times in Fig. 6.3b differs slightly from $x_{\mathrm{A}}(\omega, \rho, \langle k \rangle) = 1/2$ because the PA does not give the exact DE coordinates of the full system. Using in contrast the X-coordinates of the DE in MC simulations yields a very good match.

The scaling of convergence times τ with system size N for $\omega = 0$ and for $\omega \neq 0$ are in stark contrast, see Fig. 6.3d. For $\omega = 0$, exponential scaling is observed, as found in another modification of the adaptive voter model [95] also featuring a slow manifold connecting a stable heterogeneous state and unstable consensus. The sublinear scaling of τ with N for $\omega \neq 0$ (see inset of Fig. 6.3d) is more surprising, especially in view of the linear scaling found for the symmetric model in [38]. One would expect a stable DE on the slow manifold to counter diffusion towards consensus compared to dynamics on a line of equilibria. But since asymmetric rewiring increases overall degree heterogeneity, fluctuations in the aforementioned RW in X are enhanced, generally resulting in earlier consensus than on static networks or compared to dynamics with a symmetric rewriring rule.

Deviations from the full system

Except for the qualitative considerations above, using Eq. 6.12 to compute the splitting probability $\pi_{\mathrm{I}}\{X_0, N\}$ only yields moderately accurate predictions for the full system without rewiring (Fig. 6.3c), even when using M_{S} (as sampled from an ensemble of trajectories in corresponding MC simulations) instead of the approximate M_{A}. The reason is that since convergence times diverge quickly on static networks (Fig. 6.3d), the computation of $\pi_{\mathrm{I}}\{X_0, N\}$ is only feasible for relatively small system sizes. Yet for small N, assuming that the stochastic dynamics take place along a smooth M_{S} neglects the effect of significant transversal fluctu-

ations: Computing $\pi_{\mathrm{I}}\{X_0, N\}$ along an averaged M_{S} (taken over many stochastic trajectories) generally yields different results than directly averaging $\pi_{\mathrm{I}}\{X_0, N\}$ over the ensemble of trajectories. This remains an issue even for increasing system sizes, as M_{S} retains "problematic" segments of low x or z in the vicinity of the two consensus states where transversal fluctuations are large even for large N.

For symmetric dynamics along a line of equilibria as in [38, 94], aforementioned limitations do not apply, since there fluctuations transversal to the random walk in X are decoupled from the latter. In our asymmetric model however, a stable DE is present on M_{S} with both the drift and diffusion of the random walk in X depending on the link density z. Even if M_{S} were a line of equilibria (see Sec. 6.3), transmission and relaxation in its vicinity would generally not balance out, so that the (finite) full system with transversal fluctuations is not captured by its reduced description along M_{S}. Consequently, a new framework is needed to address metastability in the asymmetric model.

For $\omega > 0$, the sublinear scaling of convergence times τ with system size N differs from that for $\omega = 0$ (Fig. 6.3d). Moreover it poses a stark contrast to the linear scaling found for the symmetric model [38], considering that a stable DE on the slow manifold would be expected to counter diffusion towards consensus compared to dynamics on a line of equilibria. As asymmetric rewiring however increases overall degree heterogeneity, fluctuations in the aforementioned RW in X are enhanced, generally resulting in earlier consensus than on static networks or compared to dynamics with a symmetric rewriring rule.

6.3 The triple point

In the symmetric model with node update, the network magnetization $m = 1-2\cdot x$ is conserved in the thermodynamic limit for sufficiently homogeneous initial graphs [89]. With ω being the probability that a given active link is rewired instead of mediating an opinion adoption, the single ODE

$$\frac{\mathrm{d}z}{\mathrm{d}t} = \frac{2z}{\langle k\rangle}\left((1-\omega)\left(\langle k\rangle - 1\right)(1-2z) - 1\right) \tag{6.17}$$

for the time evolution of the active link density z suffices to describe the full system [38]. The symmetric model with link update on the other hand is captured with

the pairwise formalism and, using the density y of II-links, written as

$$\begin{aligned}\frac{\mathrm{d}y}{\mathrm{d}t} =&\frac{1-\omega}{2}\ z\ \left(\frac{\eta\ z}{1-x}+1\right)+\frac{\omega}{2}\ z-(1-\omega)\frac{\eta\ z\ y}{x}\\ \frac{\mathrm{d}z}{\mathrm{d}t} =&(1-\omega)\ \eta\ z\ \left(\frac{y}{x}+\frac{\langle k\rangle/2-y-z}{1-x}\right)\\ &-\omega\ z-\frac{1-\omega}{2}z\left(\eta\ z\left(\frac{1}{1-x}-\frac{1}{x}\right)+2\right)\ .\end{aligned} \tag{6.18}$$

Here $\omega \in [0,1]$ and $\eta = 1$, and the variables x, y as well as z represent the same motif densities as in Eqs. 2.2. As opinion adoption is symmetric, m and thus also x are conserved and therefore parameters of the model. In both of Eqs. 6.18, the first and last term give the gain and loss of links of the respective link type through opinion adoption, whereas the middle term quantifies the gain through the rewiring rule.

Investigating the equilibrium points yields a (frozen) fragmented phase ($z = 0$ for $x > 0$) and an active phase which features a continuum of stable steady states. The specific steady state to be reached is then determined by the parameter x. For finite system sizes and due to stochastic fluctuations, the corresponding metastable state decays into either consensus state. It does so along a slow manifold formed by the aforementioned continuum of steady states. Consequently $\pi_{\mathrm{I}}\{X_0, N\} = X_0/N$, i.e. the fixation probabilities are system-size independent and scale linearly with starting coordinates X_0 on the slow manifold. Therefore consensus in the symmetric model can only be reached from a metastable DE in the active phase - i.e. only stochastically, not dynamically. The model's symmetry encapsulated in the ODE moreover precludes any coexistence of phases; however *stochastic* bistability of the consensus states in the metastable state is given by the aforementioned fixation probabilities that do not depend on system size.

In contrast, the asymmetric model proposed here breaks the symmetry of the two node ensembles in a twofold way: Through state-dependent imitation rules and through tying the rewiring rule to just one specific node ensemble. The broken symmetry demands for additional degrees of freedom to capture the full system, yielding Eqs. 6.1. As a consequence, network magnetization is not conserved anymore, but a system variable that guides relaxation. This in turn impedes a frozen state with $0 < x < 1$, so that the asymmetric model lacks a fragmented phase. The slow manifold is generally not a line of equilibria anymore, for isolated equilibrium points - one in each consensus state and, in the active phase, an additional stable DE - replace the continuum of steady states. It follows that i) the steady state in the active phase is independent of initial conditions, particularly m ii) consensus can now be reached dynamically iii) consensus bistability is predicted by the PA and observed for the full system iv) for consensus reached stochastically in the metastable state, the fixation probabilities are now system-size dependent, converging for large system sizes to either zero or one regardless of initial conditions.

Unlike the symmetric model, the asymmetric model is not robust against varying topological backgrounds. When choosing for instance $\eta = (\langle k \rangle - 1)/\langle k \rangle$ in Eqs. 6.1 to assume an initial random regular graph [54], the intersection of the two consensus boundaries in phase diagram Fig. 6.2a disappears, and with it the active phase. Instead, bistable consensus stretches down to $\omega = 0$, featuring a slow manifold much like the active phase of the model with $\eta = 1$ does. This time however it is spanned by heteroclinics connecting two *stable* nodes in the consensus states with a saddle as the *unstable* DE. The different model phenomenology for that choice of η is corroborated by MC simulations, emphasizing the importance of initial topology for asymmetric opinion dynamics on adaptive networks. Since changing network topologies may shift the balance in opinion competition, the initial topology can be crucial for the outcome of the asymmetric dynamics [96]. The (also asymmetric) adaptive SIS model on the other hand generally allows for sufficiently enduring coevolutionary dynamics to wash out initial differences in network structure. This is because its active phase does not feature a slow manifold along which stochastic fluctuations towards consensus could be facilitated.

The triple point in the PA

Tuning the rates of the asymmetric model's three elementary processes strengthens or loosens its asymmetry. As indicated in Sec. 6.1, there exists a choice of parameters where symmetry is restored: At the coordinates given by Eqs. 6.19 - the system's triple point T that borders all phases - Eq. 6.9 holds. It follows that the PA in steady-state is exactly captured by the slow manifold in Eq. 6.8, now referred to as $M_{\mathrm{A}}^{\mathrm{T}}$.

This slow manifold is exactly the line of equilibria obtained in Eqs. 6.18 for the symmetric model without rewiring (the *classic symmetric model*), varying the parameter x from 0 to 1. Therefore at T, i.e. for a nontrivial choice of parameters, the asymptotic behavior of the asymmetric model with rewiring replicates the symmetric model with $\omega = 0$. As a consequence and according to Eq. 6.8, $M_{\mathrm{A}}^{\mathrm{T}}$ then yields at parameters (ω_T, ρ_T) two symmetries it does not display anywhere else in the active phase of the asymmetric model: For all $0 \leq x \leq 1$, one then finds that

1. $M_{\mathrm{A}}^{\mathrm{T}}$ is formed by equilibrium points, as relaxation and transmission events balance out according to $\rho \cdot z_{\mathrm{A}}\{x\} = 2 \cdot (1-\rho) \cdot (1-x) \cdot x$.

2. $\langle k_{\mathrm{S}} \rangle = \langle k_{\mathrm{I}} \rangle = \langle k \rangle$ for mean degrees $\langle k_{\mathrm{S}} \rangle = (z + 2 \cdot (\langle k \rangle/2 - y - z))/(1-x)$ and $\langle k_{\mathrm{I}} \rangle = (z + 2 \cdot y)/x$ of the S- and I-ensemble, respectively.

These two steady-state equalities moreover yield

$$\begin{aligned} z_{\mathrm{A}}\{1-x\} &= z_{\mathrm{A}}\{x\} \\ y_{\mathrm{A}}\{1-x\} &= \langle k\rangle/2 - y_{\mathrm{A}}\{x\} - z_{\mathrm{A}}\{x\} \end{aligned} \tag{6.19}$$

as a noteworthy consequence. The first of Eqs. 6.19 is a direct consequence of aforementioned balance of events that determines $z_{\mathrm{A}}(x)$, whereas the second can be easily established by solving $\langle k_{\mathrm{S}}\rangle = \langle k_{\mathrm{I}}\rangle$ for $y_{\mathrm{A}}(x)$ through the given $z_{\mathrm{A}}(x)$. It follows from Eqs. 6.19 that at T in the asymmetric model and generally in classic symmetric model, the system stays in DE even if all node states are flipped.

An additional feature unique to the asymmetric model contrasts topology change with opinion spreading: At T, transmission along and rewiring of active links happen at the same *rate* $(1-\omega)\cdot\rho = \omega$. Combined with the aforementioned balance of transmission and relaxation *events*, this implies the equipartition of processes in steady state at T: Rewiring, relaxation and transmission then each account for exactly one third of events. As soon as rewiring dominates through $\omega > \omega_{\mathrm{T}}$, topology change impedes a dynamic equilibrium (Fig. 6.2a).

The vicinity of the slow manifold

For the symmetric model with any rewiring rate, describing metastability of the DE with a one-step process in x as in Sec. 6.2 gives excellent quantitative results. This is i) because of the lack of drift on its slow manifold, but ii) also due to the homogeneity of the outside flow, in particular in the vicinity of $M_{\mathrm{A}}^{\mathrm{T}}$: As x is conserved throughout, the projection of the three-dimensional flow on the xz-plane yields a parallel vector field, evading complications that arose in the case of the asymmetric model.

At the triple point, i) is also given for the asymmetric model, since the slow manifolds of the two model flavors then concide. To have any hope for quantitatively describing metastability at T in the spirit of Sec. 6.2, one should moreover ask whether at least a weak version of ii) holds: In the xz-projection of the flow, are vectors in the vicinity of $M_{\mathrm{A}}^{\mathrm{T}}$ perpendicular to the x-axis or at least parallel to each other?

The latter scenario can be investigated by a) linearizing Eqs. 6.1 along $M_{\mathrm{A}}^{\mathrm{T}}$ b) for each x parametrizing $M_{\mathrm{A}}^{\mathrm{T}}$, computing the two-dimensional subspace spanned by the fast eigenvectors $\mathbf{u}_{\mathrm{x}}$ and $\mathbf{v}_{\mathrm{x}}$ of the respective Jacobian 3) checking whether any two subspaces at x and x' are parallel through showing that

$$(\mathbf{u}_{\mathrm{x}} \times \mathbf{v}_{\mathrm{x}}) \times (\mathbf{u}_{\mathrm{x}'} \times \mathbf{v}_{\mathrm{x}'}) = 0$$

for any $x, x' \in [0,1]$. This equality turns out to hold only if $x = x'$, and it can be moreover shown that the resulting contortion of the flow in the vicinity of $M_{\mathrm{A}}^{\mathrm{T}}$

is generally very pronounced. It follows that for the full system at T, transversal fluctuations of a trajectory along the slow manifold should still experience a coordinate-dependent drift in the x-direction. Consequently, the ansatz of Sec. 6.2 to characterize metastability of DEs is of limited use, as simulations will reveal in the next section. Furthermore, it is remarkable that although the symmetric model with $\omega = 0$ and the asymmetric model at T share the same line of equilibria in the PA description, the respective flows are fundamentally different even in the vicinity of the line.

The triple point in the full system

It is found that for the approximate coordinates ($\omega_T^* \approx 0.150, \rho_T^* \approx 0.325$) instead of ($\omega_\mathrm{T} = 1/4, \rho_\mathrm{T} = 1/3$), the full system with $\langle k \rangle = 5$ features a drift-free attracting curve M_S along which, on average,

$$\rho \; z\{x\} = 2(1-\rho)(1-x)x$$

and magnetization is conserved (Fig. 6.4a). Indeed MC simulations suggest that T^* is unique and marks the end of the active phase, similar to the triple point T in the PA.

For (ω, ρ) approaching T^* along the curve of maximum convergence times in Fig. 6.3b), stochastic trajectories drift towards $x = 1/2$ on the curve M_S before slowly diffusing to consensus with increasingly small drift velocities. At T^* the drift velocity is effectively zero, and for higher values of ω the stochastic trajectories drift towards, instead of away from, the consensus states. This behavior agrees qualitatively with the description given by the PA for the thermodynamic limit, in that the whole M_A is formed by equilibria when the change of stability of the equilibrium point on M_A occurs.

While the shape of M_S at T^* encodes the dynamical aspect of a line of equilibria (the global balance of transmission and relaxation events), its stochastic features should also emerge, e.g. $\pi_\mathrm{I}\{X_0, N\} \approx X_0/N$ for all initial X_0 considered. Fluctuations transversal to M_S still hinder a qualitative description with frameworks like Eq. 6.10 (as they do away from T^* in the active phase), since the flow in the PA close to M_A is very contorted (Sec. 6.2). As T^* is an isolated point, a high volatility of steady-state characteristics with respect to small parameter deviations is observed. Nonetheless fixation probabilities for the approximate T^* do not display the usual convergence towards 0 or 1 values for increasing system sizes (Fig. 6.4b). This is another indication, at the level of the stochastic properties of the system, of the vicinity of a point where transmission and relaxation events balance out along M_S.

In contrast to T in the PA description, the steady-state subensemble mean degrees of the full system are not equal at T^* (inset of Fig. 6.4a). This is to be expected, as

zero drift and degree equality are independent constraints on M_S, with the former occuring only at T^* for a given $\langle k \rangle$. Consequently, asymmetric voter dynamics in the full system generally cannot fully emulate the classic voter model in DE, featuring only a "weak" triple point T^* as a ghost remnant of T in the approximate pairwise description.

The adaptive SIS model on the other hand, for chosen parameter combinations, yields node-ensemble symmetries in steady state that are also displayed by the full system: The respective PA features $\langle k_S \rangle = \langle k_I \rangle$ at $(1-\omega) \cdot \rho = \omega$ as does the asymmetric model, while in contrast this equality not only holds in MC simulations, but extends to steady-state subensemble degree distributions (Sec. 2.3).

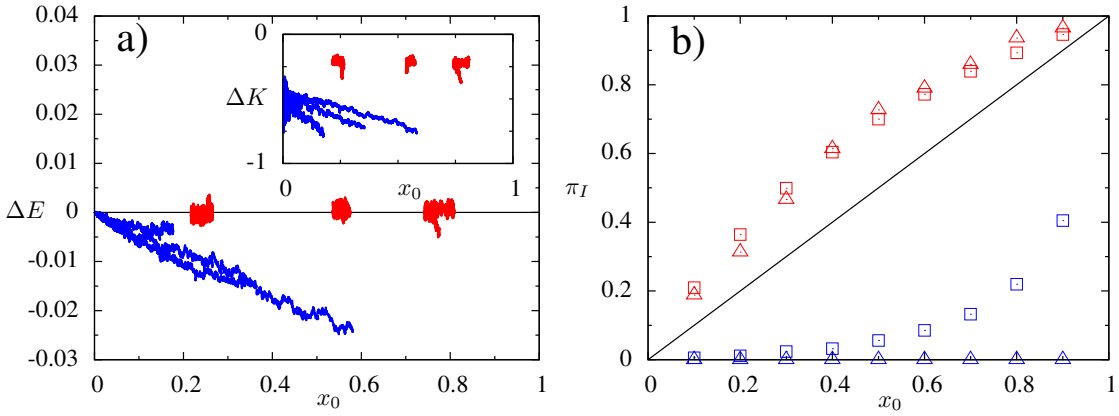

Figure 6.4: Identifying the triple point in the full system with plots for (ω_T^*, ρ_T^*) (red symbols) and $(\omega = 0.05, \rho = 0.3)$ (blue symbols) **a)** *dynamically* through balance of events $\Delta E = \rho \cdot z - 2 \cdot (1-\rho) \cdot (1-x) \cdot x$ and of mean degrees $\Delta K = (\langle k_S \rangle - \langle k_I \rangle)$ (inset) for bursts of simulations from fractions $x_0 = 0.2$, 0.5 and 0.8 of randomly primed I-nodes **b)** *stochastically* through the fixation probability for I-consensus as a function of x_0 for $N = 100$ (squares) and $N = 1000$ (triangles). Simulations in a) recorded for $N = 10^5$ and $10 \leq t \leq 100$ and in b) averaged over 10^4 runs and with error bars smaller than markers. All simulations from initially connected ER graphs and with mean degree $\langle k \rangle = 5$.

6.4 Summary

An adaptive network process of two asymmetrically competing opinions is introduced and described with a pair-approximation model. The model generally yields a good description of the network process, revealing asymptotic regimes that differ from both the symmetric voter model and adaptive contact process. Unlike in the latter, it is found that the proposed asymmetric process is sensitive with respect to initial network topology. In order to account for coexisting consensus

states, conditions and procedures are formulated to check predictions of the pair approximation against simulational results. One parameter region and a particular parameter combination are identified that warrant a closer inspection: The active phase and the triple point.

The metastability of the dynamic equilibrium in the active phase is then modeled as a random walk along a slow manifold. For the simplest case of no topological coevolution, expressions for splitting probabilities and mean first-passage times are extracted, capturing the fixation probabilities and convergence times in the full system. It is subsequently discussed why this ansatz only qualitatively describes the full system.

At the triple point, asymmetric coevolutionary dynamics in dynamic equilibrium (as described by the pair approximation) emulate the symmetric voter model without coevolution. In the full system, a "weak" triple point is identified that partially replicates the phenomenology of the triple point in the pair approximation.

7 MODIFYING THE VOTER MODEL

In the asymmetric coevolutionary voter model dealt with in Chapter 6, the overall network magnetization m steered opinion adoption of I-nodes. One can modify this mechanism to let relaxation of an I-node to the ground state be guided by a *local* majority in opinions. This yields a more realistic representation of peer influence in opinion formation, with node-update voter dynamics being more accurately emulated on part of the I-nodes than through relaxation coupled to a mean field m.

7.1 The model in the pair approximation

Let the neighborhood of a node of degree k consists of k_{I} adjacent I-nodes and $(k - k_{\mathrm{I}})$ adjacent S-nodes. The neighborhood's magnetization is then defined as

$$m_{\mathrm{L}} = \frac{k - 2k_{\mathrm{I}}}{k} \tag{7.1}$$

with $m_L := 0$ for $k = 0$, characterizing the *local* magnetization of the network as experienced by the node in question. Instead of m, m_{L} shall now guide the relaxation in the asymmetric voter model of Sec. 6.1, with the transmission and rewiring rule remaining in place. Thus S-nodes engage in the same coevolutionary link-update voter dynamics as laid out in Sec. 6.1, while relaxation to the S-state can now be seen as a more refined imitation of node-update voter dynamics on the part of I-nodes.

The PA equations for the new process (labeled m_{L}-model) are

$$\begin{aligned}
\frac{dx}{dt} &= (1-\omega)\left(\rho z - (1-\rho)\boxed{r_{\mathrm{x}}}x\right) \\
\frac{dy}{dt} &= (1-\omega)\left(\rho z\left(\frac{z}{1-x}+1\right) - 2(1-\rho)\boxed{r_{\mathrm{y}}}y\right) \\
\frac{dz}{dt} &= -z\left(\omega + (1-\omega)\left(\rho + (1-\rho)\boxed{r_{\mathrm{z}}}\right)\right) - (1-\omega)\rho\frac{z^2}{1-x} \\
&\quad + 2(1-\omega)(1-\rho)\boxed{r_{\mathrm{y}}}y + 2(1-\omega)\rho\frac{(\langle k\rangle - y - z)z}{1-x}
\end{aligned} \tag{7.2}$$

and resemble Eqs. 6.1 (now referred to as m-model), but with

$$\begin{aligned} r_{\mathrm{x}} &= 1 + \frac{z - 2y}{z + 2y} \\ r_{\mathrm{y}} &= 1 + \frac{z - 2y - x}{z + 2y + x} \\ r_{\mathrm{z}} &= 1 + \frac{z - 2y + x}{z + 2y + x} \end{aligned} \tag{7.3}$$

instead of $r_{\mathrm{x}} = r_{\mathrm{y}} = r_{\mathrm{z}} = 2 \cdot (1 - x)$. The fractions in Eqs. 7.3 are estimates of m_{L} under different circumstances, i.e. given that the I-node in question is connected to another I-node (r_{y}), S-node (r_{z}) or without considering state correlations between connected nodes (r_{x}).

All steady states obtained in the m-model are retained, and the phase boundaries of the DE and I-consensus differ only slightly compared to Fig. 6.2a. Additionally, Eqs. 7.2 yield a fragmentation phase that pervades parameter space, because unlike in the m-model, network dynamics come to a halt when active links are depleted (see below).

I-consensus and the DE

Through a linear stability analysis of Eqs. 7.2 along the lines of Appendix A.1, I-consensus is found to be stable for

$$\rho > \frac{2}{2 + \langle k \rangle}\,, \tag{7.4}$$

and the DE for

$$\frac{2 - \omega}{(3 + \langle k \rangle)(1 - \omega)} < \rho < \min\left(\frac{2}{2 + \langle k \rangle}, 1 - \frac{1}{\sqrt{5}}\right)\,. \tag{7.5}$$

The phenomenology of the active phase in both the PA and MC simulations is similar to what is observed in Sec. 6.2. Steady-state subensemble mean degrees are calculated as

$$\begin{aligned} \langle k_{\mathrm{S}} \rangle &= \frac{2 - \omega}{(1 - \omega)\,\rho} - 3 \\ \langle k_{\mathrm{I}} \rangle &= 2\left(\frac{1}{\rho} - 1\right)\,, \end{aligned} \tag{7.6}$$

hence remarkably, the mean degree of I-nodes in DE only depends on ρ, i.e. the balance of transmission and relaxation. Like for the adaptive SIS model and the m-model, Eq. 2.7 holds, underlining the kinship of the three models indicated in Sec. 2.3. Since however the DE in the active phase is only stable for $\omega \leq (1 - \omega) \cdot \rho$, $\langle k_{\mathrm{S}} \rangle \leq \langle k_{\mathrm{I}} \rangle$ across the active phase.

Fragmentation

As mentioned above, any point on the z-plane - any fragmented state without active links - is a steady state. Its stability depends on the corresponding sole nonzero eigenvalue $\lambda_z(x, y)$ of the linearized Eqs. 7.2. Because

$$\begin{aligned}\lambda_z(x,y)(x-1)(x+2y) =&(2-\rho(1-\omega)-\omega)x^2 \\ &+2(2-3\omega+\rho(1-\omega)(\langle k\rangle-2y-3))y \\ &+x(\omega-2-4y+6\omega y+\rho(1-\omega)(1+\langle k\rangle+4y))\end{aligned} \quad (7.7)$$

is linear in each parameter and quadratic in variables x and y, a stability analysis of the fragmented state is straightforward. For all $\langle k\rangle > 3$, there exists the parameter region

$$\frac{2-\omega}{(1+\langle k\rangle)(1-\omega)} \leq \rho \leq 1-\frac{1+\langle k\rangle}{(3\langle k\rangle-1)(1-\omega)} \quad (7.8)$$

for which $\lambda_z(x, y) > 0$, i.e. where the system does not display fragmentation, as stable fragmentation configurations do not exist (shown in Fig. 7.1a for $\langle k\rangle = 5$). This fragmentation-free patch in parameter space grows with $\langle k\rangle$, for higher network connectivities increase robustness towards fragmentation. Yet it never occupies a fraction larger than one third of the parameter space spanned by $\omega, \rho \in [0, 1]$, so that especially for small mean degrees $\langle k\rangle$, fragmentation is almost ubiquitous.

Further increasing ω or starting off with a small rewiring rate for different ρ, plotting $\lambda_z(x, y) = 0$ yields two hyperbolic branches enclosing regions of negative $\lambda_z(x, y)$ on the z-plane (Fig. 7.1b). These branches pass through the consensus states $(0, 0, 0)$ and $(1, \langle k\rangle/2, 0)$, respectively. For any given nonzero initial z in the system, they mark a region of realizable fragmented states, whereas the system cannot fragment into unstable configurations given by $\lambda_z(x, y) > 0$. As rewiring is further increased, the two branches approach each other and merge, giving rise to two new branches that now enclose regions of instability (Fig. 7.1c). For ω close to one, the branch at lower x disappears, so that all fragmentation configurations in the vicinity of the origin $(0, 0, 0)$ are stable (Fig. 7.1d).

The somewhat counterintuitive fact that Eqs. 7.2 predict stable fragmentation even for no rewiring is a useful reminder of their limitations: As the PA treats the network process as the unconstrained interaction of chemical species x, y and z, it allows for depletion of active links outside the two consensus states through relaxation and transmission alone. It is furthermore worth noticing that for every choice of parameters in the PA, there are unstable steady states on the z-plane the system cannot fragment into.

S-consensus

Unlike for I-consensus, obtaining the phase boundaries for S-consensus partially relies on heuristic arguments. In a large parameter region the z-plane is attractive in the vicinity of $(0, 0, 0)$, so that a stable fixed point at the origin has to compete with fragmentation arbitrarily nearby. A plausible necessary condition for a three-dimensional basin of attraction of the S-consensus state is the absence of the scenario depicted in Fig. 7.1d, i.e. there should exist unstable fragmentation configurations on the z-plane arbitrarily close to the origin. This is the case for

$$\omega < 1 - \frac{1}{3 - 3\rho + \langle k \rangle \rho}\,. \tag{7.9}$$

Determining the stability of S-consensus is more involved, since Eqs. 7.2 are singular (and difficult to regularize) at $(0, 0, 0)$. One has to resort to numerical integration to investigate whether nearby trajectories converge to $(0, 0, 0)$. Judging from Figs. 7.1b-d, it cannot be excluded that particularly with increasing ω, the basin of attraction of the fragmented state $(x > 0, y > 0, z = 0)$ occupies almost the entire vicinity of S-consensus for sufficiently small z. Hence integration runs are started within a quarter-cone around the z-axis, with its apex at $(0, 0, 0)$, a narrow opening angle and small lateral height. Obtained results are consistent with

$$\rho < \frac{2 - \omega}{(3 + \langle k \rangle)(1 - \omega)} \tag{7.10}$$

as a condition for the stability of S-consensus.

It follows that integrating the PA with a series of initial conditions close to the origin, but away from potentially competing fragmentation at $z = 0$, reveals a parameter region of stable S-consensus that, for low rewiring, resembles that of the m-model and is in line with S-consensus boundaries computed in Sec. 6.1. Fragmentation at sufficiently high rewiring rates however outcompetes S-consensus, with Eq. 7.9 giving a good estimate for the upper bound of competitive S-consensus (Fig 7.1a).

Consequently, the coexistence of at least two attractors is the dominant scenario for a wide range of parameters in the m_{L}-model, and judging on the attractors' relevance may require consideration of their competing basins of attraction. In contrast, the fragmentation-free patch (whose sole attractor is the I-consensus state) and the fragmentation-only region for low ρ and high ω are pure phases of the system (Fig. 7.1a). Lastly, the only attractor observed to compete with the dynamic equilibrium are the stable fragmentation configurations on the z-plane.

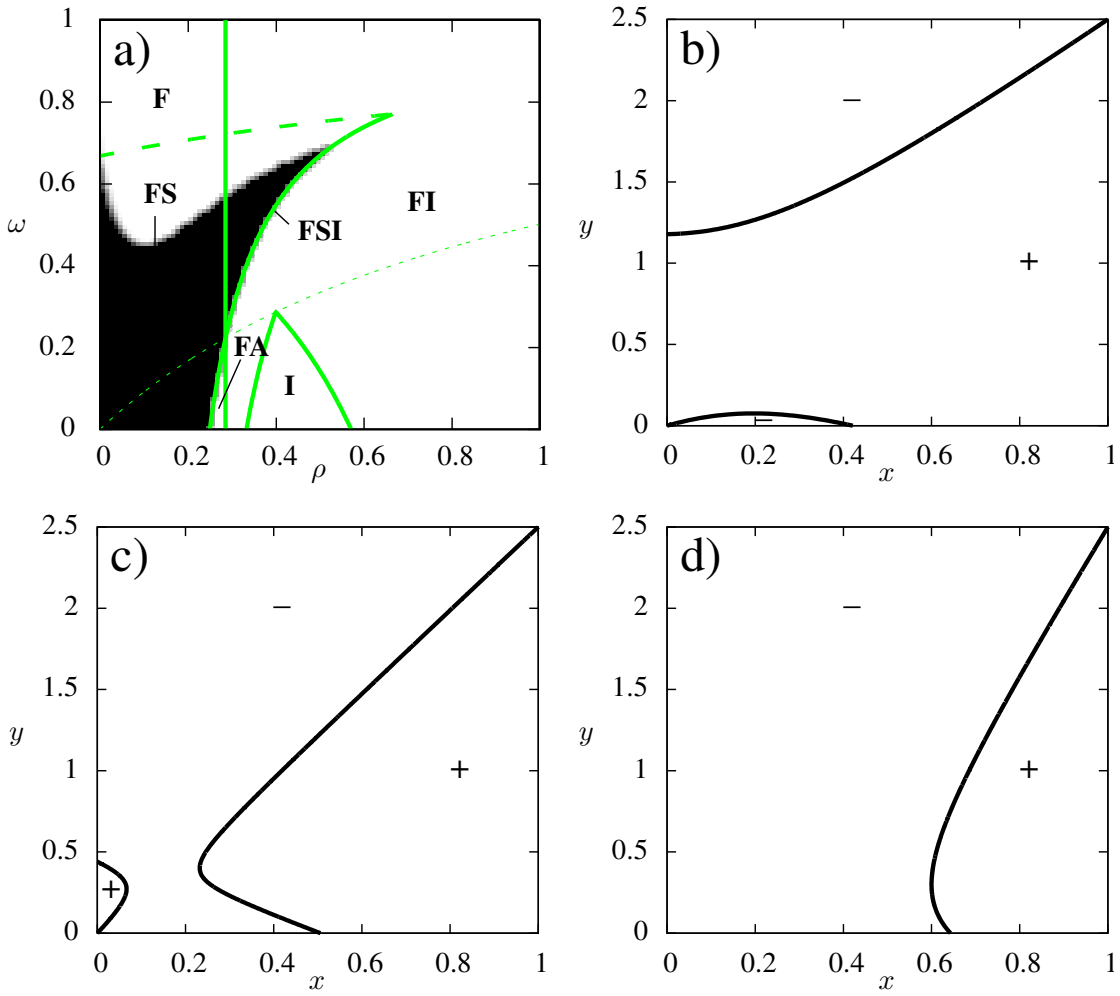

Figure 7.1: Asymptotic behavior of the m_{L}-model for mean degree $\langle k \rangle = 5$. **a)** Phase diagram with labeling as in Fig. 6.2 as well as fragmentation (**F**). Solid lines mark the phase boundaries for I-consensus (Eq. 7.4), S-consensus (Eq. 7.10 for $0 \leq \rho \leq 2/3$) and the fragmentation-free region (Eq. 7.8). The thin dotted curve is $\omega = (1-\omega) \cdot \rho$, the thick dashed line signifies the equality in Eq. 7.9 for $0 \leq \rho \leq 2/3$. Shaded regions indicate a non-zero fraction of 100 PA-integration runs converging towards $(0, 0, 0)$, with initial conditions evenly spaced on the edge of a quarter-cone around the z-axis, apex at $(0, 0, 0)$, opening angle $\pi/100$ and lateral height 0.001. **b)-d)** Fragmentation on z-plane for $\rho = 0.4$. Solid black lines (representing $\lambda_{\mathrm{z}}(x, y) = 0$) separate regions of stable fragmentation configurations ($-$) from unstable ones ($+$) for b) $\omega = 0.6$, c) $\omega = 0.71$ and d) $\omega = 0.8$.

7.2 Pitfalls in Monte-Carlo simulations

Initial conditions

Not only does network connectivity impose a lower bound $N \geq (\langle k \rangle/2+1)$ on the system size used in MC simulations, but similar combinatorical considerations of the maximal connectivity in both subensembles account for additional constraints. These are given as

$$\frac{\langle k \rangle}{2} - \frac{1-x}{2}\left((1-x)\,N-1\right) - z \leq y \leq \frac{x}{2}\left(xN-1\right)\,, \tag{7.11}$$

where the left inequality arises from considering that the maximum number of SS-links is bounded by the number of S-nodes, whereas the right equality applies the same argument to II-links. Those are weak constraints on graphical (i.e. realizable) initial conditions in MC simulations in that, for all practical purposes, they become irrelevant for sufficiently large system sizes.

Following similar considerations as on the m-model in Sec. 6.1, one wants to avoid disconnected initial networks in MC simulations of the m_{L}-framework. When verifying allowed fragmentation configurations indicated in Figs. 7.1b-d, initial topologies should be chosen so as to explore the whole z-plane, requiring the construction of initial random graphs only constrained by a state vector (x_0, y_0, z_0) (through the procedure given in the caption of Fig. 6.3). Unlike in the case of ER networks however, disconnectedness of such random graphs is inherent for a considerable range of initial conditions and cannot be averted. The space of all graphical initial network configurations expressible in the PA will thus have to be narrowed down further as to only contain connected networks. Apart from demanding $\langle k \rangle \geq 2$, this also implies that initially, every member of each subensemble shall at least have degree 2. It follows that

$$2x - z \leq 2y \leq 2x - z + \langle k \rangle - 2 \tag{7.12}$$

is a necessary condition for connectedness in the thermodynamic limit. Unlike the weak conditions imposed by *maximal* connectivity in Eq. 7.11, this constraint for *minimal* connectivity persists for any system size.

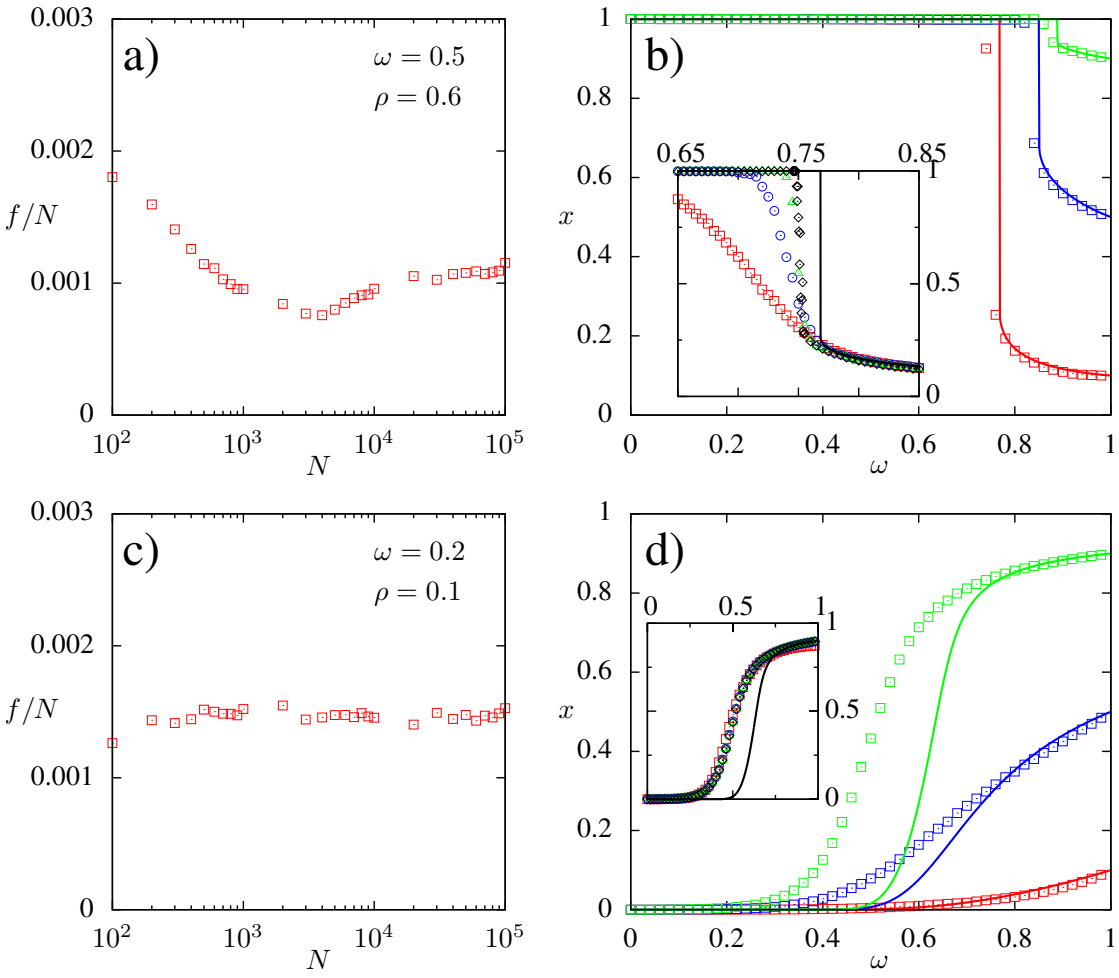

Figure 7.2: Consensus states competing with fragmentation in m_L-dynamics. **a)-b)**: Competing I-consensus at $\rho = 0.6$. **c)-d)**: Competing S-consensus at $\rho = 0.1$. **a)** and **c)**: Quantifying system-size dependent premature fragmentation through density f/N of the minority opinion, averaged over 10^4 runs for $N = 100..900$, over 10^3 runs for $N = 1000..9000$ and over 10^2 runs for $N = 10^4..10^5$ from initial network with 50% randomly primed I-nodes. **b)** and **d)**: Final node densities x in frozen networks, indicating the transition from consensus to fragmentation in MC simulations (symbols, $N = 5000$, averaged over 100 runs) as well as PA integration (solid lines). Initial conditions $(0.1, 0.025, 0.45)$ (red), $(0.5, 0.625, 1.25)$ (blue) and $(0.9, 2.025, 0.45)$ (green). The insets in b) and d) depict the system-size dependence of the respective phase transition for initial conditions $(0.1, 0.025, 0.45)$ or $(0.9, 2.025, 0.45)$ (b) and d), respectively). $N = 10^2$ (red squares),$N = 10^3$ (blue circles), $N = 10^4$ (green triangles), $N = 10^5$ (black diamonds); black solid lines are PA integration. Initial ER graphs for all simulations, mean degree $\langle k \rangle = 5$ in all computations.

Principal difficulties

Any network with N nodes and m_{L}-dynamics that approaches one of the three frozen states features an ever-decreasing density of active links. For networks sufficiently close to either of those states, stochasticity will eventually dominate over system dynamics regardless of system size. Moreover, either consensus state is at most one node-state change - or *spin flip* in voter-model literature - and one link rewiring away from a fragmented configuration (in the state space of the PA, the respective frozen states lie arbitrarily close to the z-plane). Therefore networks in MC simulations that initially are dynamically driven to consensus usually fragmentate a small number $f \ll N$ of spin flips short of it - the network on its route to consensus generally experiences 'premature fragmentation'. Since for various model parameters, f/N itself does not decrease with system size (Figs. 7.2a and 7.2c), this implies that either the thermodynamic limit at that stage of system evolution is rendered obsolete, or it reflects the existence of an attracting fragmentation configuration as predicted by the PA. The indistinguishability of premature and actual fragmentation complicates an inspection of phase diagram Fig. 7.1a in the spirit of Fig. 6.2, as well as a verification of the PA fragmentation scenarios in Figs. 7.1b-d.

Starting from a fixed set of initial conditions in the PA and the corresponding initial network in MC simulations, it is observed that with I-consensus and fragmentation competing, f does abruptly jump from $f \ll N$ to yield a value $f \sim N$ at a small parameter change (Fig. 7.2b). This transition appears to be discontinuous in the thermodynamic limit (inset of Fig. 7.2b). It is considered to be the end of I-consensus and the onset of fragmentation for that particular choice of initial conditions. The PA captures this transition and the subsequent fragmented state very well, the latter in both x (Fig. 7.2b,d) and y for a wide range of initial connected ER graphs (not shown).

For competing S-consensus and fragmentation, a different scenario emerges (see Fig. 7.2d). Here MC and PA results do not depend on system size, and given fixed initial conditions, a smooth transition from S-consensus to fragmentation is observed for the PA. Upon $z \to 0$ and disregarding stopping conditions for numerical integration introduced in Sec. 6.1, the PA can clearly separate those two regimes by either displaying both $x \to 0$ and $y \to 0$ (S-consensus) or not (fragmentation). In contrast, the premature fragmentation in MC simulations described earlier is now indistinguishable from fragmentation that is dynamically driven to small f. Therefore, the criterion for the onset of S-consensus in MC simulations has to remain the rather strict $x = 0$, preventing S-consensus for sufficiently large systems with initial conditions other than the trivial choice $(0, 0, 0)$.

7.3 Summary

A modification of the asymmetric coevolutionary voter model is introduced, emphasizing the importance of the neighborhood composition for consensus building. All asymptotic regimes of the original asymmetric model laid out in Sec. 6.1 are retained, but the modification of the relaxation process additionally enables network fragmentation.

Fragmentation pervades almost all of parameter space of the respective pair approximation, and its coexistence with the other asymptotic regimes complicates the interpretation of simulational results: It renders the full system very sensitive to stochastic effects that do not vanish in the thermodynamic limit, so that the system's dynamical route towards absorbing states - particularly S-consensus - is distorted for all system sizes.

In the context of this work, verifying the accuracy of the pair approximation thus cannot be achieved in a satisfactory manner. Feasible criteria for a proper evaluation of coexisting asymptotic regimes in simulations are needed, in part also to evaluate the performance of other relevant frameworks [55].

8 CONCLUSIONS

This work aimed at a better understanding of asymptotic regimes in adaptive networks, placing an emphasis on dynamic equilibria. The latter are common manifestations of real-world nonequilibrium processes, and their analytical treatment is paramount to predicting and steering a wide range of complex systems. The work's main theme dealt with the detection and description of dynamic equilibria, as well as the formulation of some of their general properties [97, 98]. In the course of that, two additional research lines were explored, both revolving around dynamic equilibria that arise from asymmetric microscopic dynamics [99]: One concerned the metastability of steady states, the other the emergence of node-ensemble symmetries.

The node cycle

Chapter 2 showed that the low-dimensional pair-approximation framework, designed to capture state correlations between next neighbors, yields various averages that allow for a coarse-grained description of a steady-state network. For a more thorough treatment, a new analytic ansatz was laid out in Chapters 3 and 4: The node cycle models the state and degree evolution of a single node as a random walk, with the ergodic properties of the network process allowing to formulate constraints that consistently embed long-term single-node dynamics into the network. Fulfilling these constraints then permits to extract ensemble statistics from the node's long-term behavior, making the node cycle a fully self-contained framework.

The self-consistency approach of the node cycle detects and describes all dynamic equilibria of a given adaptive network, notably also the unstable ones. Through a cost-function evaluation, it distinguishes system phases that differ in their number of coexisting dynamic equilibria. Once a dynamic equilibrium has been identified through a specific set of constant correspondence parameters, the framework addresses the equilibrium's uniqueness observed in Chapter 2: It ties the shape of stationary joint-degree distributions solely to given model and correspondence parameters, and does so through the model-intrinsic existence and uniqueness of

a transition matrix' Perron-Frobenius eigenvector. Since the correspondence parameters can be expressed as functions of low-order motif densities, the steady state of these densities then implies stationary degree distributions. Moreover, the analytic description of each subensemble in dynamic equilibrium is widened to lifetime profiles and joint-degree distributions of newborn ensemble members, thus encapsulating the dynamical aspect of dynamic equilibria in addition to their topological characterization. Therefore, the node cycle also accounts for the observed comprehensiveness of dynamic equilibria, and furthermore links all describing subensemble distributions through simple linear transformations.

Several elaborations on and extensions of the node cycle presented in Chapter 5 deserve further consideration: Among them are the possible application to processes that are not strictly cyclic, speeding up cost-function computation, exploring the stochastic properties of the node-cycle process as well as investigating the apparent all-encompassing character of dynamic equilibria (i.e. the observation that the stationary state of the network extends to motif densities of arbitrary order). Apart from pursuing these issues, it is the framework's very accuracy in dealing with dynamic equilibria (as demonstrated in Sec. 4.3) that warrants a closer look at the node cycle's cornerstone: The assumption that long-term single-node behavior can encode ensemble statistics once stationarity and correspondence have been ensured. As remarked in Sec. 5.2, the latter is an ergodic property generally not observed for link-type dynamics, so that a clarification is desirable as to which motifs other than nodes display this behavior in dynamic equilibrium.

Absorbing states and metastability

Chapters 6 and 7 considered how the accuracy of modeling frameworks is affected by the asymmetric nature of coevolutionary dynamics. A general dependence on initial conditions was noted, owing to coexisting asymptotic regimes for wide parameter regions. While the pair approximation was shown to deliver accurate phase diagrams for coevolutionary dynamics when consensus is the only absorbing state, the latter's competition with fragmentation in a related process yielded elementary difficulties in distinguishing these two regimes. When characterizing metastability of the active phase through a reduced description along a slow manifold, satisfying results were achieved on static networks, whereas the ansatz does not capture asymmetric dynamics with topological coevolution.

Future work could include a satisfactory quantitative description of the stochastic properties of the asymmetric coevolutionary model's metastable state. In Sec. 6.2, the inadequacy of the used framework was traced back to the asymmetric nature of the microscopic dynamics. While a more elaborate framework in [95] successfully derives consensus times for a network process whose symmetry has only slightly been broken, it remains to be seen how it performs for parameter regions of strong

asymmetry. Encouraging analytic results in that direction have been obtained for fluctuations around the DE of a slow manifold [100]. To however fully characterize metastability, one would need to extend existing approaches to the entire slow manifold (see also [101]).

Ensemble symmetries

On the one hand, the node cycle has shown that for a variety of adaptive networks in dynamic equilibrium, steady-state averages (through yielding constraints for constant correspondence parameters) imply steady-state distributions they arise from, and that these steady-state distributions are solely determined by the microscopic dynamics.

On the other hand, Secs. 2.3 and 6.3 demonstrated how in dynamic equilibrium, asymmetric microscopic dynamics can give rise to macroscopic ensemble symmetries. Recurrence relations were formulated that, for a whole class of asymmetric coevolutionary processes, identify a parameter region where such symmetries hold. These symmetries are indeed observed in the adaptive contact process, and partially so in an asymmetric variant of the coevolutionary voter model.

If in dynamic equilibrium macroscopic ensemble symmetries emerge from microscopic *asymmetric* dynamics, one can plausibly ask whether and for which parameters the former can also be generated by appropriately chosen *symmetric* microscopic processes. This is motivated by findings in Sec. 6.3 where at the triple point, asymmetric coevolutionary dynamics generate the same line of equilibria as symmetric dynamics on a static graph. Consequently, the more general question arises as to what extent different microscopic dynamics can give rise to the same equilibrium ensemble statistics. Large-scale properties arising independently from system details is a familiar idea in statistical physics [14], and worth exploring in the context of dynamic equilibria in adaptive networks.

A APPENDIX

A.1 The phase diagram in the pair approximation

The equilibrium points (or fixed points) of the PA are the roots of Eqs. 2.2. Apart from the ubiquitous absorbing state $([I],[II],[SS]) = (0,0,\langle k\rangle/2)$ representing disease fadeout, the two nontrivial solutions are

$$\begin{aligned}
[I]_{1,2} &= \frac{2\omega - (1+\langle k\rangle)\rho(1-\omega) \pm \sqrt{R}}{2(\omega - \rho(1-\omega))} \\
[II]_{1,2} &= \frac{[I]_{1,2}(\rho + [I]_{1,2}(1-2\rho))}{2\rho(1-[I]_{1,2})} \\
[SS]_{1,2} &= \frac{(1-\rho(1-\omega))(1-[I]_{1,2})}{2\rho(1-\omega)}\,,
\end{aligned} \tag{A.1}$$

where

$$R \equiv (1-\omega)(\rho(4+(\langle k\rangle - 3)(1+\langle k\rangle)\rho(1-\omega)) - 4\omega)\,. \tag{A.2}$$

As a first step, the physicality of the solutions needs to be checked, i.e. they ought to be real numbers with

$$\begin{aligned}
&0 \le [I]_{1,2} \le 1 \\
&0 \le [II]_{1,2} \le \langle k\rangle/2 \\
&0 \le [SS]_{1,2} \le \langle k\rangle/2 - [II]_{1,2}
\end{aligned} \tag{A.3}$$

for all $\omega, \rho \in [0,1]$ and $\langle k\rangle > 0$. It is straightforward to show that the link densities are physical whenever $[I]_{1,2}$ is, so that considerations can be confined to the latter.

If

$$\omega < \frac{4+(\langle k\rangle - 3)(1+\langle k\rangle)\rho}{4/\rho + (\langle k\rangle - 3)(1+\langle k\rangle)\rho} \equiv \omega_{\mathrm{A}}(\rho)\,, \tag{A.4}$$

then $[I]_{1,2}$ are indeed real. Demanding moreover for $0 \le [I]_{1,2} \le 1$, the curve

$$\omega_{\mathrm{B}}(\rho) \equiv 1 - \frac{1}{\rho(\langle k\rangle + 1)} \tag{A.5}$$

plays a significant role: With $\omega_{\mathrm{A}}(\rho) \geq \omega_{\mathrm{B}}(\rho)$ for all permissible ρ and $\langle k \rangle$, these two curves share a single point

$$(\omega^*, \rho^*) = \left(\frac{1}{2}, \frac{2}{1 + \langle k \rangle} \right) \tag{A.6}$$

for all $\langle k \rangle \geq 1$. If $\rho < \rho^*$, $[I]_1$ is physical for all $\omega \leq \omega_{\mathrm{B}}(\rho)$, whereas $[I]_2$ is not for any choice of ω. For $\rho > \rho^*$ on the other hand, $[I]_1$ is physical for $\omega \leq \omega_{\mathrm{A}}(\rho)$, while $[I]_2$ is now for $\omega_{\mathrm{B}}(\rho) \leq \omega \leq \omega_{\mathrm{A}}(\rho)$. Apart from the trivial absorbing state that is physical for all permissible (ω, ρ), parameter space thus yields one dynamic equilibrium for $\omega \leq \omega_{\mathrm{B}}(\rho)$, and two for $\omega_{\mathrm{B}}(\rho) \leq \omega \leq \omega_{\mathrm{A}}(\rho)$ with $\rho > \rho^*$.

Having partitioned parameter space into regions with differing numbers of coexisting equilibrium points, the stability of the latter ought to be investigated to obtain the full phase diagram. This is achieved with the linearization of Eqs. 2.2,

$$\begin{pmatrix} \dot{[I]} \\ \dot{[II]} \\ \dot{[SS]} \end{pmatrix} = J \begin{pmatrix} [I] \\ [II] \\ [SS] \end{pmatrix} , \tag{A.7}$$

where the Jacobian J of Eqs. 2.2 is evaluated at the fixed point. If the fixed point under consideration is hyperbolic, it is stable if all of the eigenvalues of J are negative, and unstable otherwise.

Following this procedure, the absorbing state $(0, 0, \langle k \rangle/2)$ is shown to be stable for $\omega > \omega_{\mathrm{B}}(\rho)$ and unstable otherwise. Subsequent numerical analysis of the eigenvalues reveals that the fixed point $([I]_2, [SS]_2, [II]_2)$ is unstable when physical and $([I]_1, [SS]_1, [II]_1)$ is stable when $\omega < \omega_{\mathrm{B}}(\rho)$. To judge which stability the physical $([I]_1, [SS]_1, [II]_1)$ has for $\omega_{\mathrm{B}}(\rho) < \omega < \omega_{\mathrm{A}}(\rho)$, the following scenarios need to be distinguished:

1. For $\rho > \rho^*$ until intermediate ranges of ρ, $([I]_1, [SS]_1, [II]_1)$ is stable throughout considered values of ω.

2. For larger ρ and small $\omega > \omega_{\mathrm{B}}(\rho)$, $([I]_1, [SS]_1, [II]_1)$ is stable, while a subcritical Andronov-Hopf bifurcation turns it unstable for larger ω.

3. For even larger ρ, $([I]_1, [SS]_1, [II]_1)$ is again stable for small $\omega > \omega_{\mathrm{B}}(\rho)$. At larger ω, $[I]_1$ loses stability in a now supercritical Andronov-Hopf bifurcation that yields a stable limit cycle, the latter of which disappears in a cycle-fold bifurcation when further increasing ω [18].

The line $\omega_{\mathrm{B}}(\rho)$ can be shown with [61] to be a transcritical bifurcation identified with the epidemic threshold of the model, whereas for $\omega \geq 1/2$, $\omega_{\mathrm{A}}(\rho)$ is the fold bifurcation that gives rise to the bistable region.

A.2 Solving Master equations in the node cycle

S-Stage

Multiplying both sides of Eq. 3.6 with $\chi^x\gamma^y$ and summing over x and y yields

$$\begin{aligned}\sum_{x,y=0}^{\infty}\chi^x\gamma^y\frac{\mathrm{d}[x,y]}{\mathrm{d}t} =&(w+r)\,(\chi-\gamma)\,\frac{\partial}{\partial\gamma}\sum_{x,y=0}^{\infty}\chi^x\gamma^y[x,y]-p\gamma\frac{\partial}{\partial\gamma}\sum_{x,y=0}^{\infty}\chi^x\gamma^y[x,y]\\ &+\tilde{w}\,(\chi-1)\sum_{x,y=0}^{\infty}\chi^x\gamma^y[x,y]+\tilde{p}_{\mathrm{S}}\,(\gamma-\chi)\,\frac{\partial}{\partial\chi}\sum_{x,y=0}^{\infty}\chi^x\gamma^y[x,y]\,,\end{aligned} \tag{A.8}$$

where the boundary conditions of Eq. 6.10 permit the shifting of summation indices. The probability generating function $F_{\mathrm{S}}\equiv F_{\mathrm{S}}(\chi,\gamma,t|x_0,y_0)$ of $P_{\mathrm{S}}(x,y,t|x_0,y_0)$ obeys the linear first-order PDE

$$\frac{\partial F_{\mathrm{S}}}{\partial t} =\{(w+r)\chi-(w+r+p)\gamma\}\frac{\partial F_{\mathrm{S}}}{\partial\gamma}+\tilde{p}_{\mathrm{S}}(\gamma-\chi)\frac{\partial F_{\mathrm{S}}}{\partial\chi}+\tilde{w}(\chi-1)F_{\mathrm{S}}\,. \tag{A.9}$$

The method of characteristics prescribes a change of coordinates in a PDE, identifying *characteristic curves* along which the equation is reduced to an ODE. In general this ODE more amenable to analytic treatment, and its solution can subsequently be transformed back into the initial coordinates to solve the original PDE. Applied to our random walk on a degree grid in the S-stage, Eq. A.9 can be rewritten as

$$\begin{aligned}\tilde{w}(\chi-1)F_{\mathrm{S}} &= \frac{\partial F_{\mathrm{S}}}{\partial\chi}\tilde{p}_{\mathrm{S}}(\chi-\gamma)+\frac{\partial F_{\mathrm{S}}}{\partial\gamma}\left((w+r+p)\gamma-(w+r)\chi\right)+\frac{\partial F_{\mathrm{S}}}{\partial t}\\ &= \frac{\partial F_{\mathrm{S}}}{\partial\chi}\frac{\partial\chi}{\partial t}+\frac{\partial F_{\mathrm{S}}}{\partial\gamma}\frac{\partial\gamma}{\partial t}+\frac{\partial F_{\mathrm{S}}}{\partial t}\\ &= \frac{\mathrm{d}F_{\mathrm{S}}}{\mathrm{d}t}\end{aligned} \tag{A.10}$$

if the characteristic curves $\chi(t)$ and $\gamma(t)$ obey

$$\frac{\mathrm{d}}{\mathrm{d}t}\begin{pmatrix}\chi(t)\\ \gamma(t)\end{pmatrix}=\begin{pmatrix}\tilde{p}_{\mathrm{S}} & -\tilde{p}_{\mathrm{S}}\\ -w-r & w+r+p\end{pmatrix}\begin{pmatrix}\chi(t)\\ \gamma(t)\end{pmatrix}\,. \tag{A.11}$$

Solving the latter system of ODEs through matrix exponentials with initial conditions $\chi(0)=\chi_0$ and $\gamma(0)=\gamma_0$ readily yields

$$\begin{aligned}\gamma(t) =&\frac{e^{\frac{tZ}{2}}}{U}\left(U\gamma_0\cosh\left(\frac{Ut}{2}\right)-\left[2(Z-\tilde{p}_{\mathrm{S}}-p)\chi_0-(Z-2\tilde{p}_{\mathrm{S}})\,\gamma_0)\right]\sinh\left(\frac{Ut}{2}\right)\right)\\ \chi(t) =&\frac{e^{\frac{tZ}{2}}}{U}\left(U\chi_0\cosh\left(\frac{Ut}{2}\right)-\left[(Z-2\tilde{p}_{\mathrm{S}})\chi_0+2\tilde{p}_{\mathrm{S}}\gamma_0\right]\sinh\left(\frac{Ut}{2}\right)\right)\end{aligned} \tag{A.12}$$

for $Z \equiv (w + p + r + \tilde{p}_\mathrm{S})$ and $U \equiv \sqrt{Z^2 - 4 \cdot p \cdot \tilde{p}_\mathrm{S}}$. Having found the relevant characteristic curves, the solution

$$F_\mathrm{S}(\chi(t), \gamma(t), t|x_0, y_0) = Ce^{\tilde{w}\left(\int_0^t \chi(t')\mathrm{d}t' - t\right)} \tag{A.13}$$

to the ODE of Eq. A.10 can be translated back to the initial coordinates. Here initial conditions determine C (which is a constant along $\chi(t)$ and $\gamma(t)$), and it follows that

$$C = F_\mathrm{S}(\chi(0), \gamma(0), 0|x_0, y_0) = F_\mathrm{S}(\chi_0, \gamma_0, 0|x_0, y_0) = \chi_0^{x_0}\gamma_0^{y_0}\,, \tag{A.14}$$

with the third equality stemming from the definition of $F_\mathrm{S}(\chi(t), \gamma(t), t|x_0, y_0)$ combined with the fact that the random walker on the degree grid starts at coordinates (x_0, y_0). Finally, inverting Eqs. A.12 delivers $\chi_0(\chi, \gamma, t)$ and $\gamma_0(\chi, \gamma, t)$, which are then substituted into Eq. A.13 *after* exponent integration to culminate in

$$F_\mathrm{S}(\chi, \gamma, t|x_0, y_0) = \left(c_1(t)\,\chi + c_2(t)\,\gamma\right)^{x_0}\left(c_3(t)\,\chi + c_4(t)\,\gamma\right)^{y_0} \tag{A.15}$$

$$\frac{e^{c_5(t)\chi + c_6(t)\gamma + c_7(t, x_0, y_0)}}{U^{x_0+y_0}} \tag{A.16}$$

with

$$\begin{aligned}
c_1(t) =& U\cosh\left(\frac{Ut}{2}\right) + (Z - 2\tilde{p}_\mathrm{S})\sinh\left(\frac{Ut}{2}\right)\\
c_2(t) =& 2\tilde{p}_\mathrm{S}\sinh\left(\frac{Ut}{2}\right)\\
c_3(t) =& 2(Z - \tilde{p}_\mathrm{S} - p)\sinh\left(\frac{Ut}{2}\right)\\
c_4(t) =& U\cosh\left(\frac{Ut}{2}\right) - (Z - 2\tilde{p}_\mathrm{S})\sinh\left(\frac{Ut}{2}\right)\\
c_5(t) =& \frac{\tilde{w}e^{-\frac{Zt}{2}}}{\tilde{p}_\mathrm{S}pU}\left[U(\tilde{p}_\mathrm{S} - Z)\cosh\left(\frac{Ut}{2}\right) + [2p\tilde{p}_\mathrm{S} + (\tilde{p}_\mathrm{S} - Z)Z]\sinh\left(\frac{Ut}{2}\right)\right]\\
&+ \frac{\tilde{w}}{\tilde{p}_\mathrm{S}pU}U(Z - \tilde{p}_\mathrm{S})\\
c_6(t) =& \frac{\tilde{w}}{pU}\left(U - e^{-\frac{Zt}{2}}\left[U\cosh\left(\frac{Ut}{2}\right) + Z\sinh\left(\frac{Ut}{2}\right)\right]\right)\\
c_7(t, x_0, y_0) =& -\left(\tilde{w} + \frac{Z(x_0 + y_0)}{2}\right)t\,.
\end{aligned} \tag{A.17}$$

I-Stage

Similarly, transforming the Master equation 3.7 for the I-stage into a PDE for the respective probability generating function yields

$$\frac{\partial F_\mathrm{I}}{\partial t} = r\,(\chi - \gamma)\,\frac{\partial F_\mathrm{I}}{\partial \gamma} + (\tilde{p}_\mathrm{I}\gamma - (w + \tilde{p}_\mathrm{I})\chi + w)\,\frac{\partial F_\mathrm{I}}{\partial \chi} - rF_\mathrm{I} \tag{A.18}$$

whose solution, following the procedure outlined above, is

$$\begin{aligned} F_{\mathrm{I}}(\chi,\gamma,t|x_0,y_0) =& e^{-rt}\left(1-e^{-\frac{St}{2}}\left[c_1(t)\left(\chi-1\right)+c_2(t)\left(\gamma-1\right)\right]\right)^{x_0} \\ & \left(1+e^{-\frac{St}{2}}\left[c_3(t)\left(\chi-1\right)+c_4(t)\left(\gamma-1\right)\right]\right)^{y_0} \end{aligned} \tag{A.19}$$

with $S \equiv (w+r+\tilde{p}_{\mathrm{I}})$, $V \equiv \sqrt{S^2-4\cdot r\cdot w}$ and

$$\begin{aligned} c_1(t) =& \frac{(S-2r)\sinh\left(\frac{Vt}{2}\right)}{V} - \cosh\left(\frac{Vt}{2}\right) \\ c_2(t) =& \frac{2\tilde{p}_{\mathrm{I}}\sinh\left(\frac{Vt}{2}\right)}{V} \\ c_3(t) =& \frac{2r\sinh\left(\frac{Vt}{2}\right)}{V} \\ c_4(t) =& \frac{(S-2r)\sinh\left(\frac{Vt}{2}\right)}{V} + \cosh\left(\frac{Vt}{2}\right). \end{aligned} \tag{A.20}$$

A.3 Node-cycle probability densities in closed form

The probability generating function of the random walk in the S-stage is rewritten as

$$\begin{aligned} F_{\mathrm{S}}(\chi,\gamma,t|x_0,y_0) =& \left(c_1(t)\chi+c_3(t)\gamma\right)^{x_0}\left(c_2(t)\chi+c_4(t)\gamma\right)^{y_0}\frac{e^{c_5(t)\chi+c_6(t)\gamma+c_7(t)}}{U^{x_0+y_0}} \\ =& \frac{e^{c_7(t,x_0,y_0)}}{U^{x_0+y_0}}\sum_{i=0}^{x_0}\sum_{j=0}^{y_0}\sum_{l,m=0}^{\infty} c(t,i,j,l,m)\chi^{x_0+y_0+l-i-j}\gamma^{i+j+m} \end{aligned} \tag{A.21}$$

with

$$c(t,i,j,l,m) = c_1(t)^{x_0-i}c_2(t)^i c_3(t)^{y_0-j}c_4(t)^j\frac{c_5(t)^l}{l!}\frac{c_6(t)^m}{m!}\binom{x_0}{i}\binom{y_0}{j}. \tag{A.22}$$

According to Eq. 3.10, all summation terms in Eq. A.21 are canceled except when

$$\begin{aligned} l =& i+j+x-x_0-y_0 \\ m =& y-i-j \end{aligned} \tag{A.23}$$

for $l,m \geq 0$. What follows is

$$P_{\mathrm{S}}(x,y,t|x_0,y_0) = \frac{e^{c_7(t,x_0,y_0)}}{U^{x_0+y_0}}\sum_{\substack{i=0 \\ x_0+y_0-x\leq i+j\leq y}}^{x_0}\sum_{j=0}^{y_0} c(t,i,j,i+j+x-x_0-y_0,y-i-j) \tag{A.24}$$

if $(x_0 + y_0) \leq (x + y)$ and $P_{\mathrm{S}}(x, y, t|x_0, y_0) = 0$ otherwise, since a S-node does not experience a loss in total degree. According to Eqs. A.17, A.22 and A.24, $P_{\mathrm{S}}(x, y, t|x_0, y_0)$ is a finite sum of exponential functions.

Arguing along the same lines, the time-dependent probability densities encapsulated in the generating function F_{I} also consist of finite sums of exponential functions in time. It follows that, as in the S-stage, the respective tensors P_{I} and Φ_{I} describing the I-stage can be set up fully analytically, with each entry consisting of a finite sum of closed-form expressions.

A.4 Reducing the rank of tensors in the node cycle

With the maximum degree $k_{\mathrm{M}} \geq (x + y) \geq 0$, one can map index doublets (x, y) representing joint degrees on a single index variable z as

$$z = y + 1 + \sum_{i=1}^{x} (k_{\mathrm{M}} + 2 - i) = y + 1 + \left(k_{\mathrm{M}} + 2 - \frac{x+1}{2}\right) x \tag{A.25}$$

with $z \in [1, (k_{\mathrm{M}} + 1) \cdot (k_{\mathrm{M}} + 2)/2]$.

The map $(x, y) \to (z)$ is bijective, so that z can reversely be assigned a unique doublet (x, y). Then

$$z \leq \left(k_{\mathrm{M}} + 2 - \frac{(x+1)+1}{2}\right)(x+1) \tag{A.26}$$

from which follows

$$\left(\frac{2k_{\mathrm{M}}+1}{2} - x\right)^2 \leq \sqrt{\frac{(2k_{\mathrm{M}}+1)^2}{4} + 2(k_{\mathrm{M}} + 1 - z)} \tag{A.27}$$

and finally

$$x \geq \frac{2k_{\mathrm{M}}+1}{2} - \sqrt{\frac{(2k_{\mathrm{M}}+1)^2}{4} + 2(k_{\mathrm{M}} + 1 - z)}\,, \tag{A.28}$$

where the third inequality follows from $x \leq k_{\mathrm{M}}$. Considering Eq. A.28 as an equality, it yields a (generally non-integer) solution x_R on its left-hand side, and clearly x is then equal to the smallest integer that is not less than x_R. Having both z and x at hand, y is calculated through Eq. A.25 as a last step.

Hence tensors $P_{\mathrm{S,I}}(x, y|x_0, y_0)$ and $\Phi_{\mathrm{S,I}}(x, y|x_0, y_0)$ with $(k_{\mathrm{M}} + 1)^4$ elements are expressd as matrices with $[(k_{\mathrm{M}} + 1) \cdot (k_{\mathrm{M}} + 2)/2]^2$ entries, and similarly the matrices $P_{\mathrm{S,I}}(x, y)$ and $\Phi_{\mathrm{S,I}}(x, y)$ are turned into vectors of $(k_{\mathrm{M}} + 1) \cdot (k_{\mathrm{M}} + 2)/2$ elements.

A.5 Regularizing absorbing states

S-Consensus

In the spirit of Appendix A.1, the Jacobian of Eqs. 6.1 is computed at $(0, 0, 0)$, yielding the eigenvalues

$$\begin{aligned}\lambda_1 &= -2(1-\rho)(1-\omega)\\ \lambda_{2,3} &= \frac{1}{2}\left(-6-(5+\langle k\rangle)\rho(-1+\omega)+5\omega \pm \sqrt{R}\right)\end{aligned} \tag{A.29}$$

with

$$\begin{aligned}R \equiv &(2-3\omega)^2 + (-7+\langle k\rangle)(1+\langle k\rangle)\rho^2(-1+\omega)^2\\ &+ 2\rho(-1+\omega)(-2-2\langle k\rangle-\omega+3\langle k\rangle w)\,.\end{aligned} \tag{A.30}$$

For considered $\omega, \rho \in [0, 1]$, $\lambda_1 \leq 0$ always, and eigenvalues $\lambda_{2,3}$ are real numbers. The larger of them (λ_3) is then negative for

$$\rho \leq \frac{2-\omega}{(2+\langle k\rangle)\,(1-\omega)}, \tag{A.31}$$

giving the phase boundary for stable S-consensus.

I-Consensus

Expressing Eqs. 6.1 in spherical coordinates $\theta, \phi \in [0, \pi/2]$ and $r \in [0, 1]$ with $x = (1 - r \cdot \sin(\theta) \cdot \cos(\phi))$, $y = (\langle k\rangle/2 - r \cdot \sin(\theta) \cdot \sin(\phi))$ and $z = r \cdot \cos(\theta)$, one is interested in the flow's behavior in the vicinity of I-consensus, i.e. for $r \to 0$.

In these coordinates, the singularity at I-consensus can be regularized, and it is found that $\dot{r} = 0$ for $r = 0$ and all angular coordinates. Hence the sphere octant Σ at $r = 0$ is invariant and represents I-consensus, which is then indeed a steady state. Parameter regions of stable I-consensus can consequently be determined by identifying stable fixed points (θ^*, ϕ^*) of the angular flow on Σ, in conjunction with demanding stability of the radial flow at (θ^*, ϕ^*). In the following, *fixed point* will be exclusively used in the context of the two-dimensional angular flow on Σ, whereas I-consensus in the full system is referred to as such.

It is straightforward to classify the parameter dependence of the angular flow into six typical phase portraits, each of which yields three fixed points at the boundary $\phi = \pi/2$ and none, one or two in the interior of Σ. With these phase portraits at hand, the stability of fixed points is separately investigated for those two regions.

At the boundary $\phi = \pi/2$, the angular flow has fixed points (θ^*, ϕ^*) at coordinates $(\arccos(2/\sqrt{5}), \pi/2)$, $(\pi/4, \pi/2)$ and $(\pi/2, \pi/2)$. The first one is unstable, whereas the remaining two are non-hyperbolic with one zero and one negative eigenvalue each. The radial flow is unstable at $(\pi/2, \pi/2)$ and stable at $(\pi/4, \pi/2)$, so that only the latter fixed point is of further interest. Aforementioned phase portraits reveal it to be stable as soon as there are two (for $\rho < 2/(1 + \langle k \rangle)$) or no (for $\rho > 2/(1 + \langle k \rangle)$) fixed points in the interior of Σ. For both cases, this criterion translates into a comparison of tangent slopes of respective nullclines at $(\pi/4, \pi/2)$ and yields

$$\rho > (2 - 3\omega)/(1 - \omega) \tag{A.32}$$

as a sufficient condition for stable I-consensus.

Thus for $\rho < (2 - 3 \cdot \omega)/(1 - \omega)$, there is exactly one fixed point in the interior of Σ, and it follows from aforementioned phase portraits that it is always stable. It can moreover be shown that the radial flow at this fixed point is stable if

$$\rho > 2/(1 + \langle k \rangle) \ , \tag{A.33}$$

so that overall, I-consensus is stable for

$$\rho > \min\{2/(1 + \langle k \rangle), (2 - 3\omega)/(1 - \omega)\} \ . \tag{A.34}$$

Note that there can be coexisting stable fixed points for the angular flow - one at $(\pi/4, \pi/2)$ (automatically implying stable I-consensus) and one in the interior of Σ. For the $\langle k \rangle$ chosen here, the basin of attraction of the former is significantly smaller than that of the latter. If the radial flow is unstable at the interior fixed point, trajectories in the vicinity of I-consensus usually get attracted to those angular coordinates and are consequently repelled from I-consensus in the r-direction. This is the case for low ρ and large ω, so that reaching I-consensus for that parameter region requires careful selection of initial conditions (Fig. 6.2b). If however the radial flow is also stable at the interior stable fixed point, then there are two routes towards I-consensus, characterized by the two different angles under which the trajectory approaches it.

A.6 Quantifying metastability

In what follows, a condensed version of the relevant section in [58] is laid out: Considering a general one-step process in the positive integer variable $0 \leq i \leq N$, transition rates g_i (mediating a gain in i), r_i (descending i) and the two absorbing integer boundaries 0 and $N \geq 0$ are defined.

Splitting probabilities

The splitting probability π_i for the random walker to reach N before 0 when starting from i,

$$\pi_i = \frac{g_i}{g_i + r_i}\pi_{i+1} + \frac{r_i}{g_i + r_i}\pi_{i-1} \tag{A.35}$$

and equivalently

$$0 = g_i(\pi_{i+1} - \pi_i) + r_i(\pi_{i-1} - \pi_i) \tag{A.36}$$

obviously hold for $2 \leq i \leq (N-2)$ as a recursive definition of π_i. As the boundary conditions are $\pi_0 = 0$ and $\pi_N = 1$, Eq. A.36 extends its validity to $1 \leq i \leq (N-1)$. For the same interval of i, setting $\Delta_i \equiv (\pi_{i+1} - \pi_i)$

yields

$$g_i\Delta_i = r_i\Delta_{i-1}\,, \tag{A.37}$$

so that

$$\Delta_i = \prod_{j=1}^{i} \frac{r_j}{g_j}\Delta_0 \tag{A.38}$$

with $\Delta_0 = \pi_1$. It follows that

$$\pi_i = \sum_{j=0}^{i-1} \Delta_j = \pi_1 + \sum_{j=1}^{i-1}\prod_{k=1}^{j} \frac{r_k}{g_k}\pi_1\,. \tag{A.39}$$

Considering that $\pi_N = 1$ delivers π_1, so that finally

$$\pi_i = \frac{1 + \sum_{j=1}^{i-1}\prod_{k=1}^{j} r_k/g_k}{1 + \sum_{j=1}^{N-1}\prod_{k=1}^{j} r_k/g_k} = \left(1 + \frac{\sum_{j=i}^{N-1}\prod_{k=1}^{j} r_k/g_k}{1 + \sum_{j=1}^{i-1}\prod_{k=1}^{j} r_k/g_k}\right)^{-1}\,. \tag{A.40}$$

Inserting the transition rates of Sec. 6.1 readily yields the splitting probabilities for the asymmetric model, which for large N and i are calculated according to the second equality of Eq. A.40 to minimize computation times.

Mean first-passage times

In the same recursive manner as above, one can compute the mean first-passage time τ_i of the random walker to hit coordinate N before 0 when starting at coordinate $0 \leq i \leq N$. Within the first time step Δt, the random walker jumps to $(i+1)$ with probability $g_i \cdot \Delta t$, to $(i-1)$ with probability $r_i \cdot \Delta t$, and stays at i with probability $(1 - g_i \cdot \Delta t - r_i \cdot \Delta t)$. Obviously $(\tau_i - \Delta t)$ is equal to a weighted sum

of τ_{i+1}, τ_i and τ_{i-1}, with the weights being aforementioned transition probabilities to the respective coordinates. Hence

$$\tau_i - \Delta t = \tau_{i+1} g_i \Delta t + \tau_{i-1} r_i \Delta t + \tau_i (1 - g_i \Delta t - r_i \Delta t) \tag{A.41}$$

and, by multiplying both sides with $\pi_i / \Delta t$ as well as introducing $\nu_i \equiv \pi_i \cdot \tau_i$ and redefining $\Delta_i \equiv (\nu_{i+1} - \nu_i)$,

$$\Delta_i = -\frac{\pi_i}{g_i} + \frac{r_i}{g_i} \Delta_{i-1} \,. \tag{A.42}$$

It is straightforward to check that this recursive equation can be given the closed form

$$\Delta_i = \nu_1 \prod_{k=1}^{i} \frac{r_k}{g_k} - \sum_{j=1}^{i} \frac{\pi_j}{r_j} \prod_{k=j}^{i} \frac{r_k}{g_k} \,, \tag{A.43}$$

so that then

$$\nu_i = \sum_{j=0}^{i-1} \Delta_j = \nu_1 \left(1 + \sum_{j=1}^{i-1} \prod_{k=1}^{j} \frac{r_k}{g_k} \right) - \sum_{j=1}^{i-1} \sum_{k=1}^{j} \frac{\pi_k}{r_k} \prod_{l=k}^{j} \frac{r_l}{g_l} \,. \tag{A.44}$$

Since $\nu_N = 0$ due to $\tau_N = 0$, ν_1 can be calculated from Eq. A.44 as

$$\nu_1 = \frac{\sum_{j=1}^{N-1} \sum_{k=1}^{j} \pi_k / r_k \prod_{l=k}^{j} r_l / g_l}{1 + \sum_{j=1}^{N-1} \prod_{k=1}^{j} r_k / g_k} \,. \tag{A.45}$$

Inserting Eq. A.45 into Eq. A.44 while considering Eq. A.40 finally yields

$$\begin{aligned} \nu_i &= \pi_i \sum_{j=1}^{N-1} \sum_{k=1}^{j} \frac{\pi_k}{r_k} \prod_{l=k}^{j} \frac{r_l}{g_l} - \sum_{j=1}^{i-1} \sum_{k=1}^{j} \frac{\pi_k}{r_k} \prod_{l=k}^{j} \frac{r_l}{g_l} \\ &= \pi_i \sum_{j=i}^{N-1} \sum_{k=1}^{j} \frac{\pi_k}{r_k} \prod_{l=k}^{j} \frac{r_l}{g_l} - (1 - \pi_i) \sum_{j=1}^{i-1} \sum_{k=1}^{j} \frac{\pi_k}{r_k} \prod_{l=k}^{j} \frac{r_l}{g_l} \end{aligned} \tag{A.46}$$

with $\tau_i = \nu_i / \pi_i$, where for large N and i, the second equality is to be preferred to ensure fast computation of ν_i.

To calculate the mean passage time $\tau_i^{'}$ for hitting coordinate 0 first when starting from i, the variable $\nu_i^{'} \equiv (1 - \pi_i) \cdot \tau_i^{'}$ is introduced. Then $\nu_i^{'}$ is easily obtained from Eq. A.46 by reversing the direction of the considered first passage, so that

$$\nu_i^{'} = (1 - \pi_i) \sum_{j=N-i}^{N-1} \sum_{k=1}^{j} \frac{\pi_{N-k}}{g_{N-k}} \prod_{l=k}^{j} \frac{g_{N-l}}{r_{N-l}} - \pi_i \sum_{j=1}^{N-i-1} \sum_{k=1}^{j} \frac{\pi_{N-k}}{g_{N-k}} \prod_{l=k}^{j} \frac{g_{N-l}}{r_{N-l}} \tag{A.47}$$

and $\tau_i^{'} = \nu_i^{'} / (1 - \pi_i)$.

Bibliography

[1] C. R. Darwin. *The descent of man, and selection in relation to sex.* Project Gutenberg, 2nd edition, 2000.

[2] N. Copernicus. *On the revolutions of the heavenly spheres.* Prometheus Books, 1995.

[3] E. P. Hubble. Extra-galactic nebulae. *The Astrophysical Journal*, 64:321–369, 1926.

[4] B. Libet, C. A. Gleason, E. W. Wright, and D. K. Pearl. Time of conscious intention to act in relation to onset of cerebral activity (readiness-potential). The unconscious initiation of a freely voluntary act. *Brain*, 106:623–42, 1983.

[5] D. Fagen. *I.G.Y.* Warner, 1982.

[6] K. Marx and F. Engels. *Manifesto of the communist party.* Project Gutenberg, 2005.

[7] R. Axelrod and W. D. Hamilton. The evolution of cooperation. *Science*, 211:1390–1396, 1981.

[8] E. J. Gumbel. *Statistics of extremes.* Dover Books on Mathematics, 2004.

[9] M. Gardner. The fantastic combinations of John Conway's new solitaire game "life". *Sci. Am.*, 223:120–123, 1970.

[10] G. Lebon, D. Jou, and J. Casas-Vázquez. *Understanding non-equilibrium thermodynamics: Foundations, applications, frontiers.* Springer, 2008.

[11] N. Goldenfeld and L. P. Kadanoff. Simple lessons from complexity. *Science*, 284:87–89, 1999.

[12] H. Haken. *Synergetics, an introduction: Nonequilibrium phase transitions and self-organization in physics, chemistry, and biology.* Springer, 3rd edition, 1983.

[13] H. Risken. *The Fokker-Planck equation: Methods of solutions and applications.* Springer, 2nd edition, 1996.

[14] N. Goldenfeld. *Lectures on phase transitions and the renormalization group*. Westview Press, 1992.

[15] S. H. Strogatz. *Nonlinear dynamics and chaos: With applications to physics, biology, chemistry, and engineering*. Westview Press, 2001.

[16] P. Hartman. A lemma in the theory of structural stability of differential equations. *Proc. AMS*, 11:610–620, 1960.

[17] D. M. Grobman. Topological classification of neighborhoods of a singularity in n-space. *Mat. Sbornik*, 56:77–94, 1962.

[18] J. Guckenheimer and P. Holmes. *Nonlinear oscillations, dynamical systems, and bifurcations of vector fields*. Springer, 2nd edition, 2002.

[19] S. Wiggins. *Introduction to applied nonlinear dynamical systems and chaos*. Springer, 2nd edition, 2003.

[20] G. Gonthier. Formal proof-the four-color theorem. *Not. AMS*, 55:1382–1393, 2008.

[21] M. Matsumoto and T. Nishimura. Mersenne Twister: A 623-dimensionally equidistributed uniform pseudo-random number generator. *ACM Transactions on Modeling and Computer Simulation*, 8:3–30, 1998.

[22] R. Albert and A.-L. Barabási. Statistical mechanics of complex networks. *Rev. Mod. Phys.*, 74:47–97, 2002.

[23] S. N. Dorogovtsev and J. F. F. Mendes. *Evolution of networks: From biological nets to the internet and WWW*. Oxford University Press, 2003.

[24] M. E. J. Newman. The structure and function of complex networks. *SIAM Review*, 45:167–256, 2003.

[25] S. Boccaletti, V. Latora, Y. Moreno, M. Chavez, and D. Hwang. Complex networks: Structure and dynamics. *Phys. Rep.*, 424:175–308, 2006.

[26] B. Bollobás. *Random Graphs*. Cambridge Studies in Advanced Mathematics, 2nd edition, 2001.

[27] D. J. Watts and S. H. Strogatz. Collective dynamics of 'small-world' networks. *Nature*, 393:440–442, 1998.

[28] A.-L. Barabási and R. Albert. Emergence of scaling in random networks. *Science*, 286:509–512, 1999.

[29] T. Gross and B. Blasius. Adaptive coevolutionary networks: A review. *J. R. Soc. Interface*, 5:259–271, 2008.

[30] T. Gross and H. Sayama, editors. *Adaptive networks: Theory, models and applications*. Springer, 2009.

[31] H. Ebel and S. Bornholdt. Coevolutionary games on networks. *Phys. Rev. E*, 66:056118, 2002.

[32] M. G. Zimmermann, V. M. Eguíluz, and M. San Miguel. Co-evolution of dynamical states and interactions in dynamic networks. *Phys. Rev. E*, 69:065102, 2004.

[33] A. Szolnoki and M. Perc. Resolving social dilemmas on evolving random networks. *EPL*, 86:30007, 2009.

[34] F. Fu, T. Wu, and L. Wang. Partner switching stabilizes cooperation in coevolutionary prisoner's dilemma. *Phys. Rev. E*, 79:036101, 2009.

[35] M. Perc and A. Szolnoki. Coevolutionary games - a mini review. *Biosystems*, 99:109–125, 2010.

[36] P. Holme and M. E. J. Newman. Nonequilibrium phase transition in the coevolution of networks and opinions. *Phys. Rev. E*, 74:056108, 2006.

[37] B. Kozma and A. Barrat. Consensus formation on adaptive networks. *Phys. Rev. E*, 77:016102, 2008.

[38] F. Vazquez, V. M. Eguíluz, and M. San Miguel. Generic absorbing transition in coevolution dynamics. *Phys. Rev. Lett.*, 100:108702, 2008.

[39] I. J. Benczik, S. Z. Benczik, B. Schmittmann, and R. K. P. Zia. Opinion dynamics on an adaptive random network. *Phys. Rev. E*, 79:046104, 2009.

[40] S. Funk, M. Salathé, and V. A. A. Jansen. Modelling the influence of human behaviour on the spread of infectious diseases: A review. *J. R. Soc. Interface*, 7:1247–1256, 2010.

[41] D. H. Zanette and S. Gil. Opinion spreading and agent segregation on evolving networks. *Phys. D.*, 224:156–165, 2006.

[42] T. Gross, C. J. Dommar, and B. Blasius. Epidemic dynamics on an adaptive network. *Phys. Rev. Lett.*, 96:208701, 2006.

[43] S. Risau-Gusman and D. H. Zanette. Contact switching as a control strategy for epidemic outbreaks. *J. Theor. Biol.*, 257:52 – 60, 2009.

[44] B. Drossel, P. G. Higgs, and A. J. McKane. The influence of predator-prey population. *J. Theor. Biol.*, 208:91–107, 2001.

[45] U. Dieckmann, M. Doebeli, J. A. J. Metz, and D. Tautz, editors. *Adaptive speciation*. Cambridge University Press, 2004.

[46] W.X. Wang, B.H. Wang, B. Hu, G. Yan, and Q. Ou. General dynamics of topology and traffic on weighted technological networks. *Phys. Rev. Lett.*, 94:188702, 2005.

[47] M. Lim, D. Braha, S. Wijesinghe, S. Tucker, and Y. Bar-Yam. Preferential detachment in broadcast signaling networks: Connectivity and cost tradeoff. *EPL*, 79:58005, 2007.

[48] Y. B. Xie, W. X. Wang, and B. H. Wang. Modeling the coevolution of topology and traffic on weighted technological networks. *Phys. Rev. E*, 75:026111, 2007.

[49] J. L. Herrera, M. G. Cosenza, K. Tucci, and J. C. González-Avella. General coevolution of topology and dynamics in networks. *EPL*, 95:58006, 2011.

[50] C. Zhang, J. Zhang, G. Xie, L. Wang, and M. Perc. Evolution of interactions and cooperation in the spatial prisoner's dilemma game. *PLoS ONE*, 6:e26724, 2011.

[51] M. G. Zimmermann and V. M. Eguíluz. Cooperation, social networks, and the emergence of leadership in a prisoner's dilemma with adaptive local interactions. *Phys. Rev. E*, 72:056118, 2005.

[52] C. Lagorio, M. Dickison, F. Vazquez, L. A. Braunstein, P. A. Macri, M. V. Migueles, S. Havlin, and H. E. Stanley. Quarantine-generated phase transition in epidemic spreading. *Phys. Rev. E*, 83:026102, 2011.

[53] O. Gräser, C. Xu, and P. M. Hui. Disconnected-connected network transitions and phase separation driven by co-evolving dynamics. *EPL*, 87:38003, 2009.

[54] G. Demirel, F. Vazquez, G. A. Böhme, and T. Gross. Moment-closure approximations for discrete adaptive networks. *arXiv:1211.0449 [nlin.AO]*, 2013.

[55] G. A. Böhme and T. Gross. Analytical calculation of fragmentation transitions in adaptive networks. *Phys. Rev. E*, 83:035101, 2011.

[56] S. Bornholdt and T. Rohlf. Topological evolution of dynamical networks: Global criticality from local dynamics. *Phys. Rev. Lett.*, 84:6114–6117, 2000.

[57] P. Holme and G. Ghoshal. Dynamics of networking agents competing for high centrality and low degree. *Phys. Rev. Lett.*, 96:098701, 2006.

[58] N. van Kampen. *Stochastic Processes in Physics and Chemistry*. North Holland, 3rd edition, 2007.

[59] R. M. May and R. M. Anderson. *Infectious diseases of humans: Dynamics and control*. Oxford University Press, 1992.

[60] K. T. D. Eames and M. J. Keeling. Modeling dynamic and network heterogeneities in the spread of sexually transmitted diseases. *PNAS*, 99:13330–13335, 2002.

[61] E. J. Doedel, A. R. Champneys, F. Dercole, T. Fairgrieve, Y. Kuznetsov, B. Oldeman, R. Paffenroth, B. Sandstede, X. Wang, and C. Zhang. *AUTO-07P: Continuation and bifurcation software for ordinary differential equations*, 2008.

[62] D. Juher, J. Ripoll, and J. Saldaña. Outbreak analysis of an SIS epidemic model with rewiring. *J. Math. Biol.*, 67:411–432, 2013.

[63] R. Pastor-Satorras and A. Vespignani. Epidemic spreading in scale-free networks. *Phys. Rev. Lett.*, 86:3200–3203, 2001.

[64] M. Boguñá, C. Castellano, and R. Pastor-Satorras. The nature of epidemic thresholds in networks. *arXiv:1305.4819 [physics.soc-ph]*, 2013.

[65] V. Marceau, P. A. Noël, L. H. Dufresne, A. Allard, and L. J. Dubé. Adaptive networks: Coevolution of disease and topology. *Phys. Rev. E*, 82:036116, 2010.

[66] D. T. Gillespie. A general method for numerically simulating the stochastic time evolution of coupled chemical reactions. *J. Comput. Phys.*, 22:403–434, 1976.

[67] U. Brandes and D. Wagner. *Visone: Analysis & visualization of social networks*, 2011.

[68] P.-A. Noël, B. Davoudi, R. C. Brunham, L. J. Dubé, and B. Pourbohloul. Time evolution of epidemic disease on finite and infinite networks. *Phys. Rev. E*, 79:026101, 2009.

[69] J. P. Gleeson. High-accuracy approximation of binary-state dynamics on networks. *Phys. Rev. Lett.*, 107:068701, 2011.

[70] S. P. Meyn and R. L. Tweedie. *Markov Chains and Stochastic Stability.* Cambridge University Press, 2nd edition, 2009.

[71] M. E. J. Newman. Assortative mixing in networks. *Phys. Rev. Lett.*, 89:208701, 2002.

[72] E. Hestenes, M. R.; Stiefel. Methods of conjugate gradients for solving linear systems. *Journal of Research of the National Bureau of Standards (NIST Virtual Library)*, 49, 1952.

[73] T. Gross and I. G. Kevrekidis. Robust oscillations in SIS epidemics on adaptive networks: Coarse-graining by automated moment closure. *EPL*, 82:38004, 2008.

[74] D. H. Zanette and S. Risau-Gusman. Infection spreading in a population with evolving contacts. *J. Biol. Phys.*, 34:135–148, 2008.

[75] H. Silk, G. Demirel, M. Homer, and T. Gross. Exploring network dynamics with a mathematical triple jump. *arXiv:1302.2743 [math.DS]*, 2013.

[76] S. Wieland, T. Aquino, A. Parisi, and A. Nunes. Characterising steady-state topologies of SIS dynamics on adaptive networks. *arXiv:1212.1060 [nlin.AO]*, 2010.

[77] R Bhatia. *Matrix analysis: Graduate texts in mathematics*. Springer, 1997.

[78] A. Mugler, A. M. Walczak, and C. H. Wiggins. Spectral solutions to stochastic models of gene expression with bursts and regulation. *Phys. Rev. E*, 80:041921, 2009.

[79] P. J. Menck, J. Heitzig, N. Marwan, and J. Kurths. How basin stability complements the linear-stability paradigm. *Nature Physics*, 9:89–92, 2013.

[80] Charo I. Del Genio, Thilo Gross, and Kevin E. Bassler. All scale-free networks are sparse. *Phys. Rev. Lett.*, 107:178701, 2011.

[81] J. M. Pacheco, A. Traulsen, and M. A. Nowak. Coevolution of strategy and structure in complex networks with dynamical linking. *Phys. Rev. Lett.*, 97:258103, 2006.

[82] S. Van Segbroeck, F. C. Santos, T. Lenaerts, and J. M. Pacheco. Reacting differently to adverse ties promotes cooperation in social networks. *Phys. Rev. Lett.*, 102:058105, 2009.

[83] S. Van Segbroeck, F. C. Santos, and J. M. Pacheco. Adaptive contact networks change effective disease infectiousness and dynamics. *PLoS Comput. Biol.*, 6:e1000895, 2010.

[84] I. Z. Kiss, L. Berthouze, T. J. Taylor, and P. L. Simon. Modelling approaches for simple dynamic networks and applications to disease transmission models. *Proc. R. Soc. A*, 468:1332–1355, 2012.

[85] L. B. Shaw and I. B. Schwartz. Fluctuating epidemics on adaptive networks. *Phys. Rev. E*, 77:066101, 2008.

[86] B. Guerra and J. Gómez-Gardeñes. Annealed and mean-field formulations of disease dynamics on static and adaptive networks. *Phys. Rev. E*, 82:035101, 2010.

[87] J. Bryden, S. Funk, N. Geard, S. Bullock, and V. A. A. Jansen. Stability in flux: Community structure in dynamic networks. *J. R. Soc. Interface*, 8:1031–1040, 2011.

[88] R. A. Holley and T. M. Liggett. Ergodic theorems for weakly interacting infinite systems and the voter model. *Ann. Probab*, 3:643–663, 1975.

[89] K. Suchecki, V. M. Eguíluz, and M. San Miguel. Conservation laws for the voter model in complex networks. *EPL*, 69:228, 2005.

[90] R. Durrett, J. P. Gleeson, A. L. Lloyd, P. J. Mucha, F. Shi, D. Sivakoff, J. E. S. Socolar, and C. Varghese. Graph fission in an evolving voter model. *PNAS*, 109:3682–3687, 2012.

[91] T. Williams and R. Bjerknes. Stochastic model for abnormal clone spread through epithelial basal layer. *Nature*, 236:19–21, 1972.

[92] A. D. Sánchez, J. M. López, and M. A. Rodríguez. Nonequilibrium phase transitions in directed small-world networks. *Phys. Rev. Lett.*, 88:048701, 2002.

[93] G. Zschaler, G. A. Böhme, M. Seißinger, C. Huepe, and T. Gross. Early fragmentation in the adaptive voter model on directed networks. *Phys. Rev. E*, 85:046107, 2012.

[94] F. Vazquez and V. M. Eguíluz. Analytical solution of the voter model on uncorrelated networks. *New Journal of Physics*, 10:063011, 2008.

[95] T. Rogers and T. Gross. Consensus time and conformity in the adaptive voter model. *arXiv:1304.4742 [physics.soc-ph]*, 2013.

[96] T. Antal, S. Redner, and V. Sood. Evolutionary dynamics on degree-heterogeneous graphs. *Phys. Rev. Lett.*, 96:188104, 2006.

[97] S. Wieland, T. Aquino, and A. Nunes. The structure of coevolving infection networks. *EPL*, 97:18003, 2012.

[98] S. Wieland, A. Parisi, and A. Nunes. Detecting and describing dynamic equilibria in adaptive networks. *EPJ-ST*, 212:99–113, 2012.

[99] S. Wieland and A. Nunes. An asymmetric coevolutionary voter model. *arXiv:1303.0314 [nlin.AO]*, 2013.

[100] G. W. A. Constable, A. J. McKane, and T. Rogers. Stochastic dynamics on slow manifolds. *arXiv:1301.7697 [cond-mat.stat-mech]*, 2013.

[101] A.J. Roberts. Normal form transforms separate slow and fast modes in stochastic dynamical systems. *Physica A*, 387:12–38, 2008.